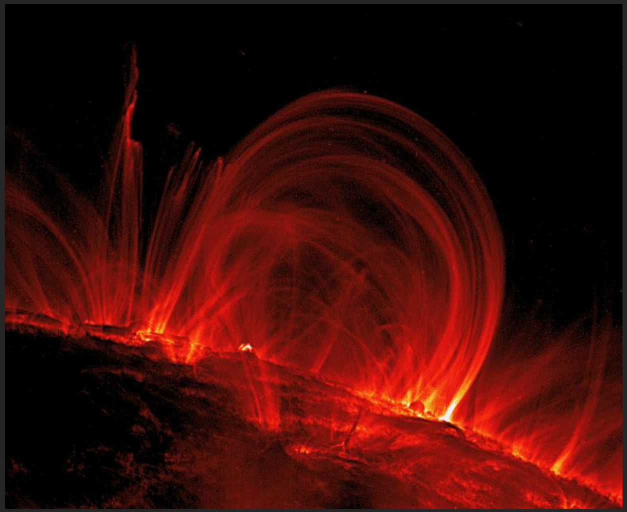

Solar Corona

Jaroslav Dudík

Astronomical Institute of the Czech Academy of Sciences

Lecture 1

Selected Chapters in Astrophysics

Faculty of Mathematics and Physics, Charles University, 2018-10-22

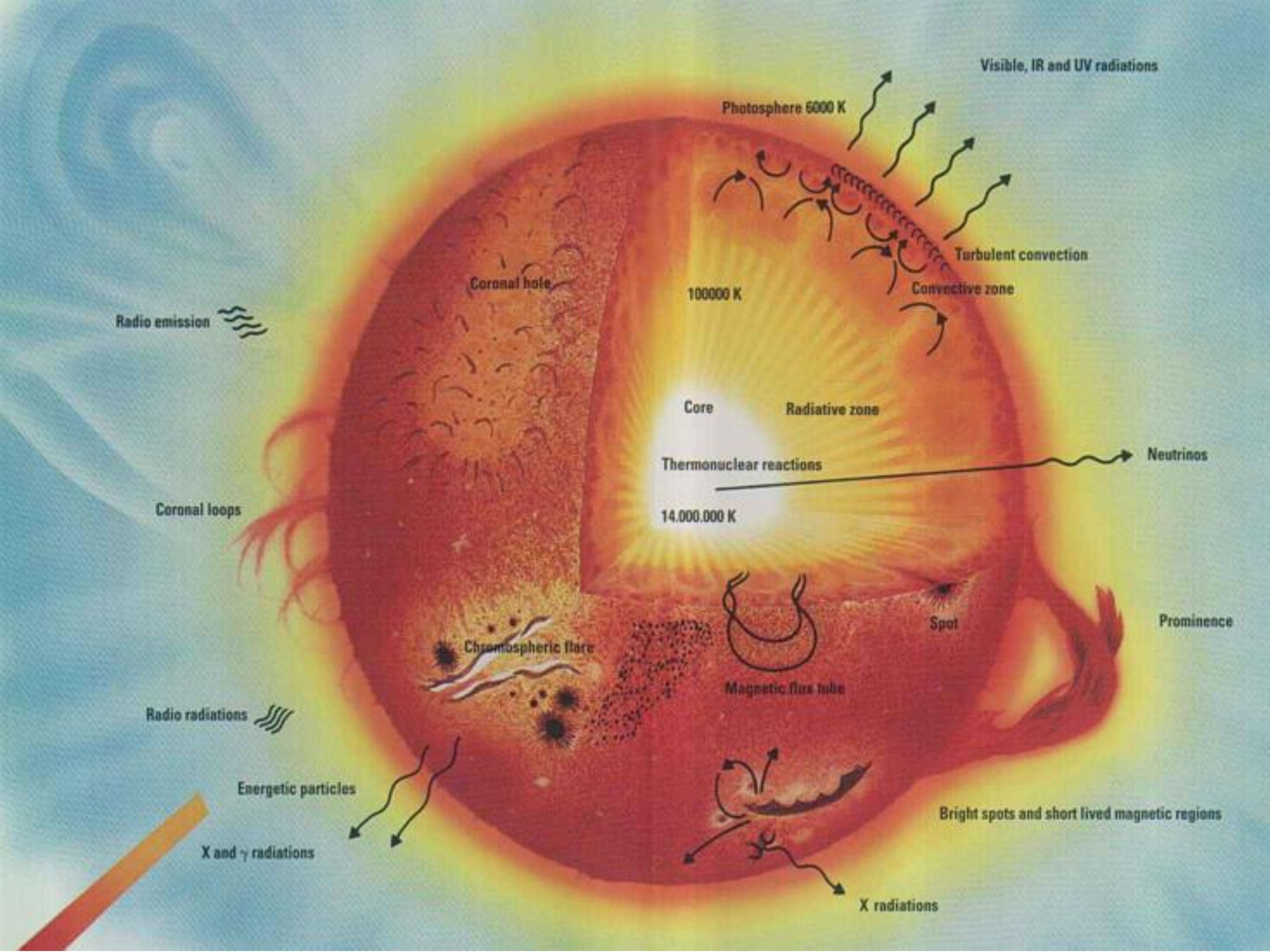

Visible, IR and UV radiations
Photosphere 6000 K
Turbulent convection
Coronal hole
100000 K
Convective zone
Radio emission
Core
Radiative zone
Thermonuclear reactions
Neutrinos
Coronal loops
14.000.000 K
Spot
Prominence
Chromospheric flare
Magnetic flux tube
Radio radiations
Energetic particles
Bright spots and short lived magnetic regions
X and γ radiations
X radiations

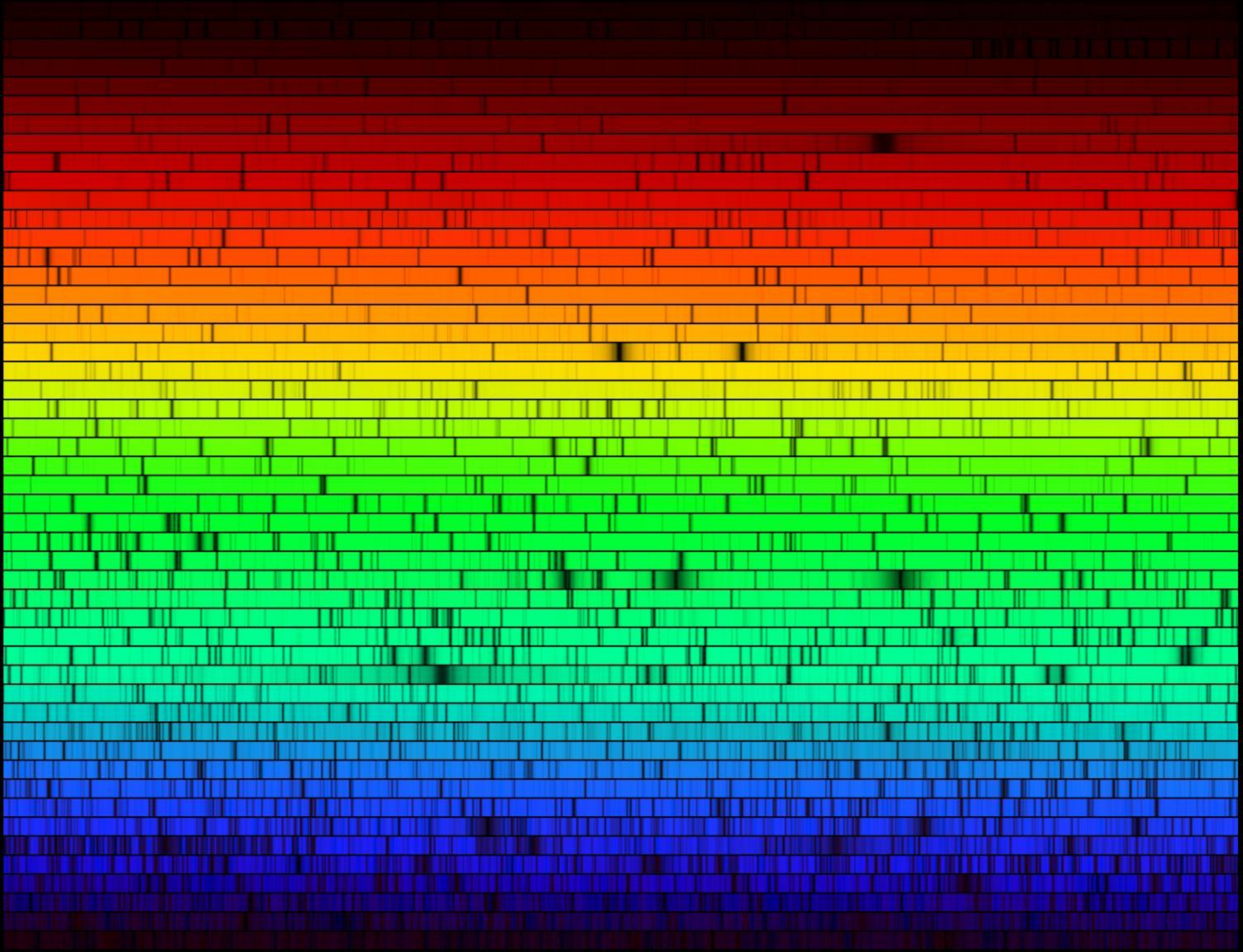

Motivation: Irradiance

The Solar "Constant"

- Energy flux budget at Earth

$$F = \frac{L_\odot}{4\pi(1\ \mathrm{AU})^2} = \frac{3.846 \times 10^{26}\ \mathrm{W}}{4\pi(1.49597\ \times 10^{11}\ \mathrm{m})^2} = 1367.6\ \mathrm{Wm}^{-2}$$

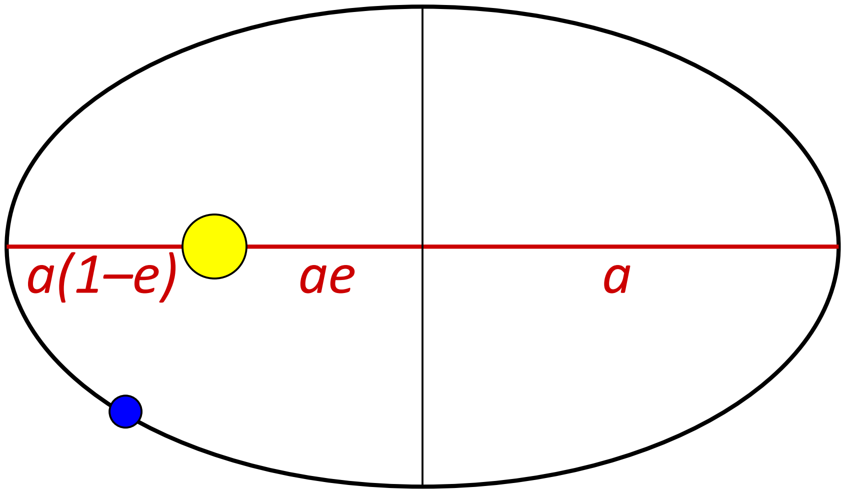

- Variations due to elipticity of the Earth's orbit (*e* = 0,0167)

  perihelion: ~ 1414,4 Wm^{-2} (+3,3%)

  aphelion: ~ 1323,0 Wm^{-2} (–3,3%)

➢ Earth's albedo *A* = 0,367 (but clouds etc.)

$\Rightarrow$ mean temperature at Earth

$$\pi R_\otimes^2 (1 - A) F = 4\pi R_\otimes^2 \sigma T_\otimes^4 \left(\frac{100}{119}\right)^4$$

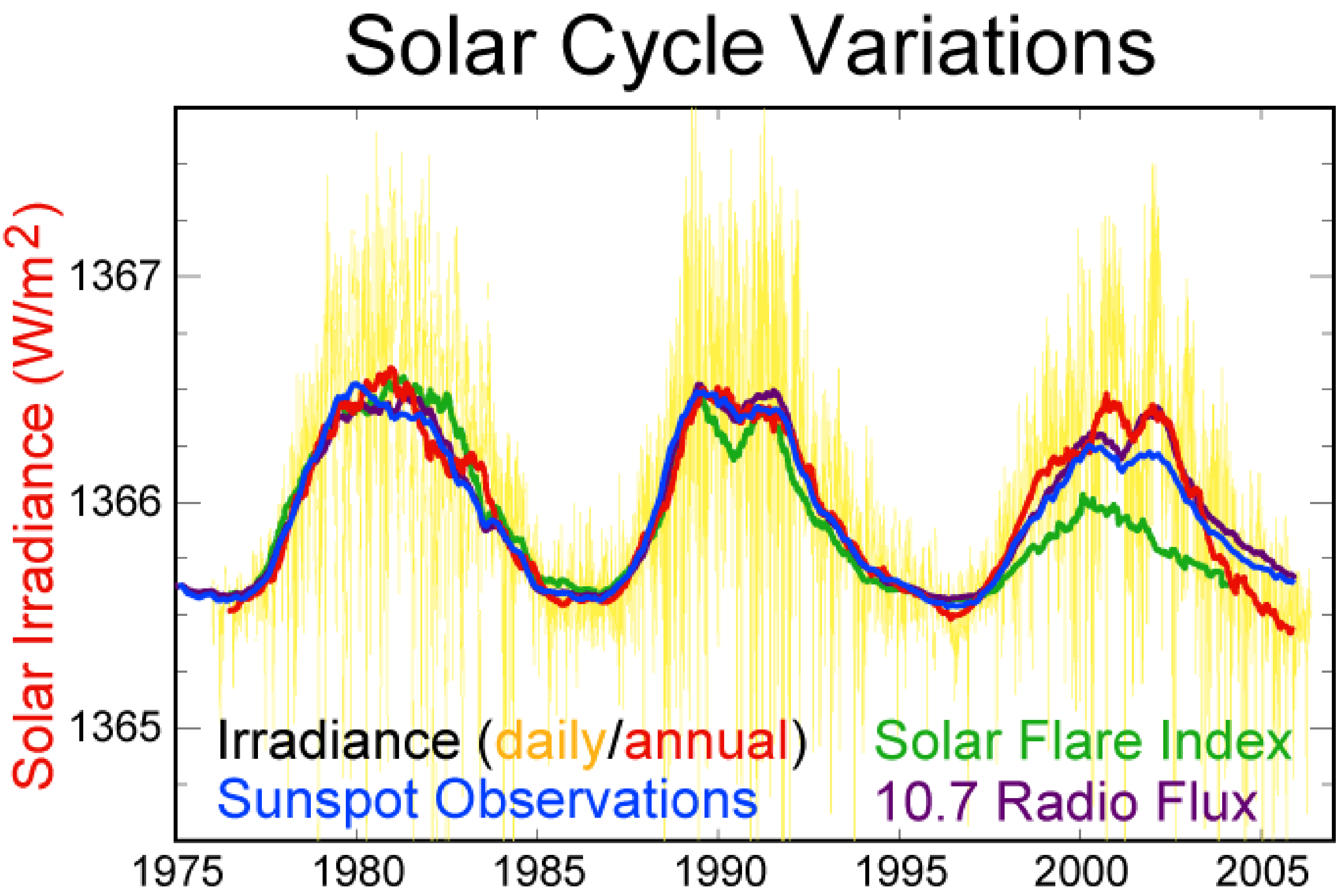

Solar Cycle Variations
Solar Irradiance (W/m2)
1367
1366
1365
Irradiance (daily/annual)
Sunspot Observations
Solar Flare Index
10.7 Radio Flux
1975
1980
1985
1990
1995
2000
2005

Irradiance at EUV wavelengths

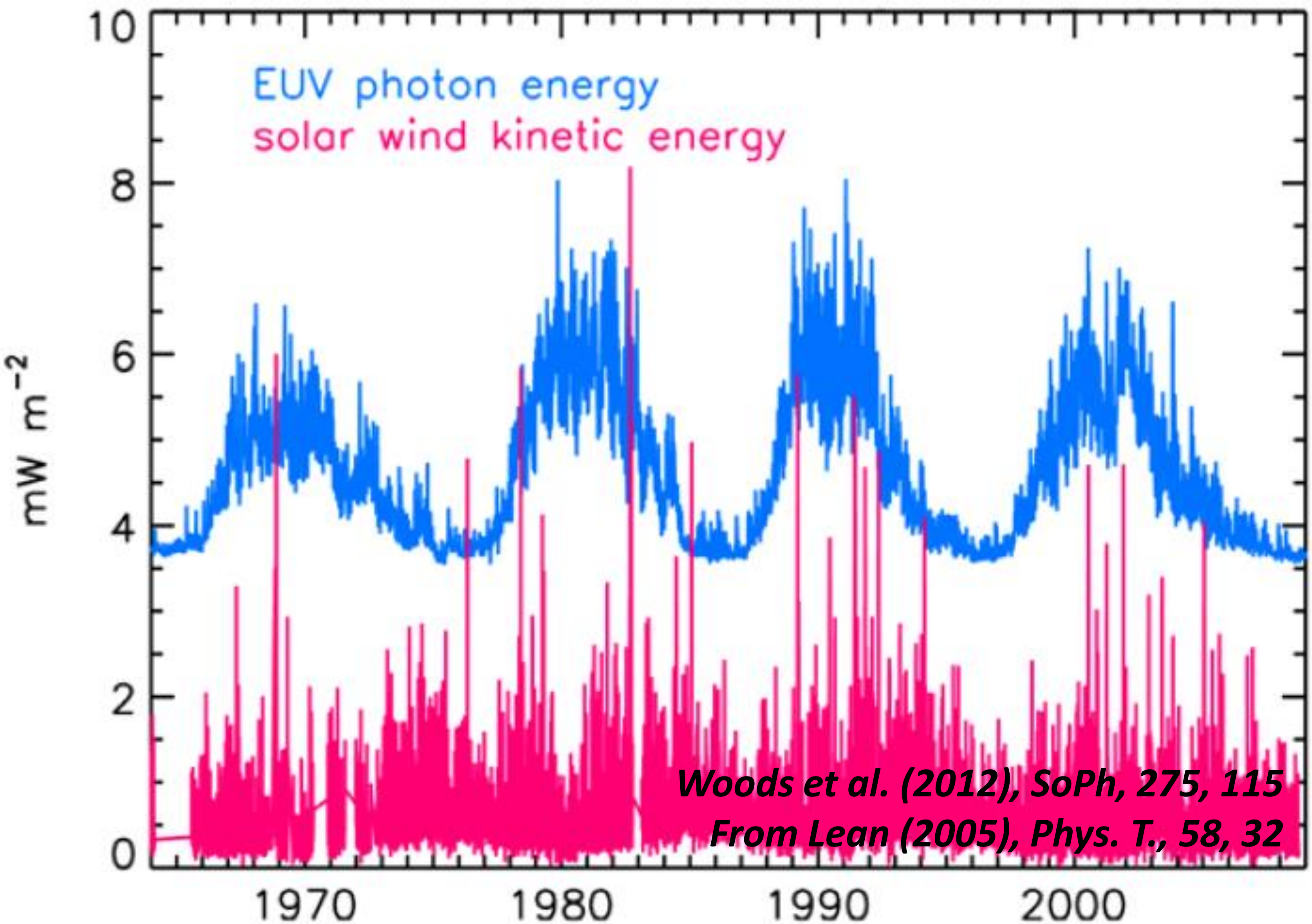

Chromosphere and Corona: *T* (*z*)

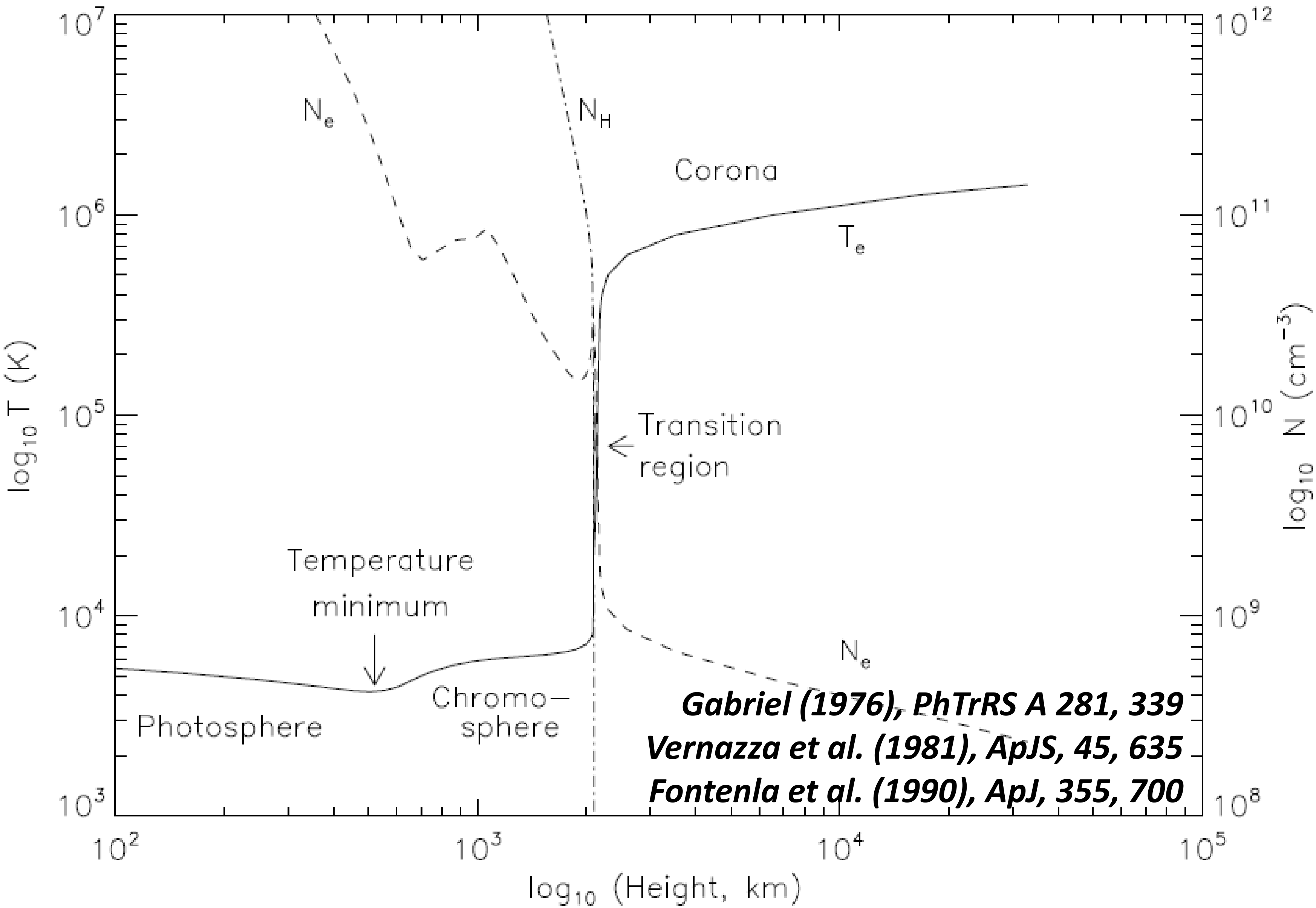

Gabriel (1976), PhTrRS A 281, 339
Vernazza et al. (1981), ApJS, 45, 635
Fontenla et al. (1990), ApJ, 355, 700

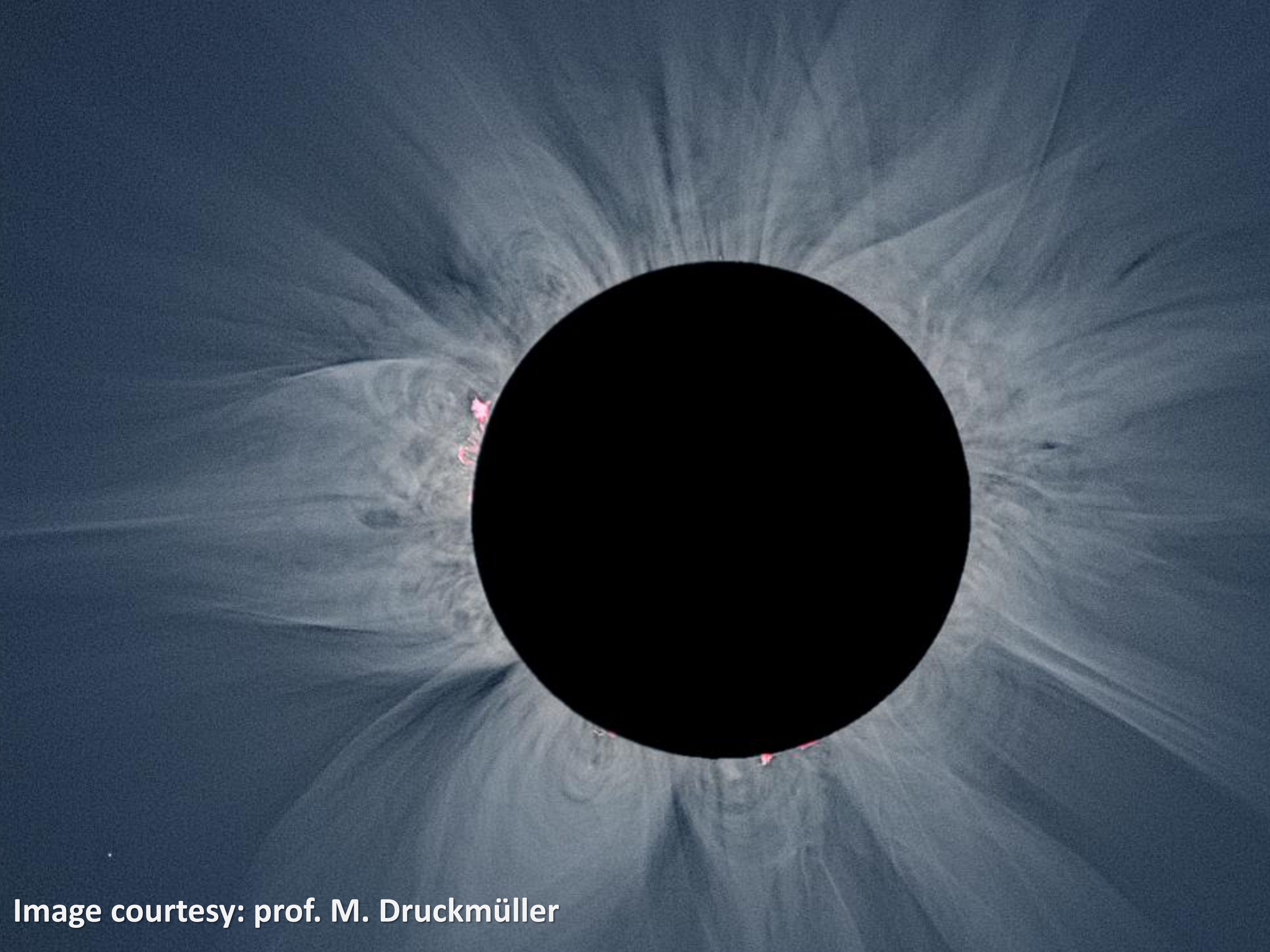

Image courtesy: prof. M. Druckmüller

Image courtesy: prof. M. Druckmüller

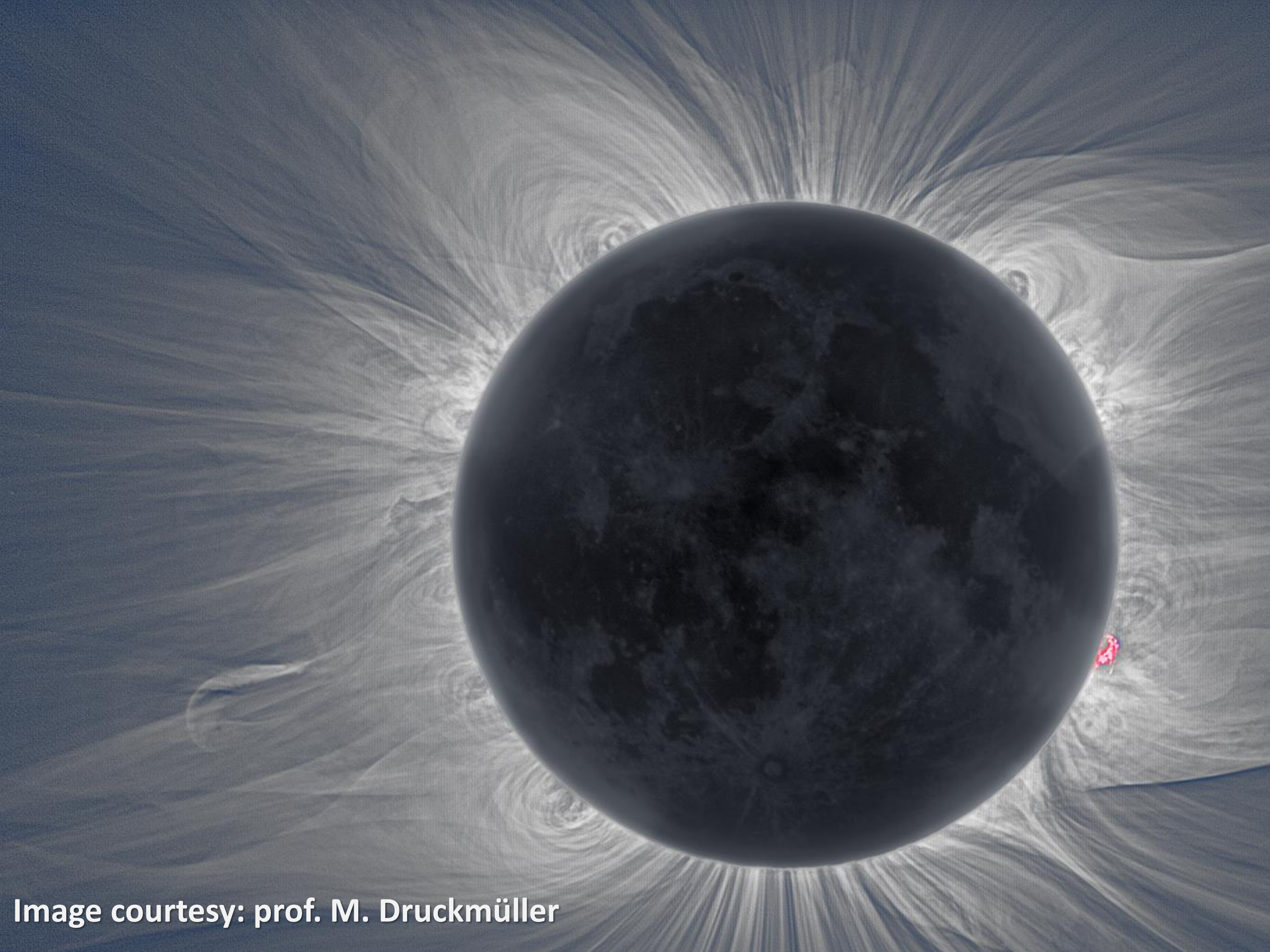
Image courtesy: prof. M. Druckmüller

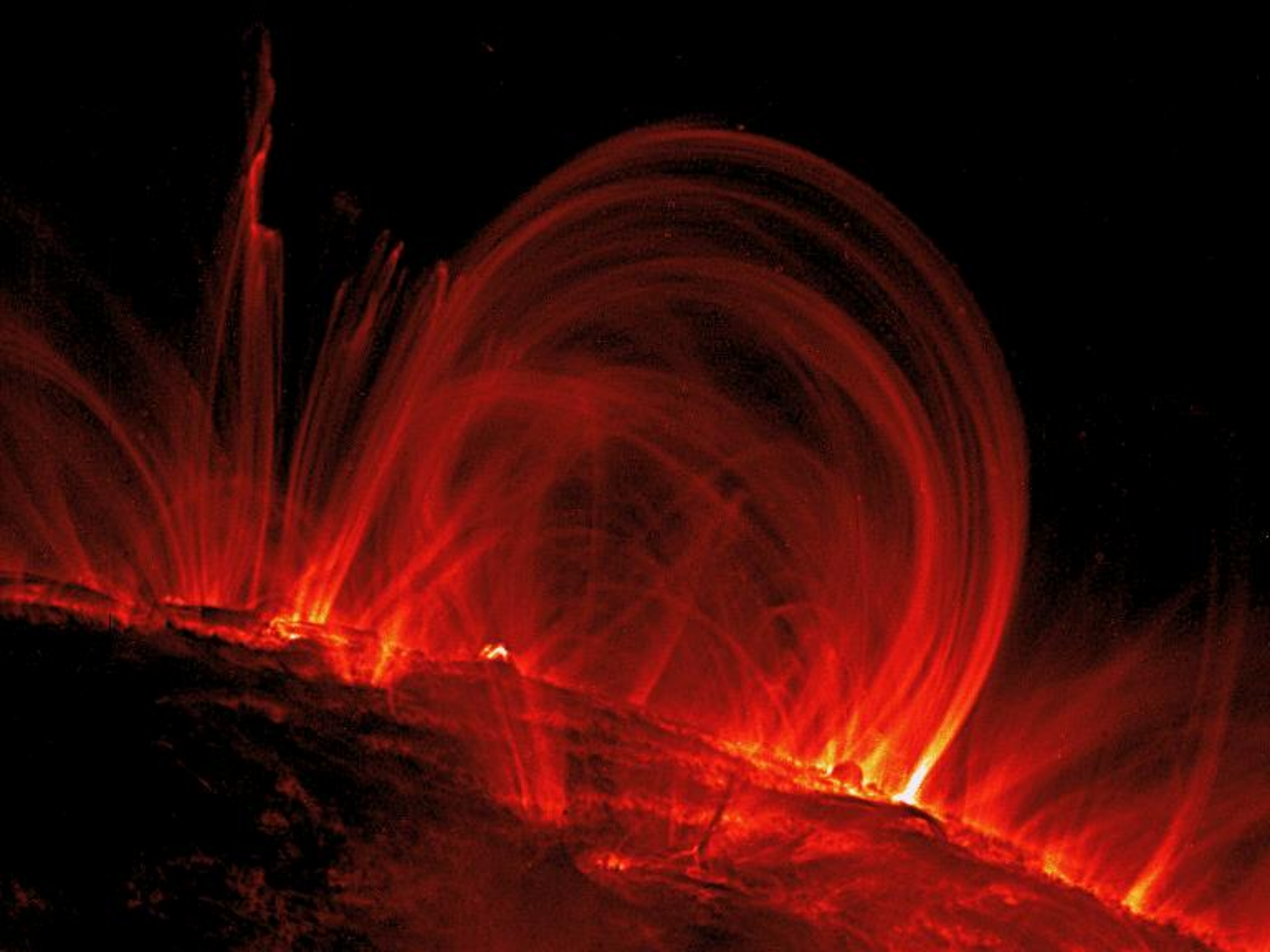

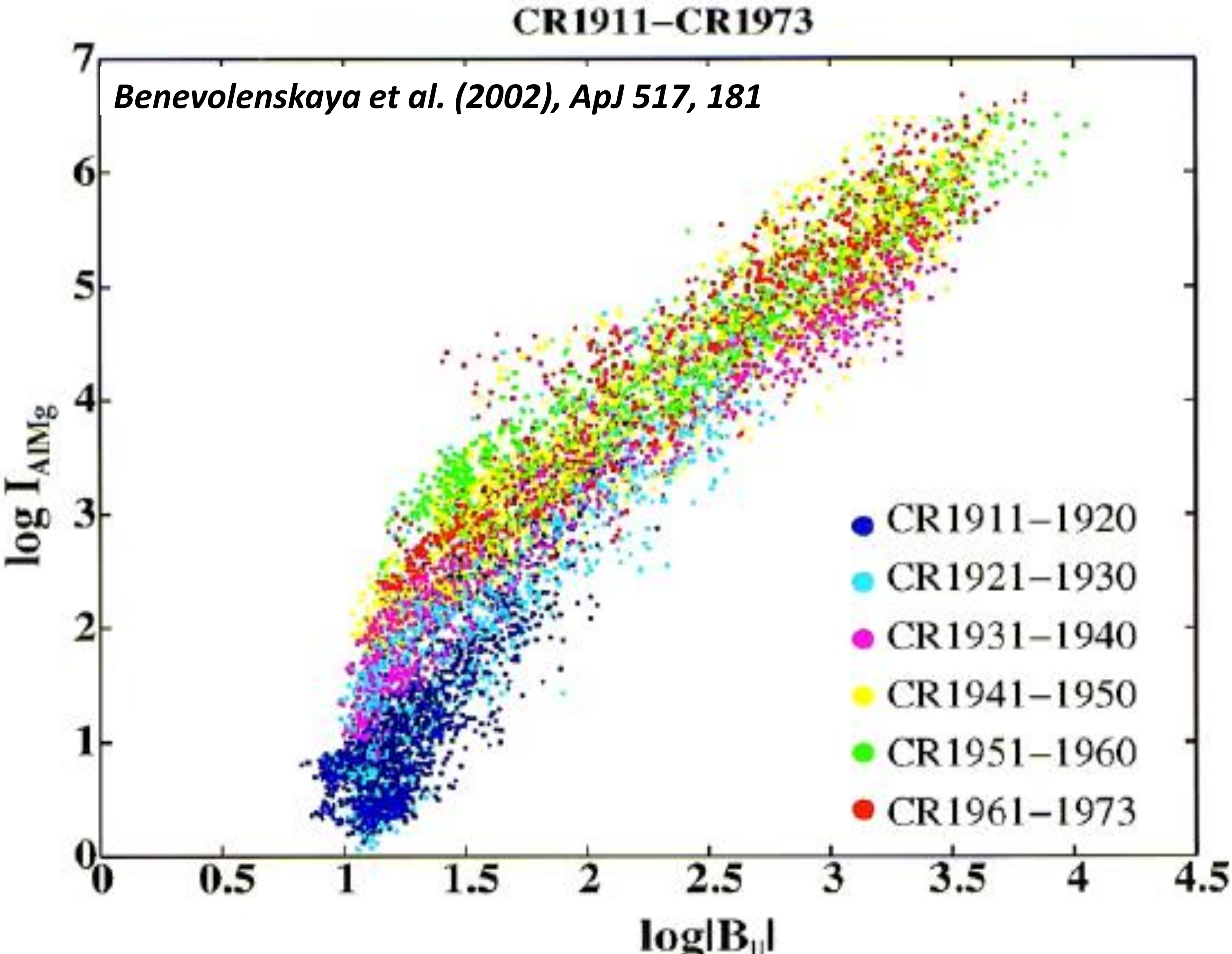

CR1911–CR1973
Benevolenskaya et al. (2002), ApJ 517, 181
CR1911–1920
CR1921–1930
CR1931–1940
CR1941–1950
CR1951–1960
CR1961–1973
log I_AIMg
log|B_∥|

Optically Thin Spectroscopy

- **Optically thin = negligible absorption (no radiative transfer) – everything emitted along the LOS will reach the observer**
- **The emissivity ε_{ij} of a spectral line λ_{ij} produced by transitions from level i to level j in a k-times ionized atom of element X is given by**

$$\varepsilon_{ij} = \frac{hc}{\lambda_{ij}} A_{ij} n\left(X_i^{+k}\right) = \frac{hc}{\lambda_{ij}} \frac{A_{ij}}{n_e} \frac{n\left(X_i^{+k}\right)}{n(X^{+k})} \frac{n(X^{+k})}{n(X)} \frac{n(X)}{n(H)} n(H) n_e$$

$$= \frac{hc}{\lambda_{ij}} C_{ji} \frac{n\left(X_i^{+k}\right)}{n(X^{+k})} \frac{n(X^{+k})}{n(X)} \frac{n(X)}{n(H)} n(H) n_e$$

$$= G(T, n_e) n(H) n_e$$

- **Assume ionization equilibrium and excitation equilibrium can be treated separately ("coronal approximation")**
- **Intensity I_{ij} of this emission line from optically thin plasma of volume V along the line of sight:**

$$I_{ij} = \int G(T, n_e) n(H) n_e dV$$

FIP Effect – Coronal Abundances

- Elements with **first ionization potential smaller than 10 keV** have greatly **enhanced abundances** in the corona: FIP effect

Feldman & Widing (2003), Space Sci. Rev. 107, 665

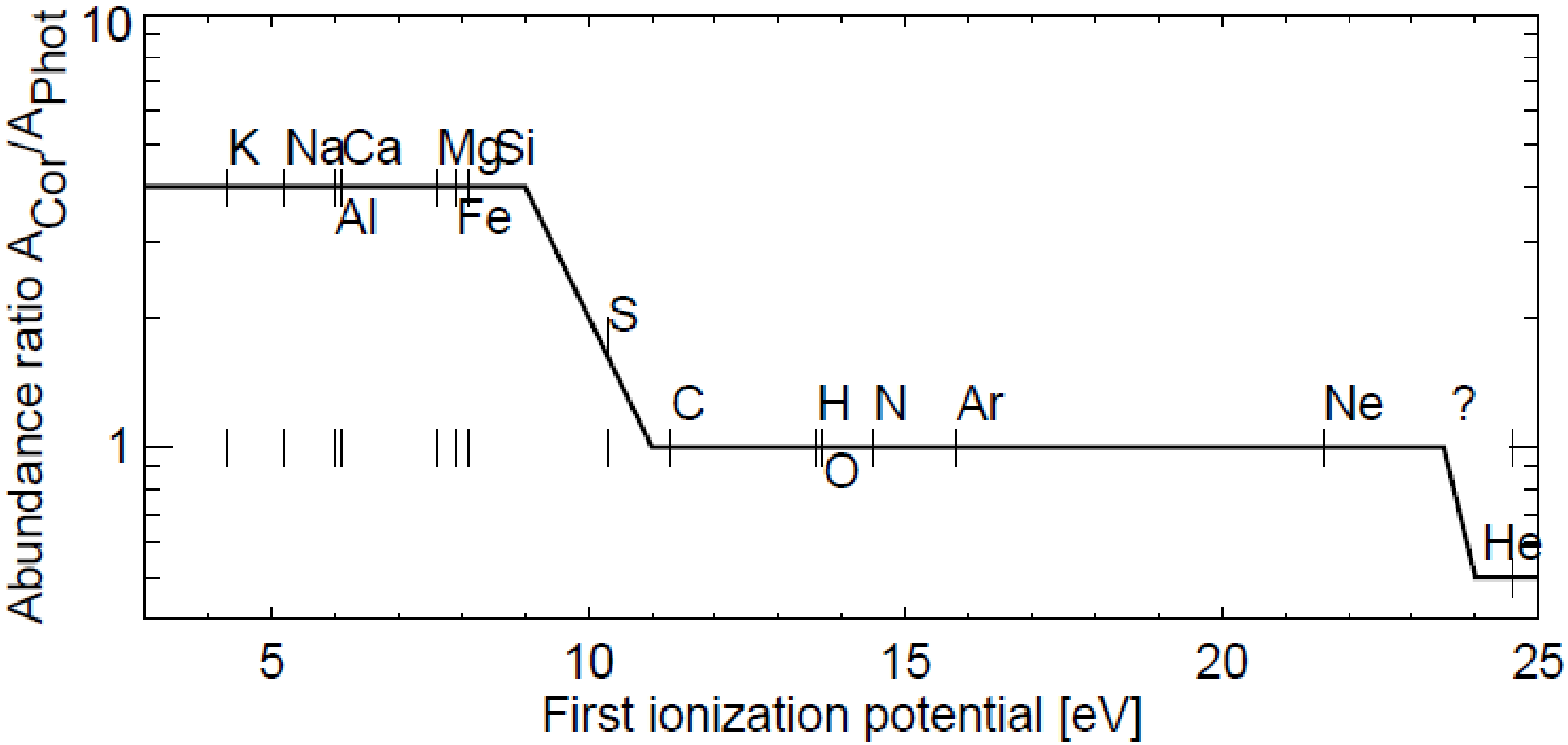

Collisional Ionization Equilibrium

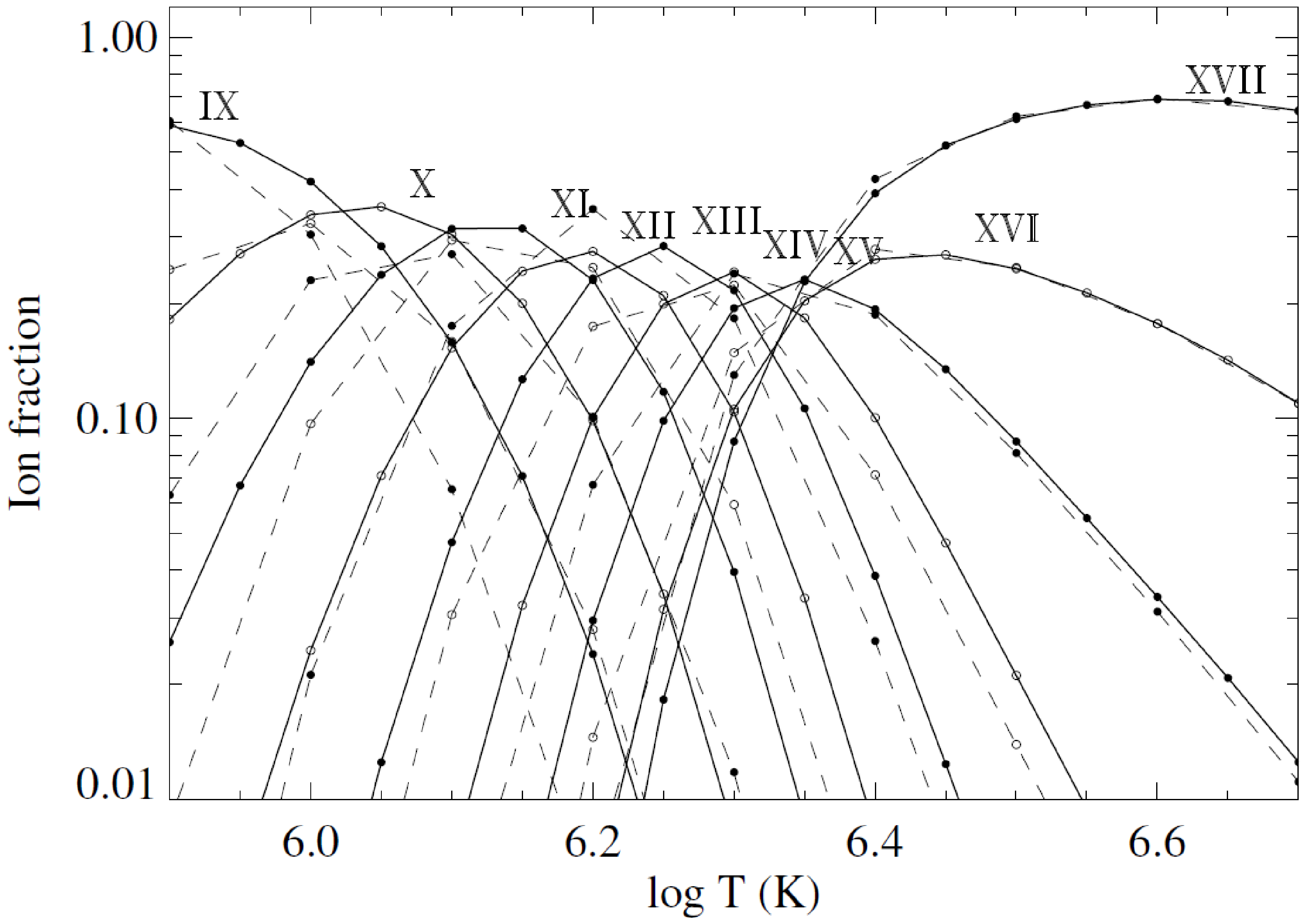

Dere et al. (2009), Astron. Astrophys. 498 915, CHIANTI 6 paper

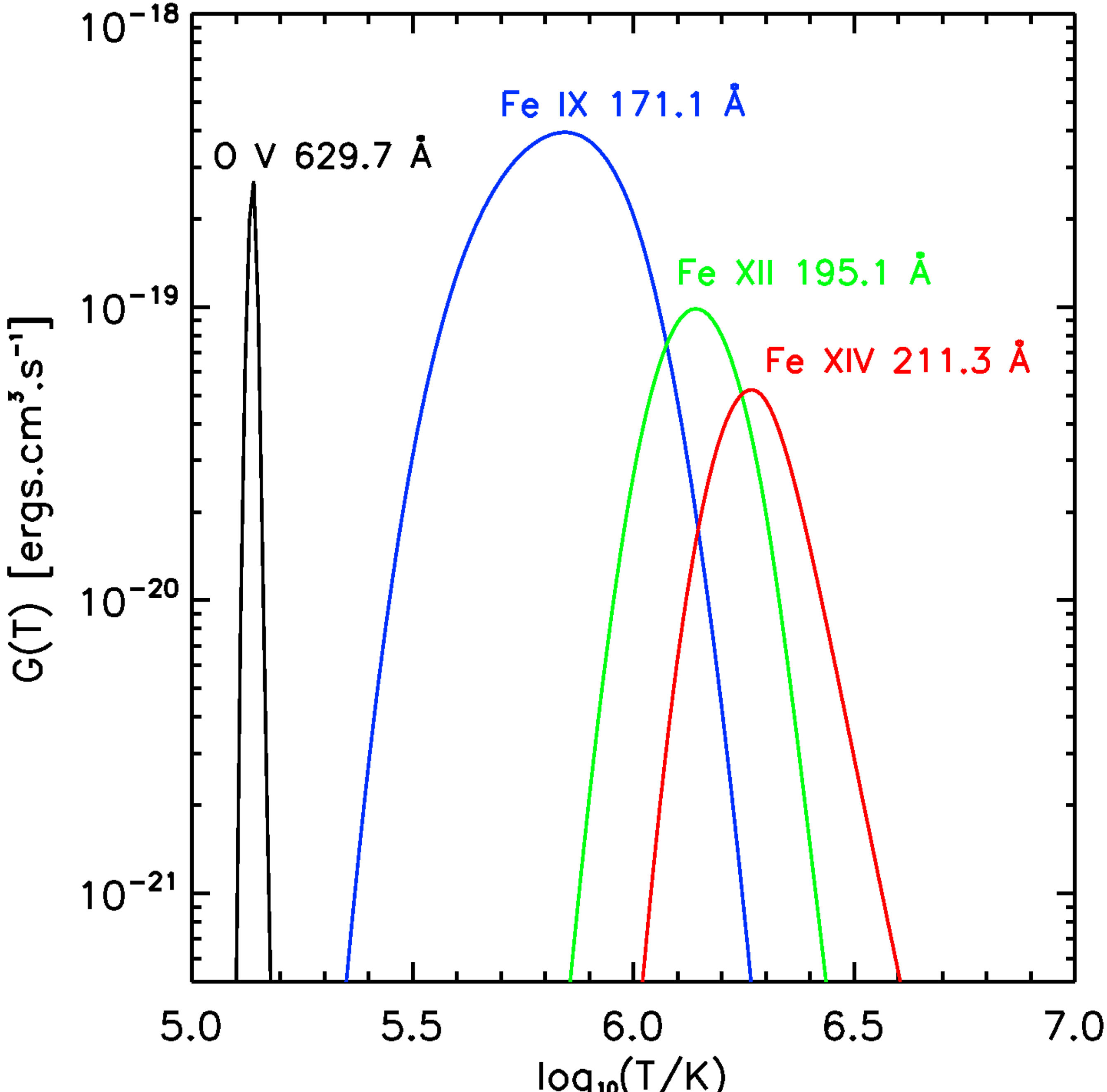

O V 629.7 Å
Fe IX 171.1 Å
Fe XII 195.1 Å
Fe XIV 211.3 Å
10^{-18}
10^{-19}
10^{-20}
10^{-21}
G(T) [ergs.cm^3.s^{-1}]
5.0
5.5
6.0
6.5
7.0
$\log_{10}$(T/K)

Coronal Radiative Losses

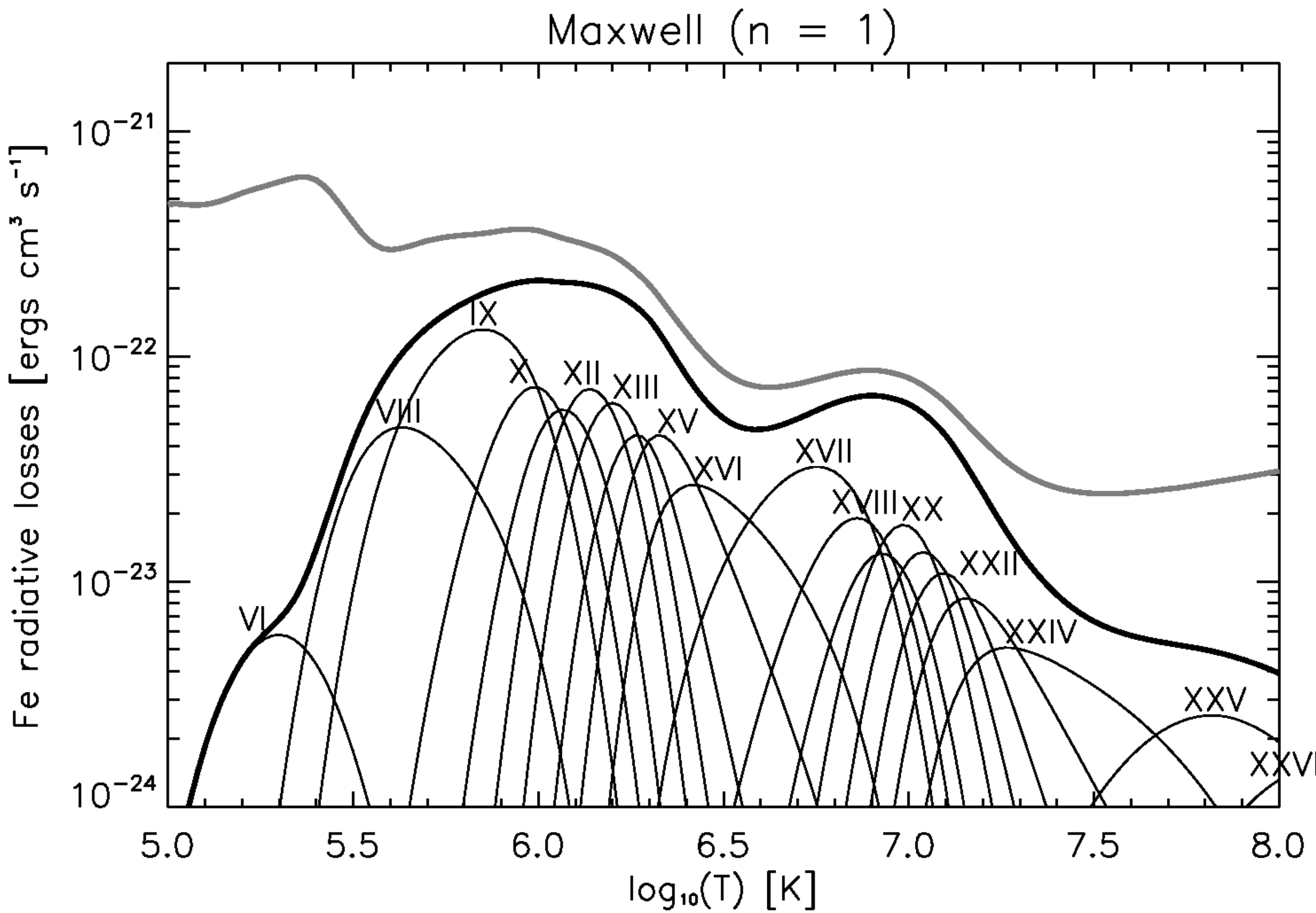

Dudík et al. (2011), Astron. Astrophys. 529, A103

Emission Measure and DEM(T)

- **If the plasma is isothermal along the LOS, the intensity is simply**

$$I_{ij} = \int G(T,n_e)n_H n_e dV = G(T,n_e)\int n_H n_e dV = G(T,n_e)EM(T)$$

- **However, if the plasma is multithermal, i.e., many different structures along the LOS, the intensity is given by**

$$I_{ij} = \int G(T,n_e)n_H n_e \frac{dV}{dT}dT = \int G(T,n_e)DEM(T)dT$$

- **where DEM(T) is the differential emission measure**

- **DEM(T) has to be determined from observations.**
- **Inverse, ill-posed problem, but corona sometimes *is* multithermal!**

EM-loci Method: Multithermality

$$EM_{\text{loci}} = \frac{I_{ij}}{G_{ij}(T, n_e)} \Rightarrow DEM(T) \leq \left\{ \frac{I_{ij}}{G_{ij}(T, n_e)} \right\} \quad \forall\, i, j$$

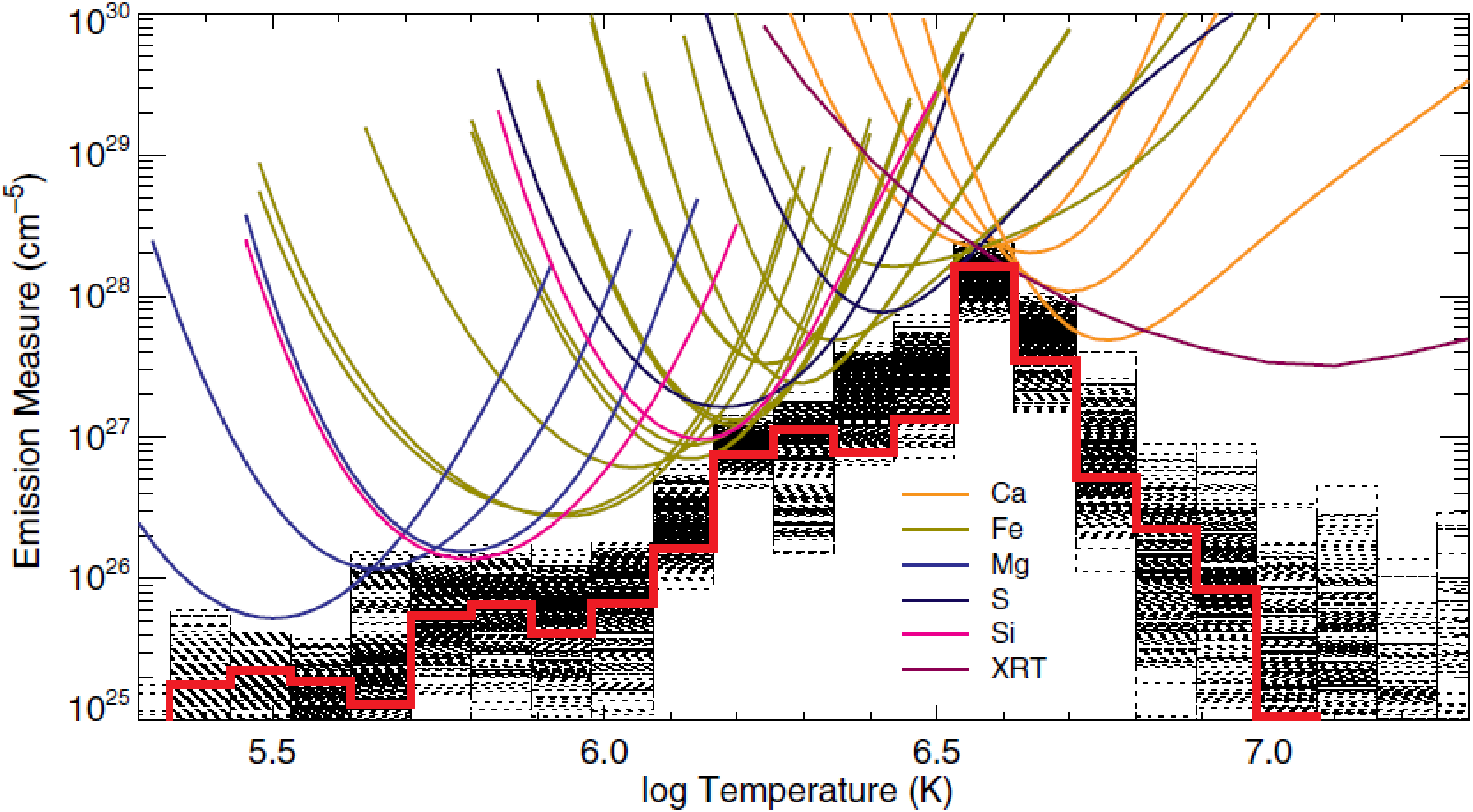

Warren et al. (2011), Astrophys. J. 734, 90

EUV and X-ray Filters

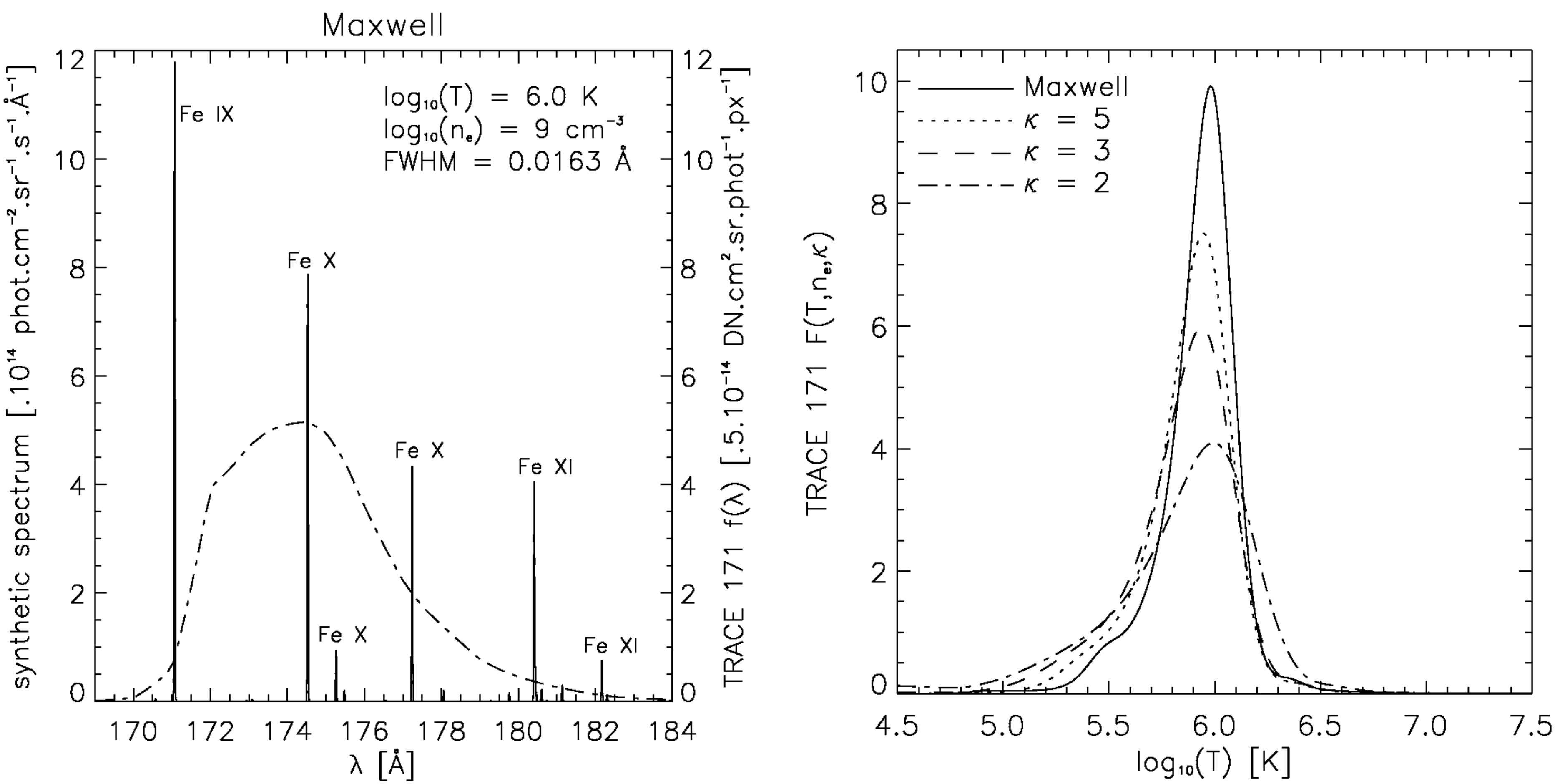

Dudík et al. (2009), Astron. Astrophys. 505, 1255

Hinode

- Hinode ("Sunrise") – Japanese mission, launched 2006
- European and US collaboration
- The X-Ray Telescope (XRT) – multi-filter telescope
- EUV Imaging Spectrometer (EIS) – 170-210 Å and 250-290 Å
  – slit-slot mech. 1", 2", 40", 266"
- Solar Optical Telescope (SOT) – 0.5 m mirror, filter packages

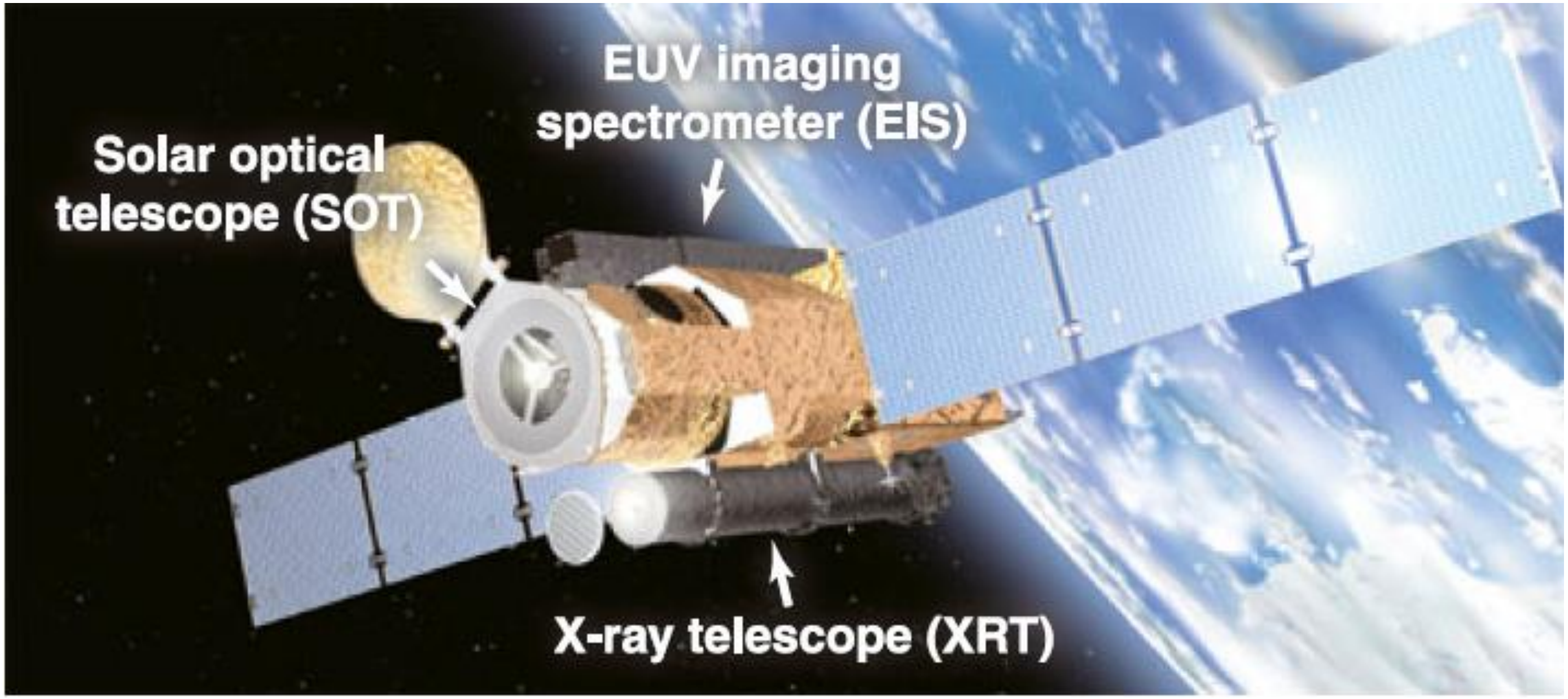

Narukage et al. (2011), Solar Phys. 269, 169

Hinode/XRT

filter wheel 1

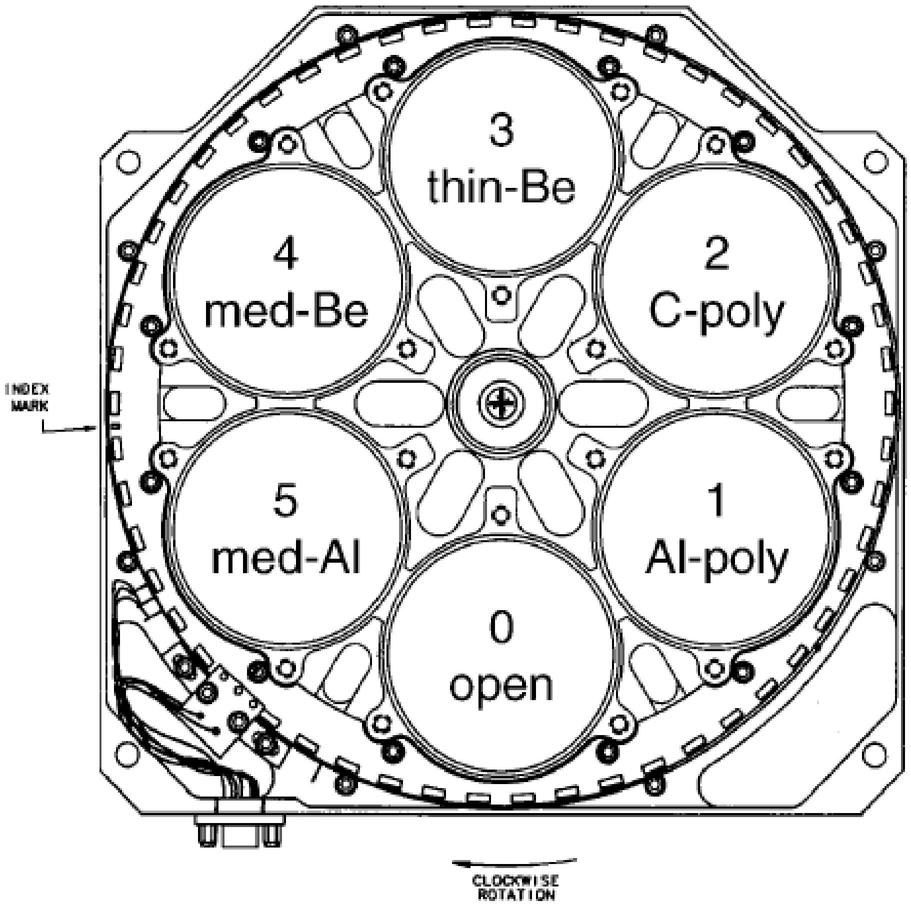

filter wheel 2

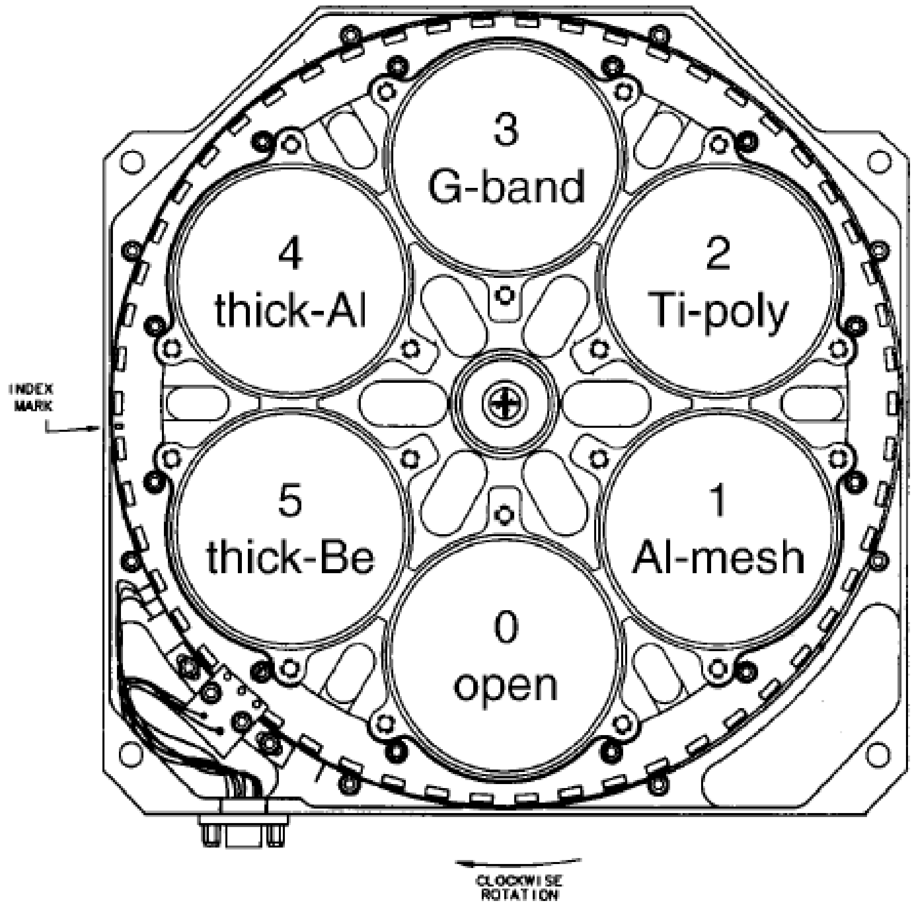

Narukage et al. (2011), Solar Phys. 269, 169

Hinode/XRT Temperature Response

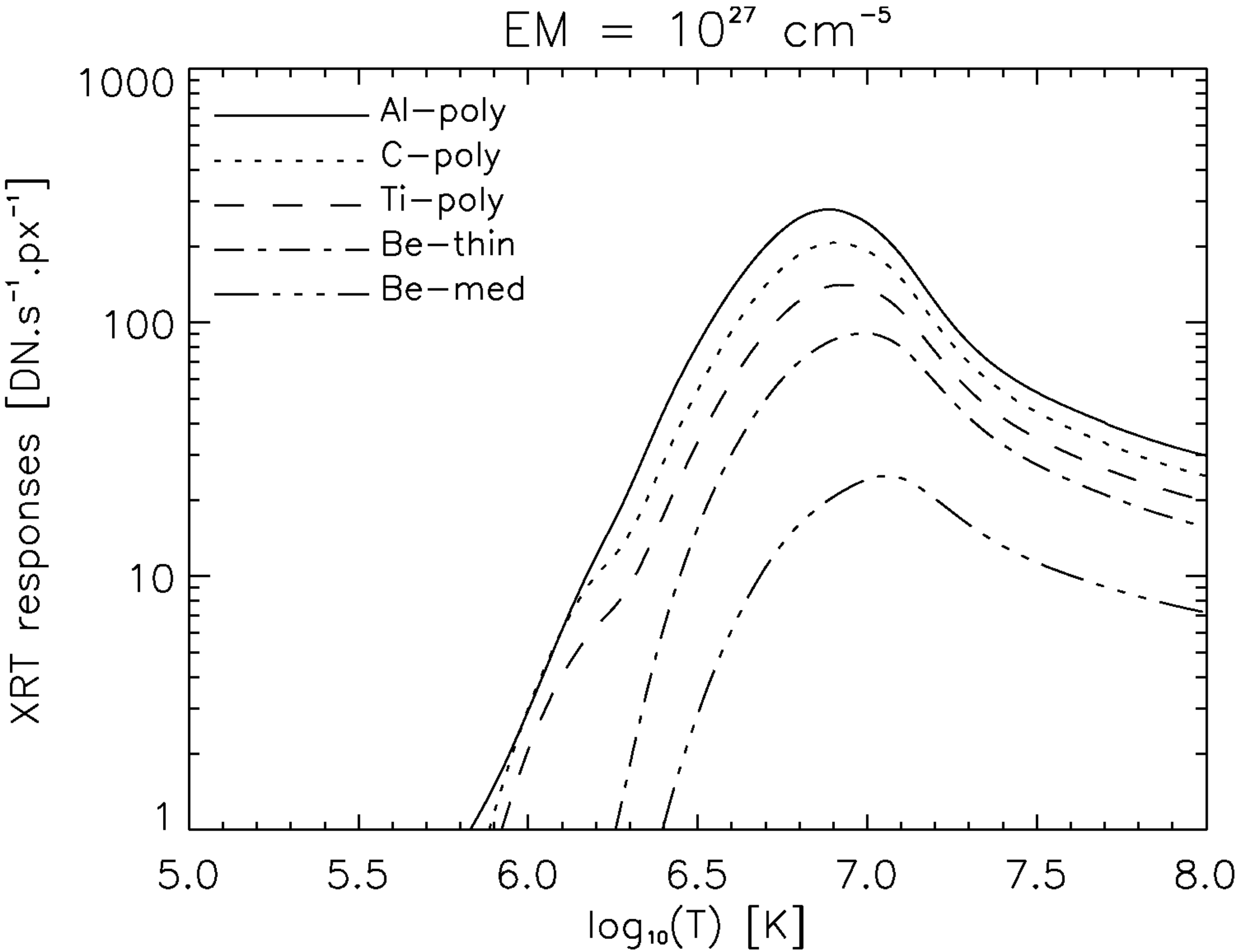

XRT Temperature Diagnostics

$$CIFR(T) = \frac{\left(\prod_{i=1}^{5} F_i(T)\right)^{2/5}}{F_1(T)F_2(T)}$$

Reale et al. (2007)
Science 317, 1582

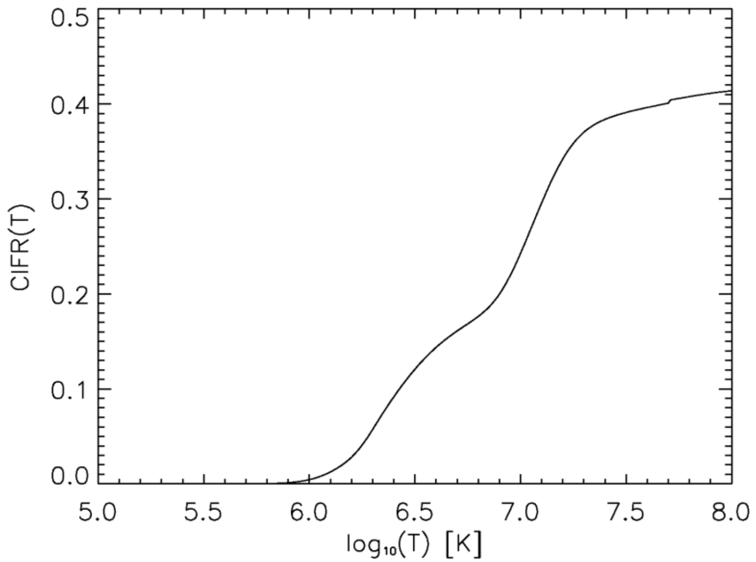

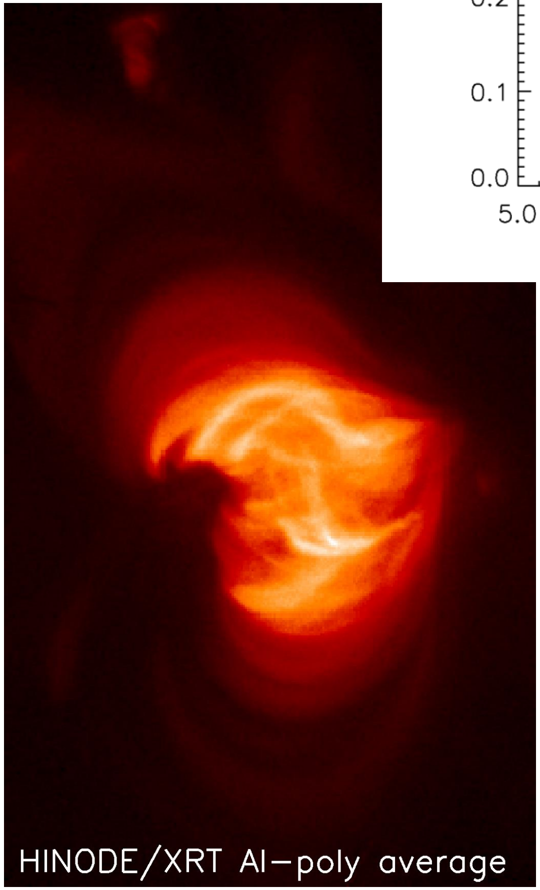

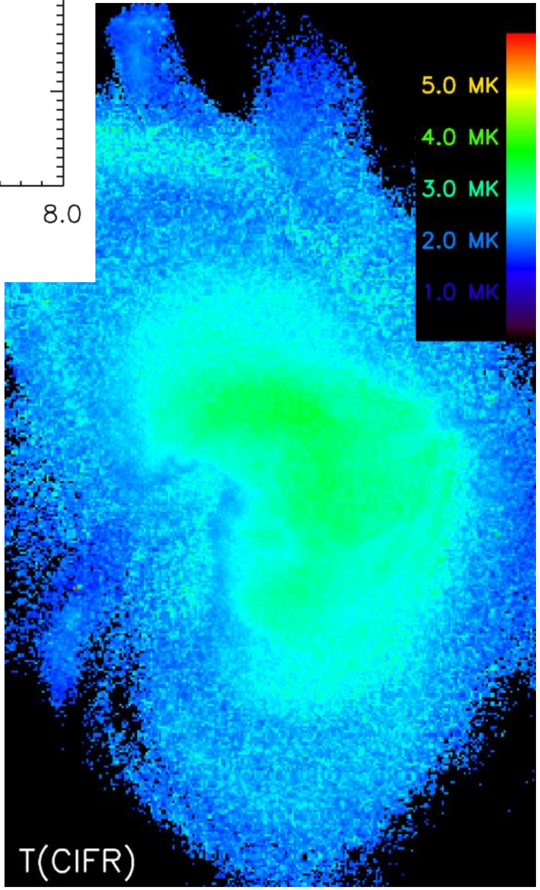

Atmospheric Imaging Assembly

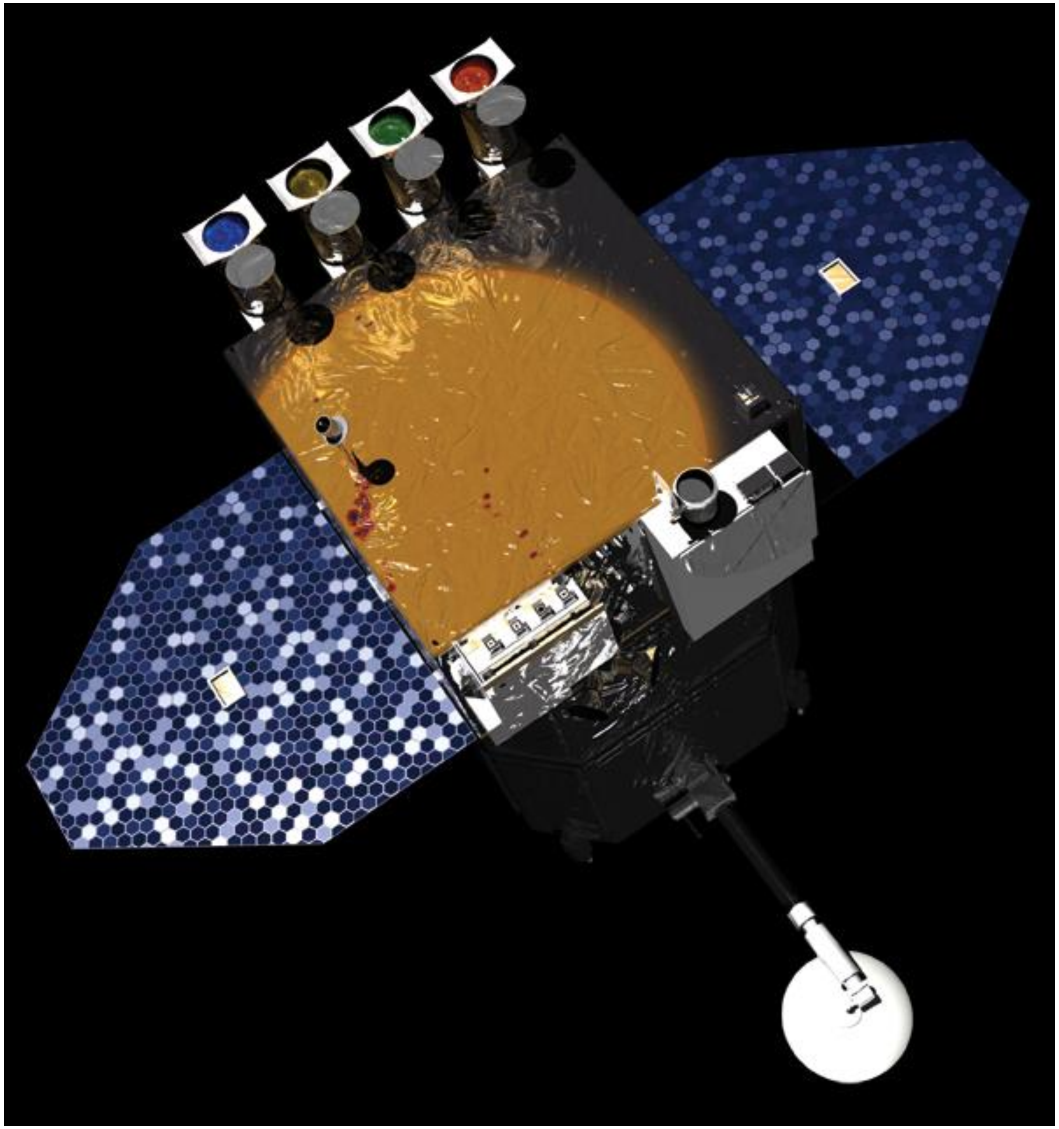

Solar Dynamics Observatory:

- NASA, launched 2010
- current workhorse for Solar Physics

Atmospheric Imaging Assembly (AIA):

- four identical EUV full-disc telescopes, state-of-the-art
- cadence of 12 seconds
- 0.6” px size, 1.5” resolution
- broad temperature coverage to study coronal and flare physics

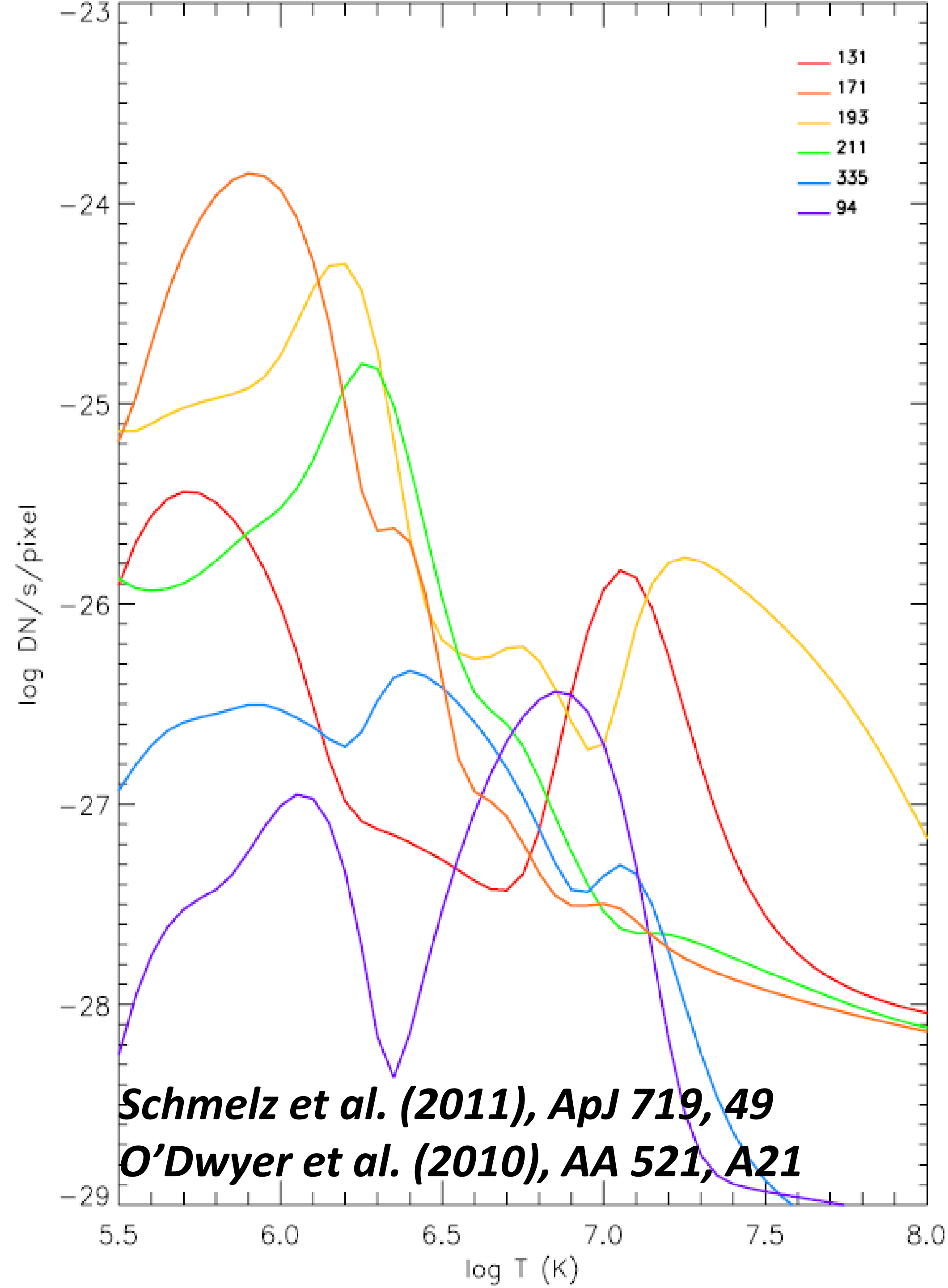

Table 1. Predicted AIA count rates.

	Ion	λ Å	$T_p{}^a$ K	Fraction of total emission CH	QS	AR	FL
94 Å	Mg VIII	94.07	5.9	0.03	–	–	–
	Fe XX	93.78	7.0	–	–	–	0.10
	Fe XVIII	93.93	6.85	–	–	0.74	0.85
	Fe X	94.01	6.05	0.63	0.72	0.05	–
	Fe VIII	93.47	5.6	0.04	–	–	–
	Fe VIII	93.62	5.6	0.05	–	–	–
	Cont.			0.11	0.12	0.17	–
131 Å	O VI	129.87	5.45	0.04	0.05	–	–
	Fe XXIII	132.91	7.15	–	–	–	0.07
	Fe XXI	128.75	7.05	–	–	–	0.83
	Fe VIII	130.94	5.6	0.30	0.25	0.09	–
	Fe VIII	131.24	5.6	0.39	0.33	0.13	–
	Cont.			0.11	0.20	0.54	0.04
171 Å	Ni XIV	171.37	6.35	–	–	0.04	–
	Fe X	174.53	6.05	–	0.03	–	–
	Fe IX	171.07	5.85	0.95	0.92	0.80	0.54
	Cont.			–	–	–	0.23
193 Å	O V	192.90	5.35	0.03	–	–	–
	Ca XVII	192.85	6.75	–	–	–	0.08
	Ca XIV	193.87	6.55	–	–	0.04	–
	Fe XXIV	192.03	7.25	–	–	-	0.81
	Fe XII	195.12	6.2	0.08	0.18	0.17	–
	Fe XII	193.51	6.2	0.09	0.19	0.17	–
	Fe XII	192.39	6.2	0.04	0.09	0.08	–
	Fe XI	188.23	6.15	0.09	0.10	0.04	–
	Fe XI	192.83	6.15	0.05	0.06	–	–
	Fe XI	188.30	6.15	0.04	0.04	–	–
	Fe X	190.04	6.05	0.06	0.04	–	–
	Fe IX	189.94	5.85	0.06	–	–	–
	Fe IX	188.50	5.85	0.07	–	–	–
	Cont.			–	–	0.05	0.04
211 Å	Cr IX	210.61	5.95	0.07	–	–	–
	Ca XVI	208.60	6.7	–	–	–	0.09
	Fe XVII	204.67	6.6	–	–	–	0.07
	Fe XIV	211.32	6.3	–	0.13	0.39	0.12
	Fe XIII	202.04	6.25	–	0.05	–	–
	Fe XIII	203.83	6.25	–	–	0.07	–

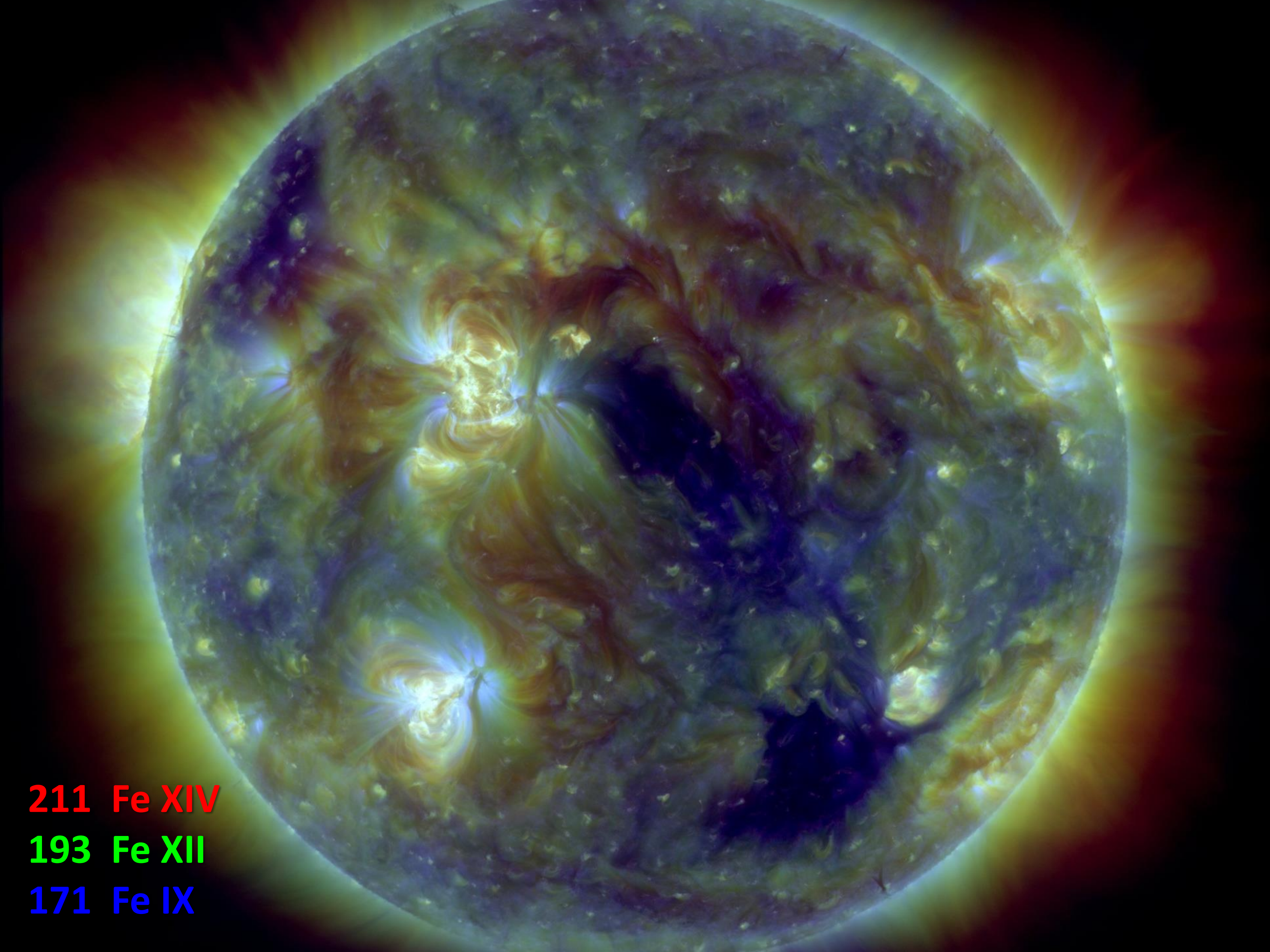
211 Fe XIV
193 Fe XII
171 Fe IX

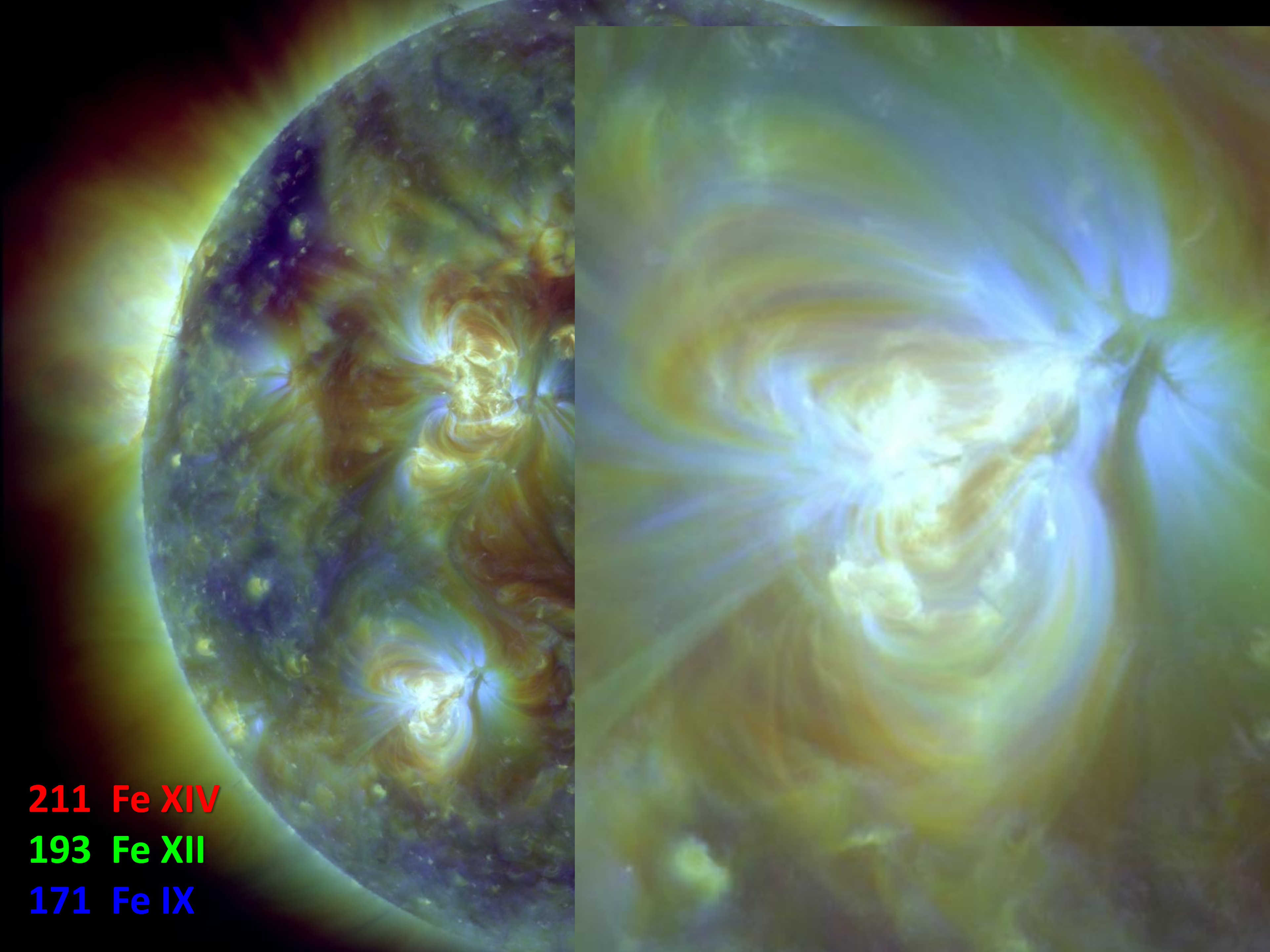
211 Fe XIV
193 Fe XII
171 Fe IX

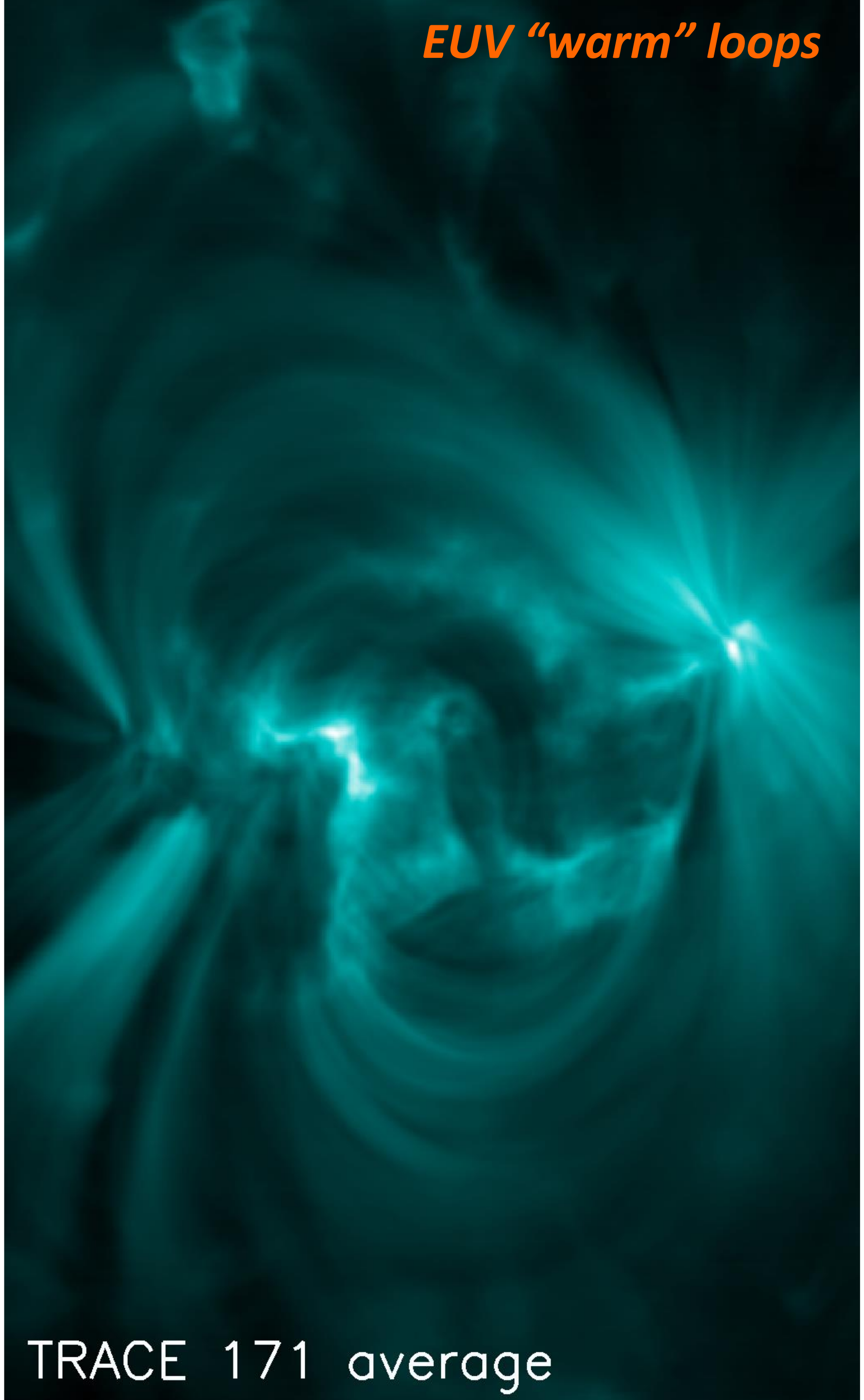
EUV “warm” loops
TRACE 171 average

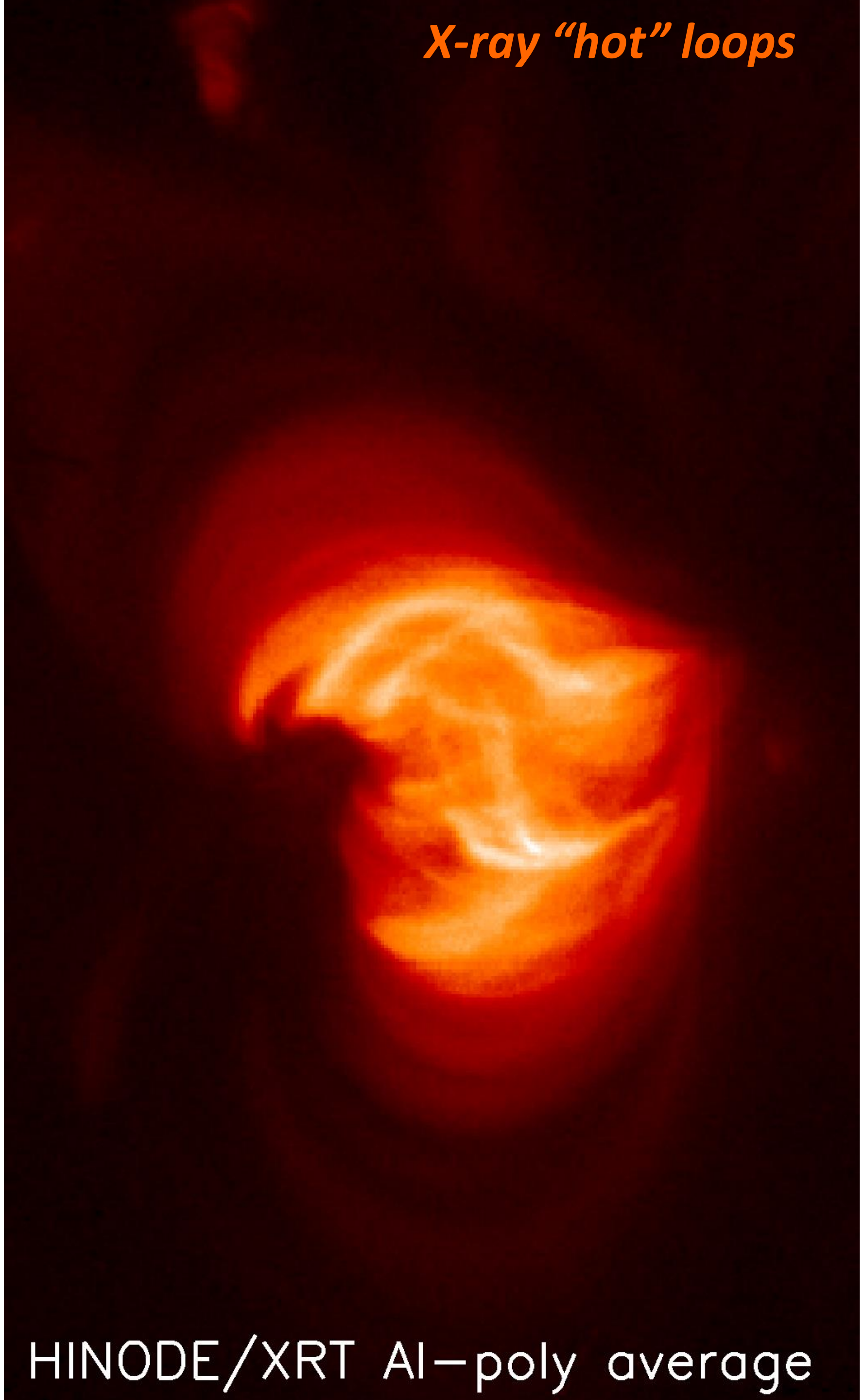
X-ray “hot” loops
HINODE/XRT Al-poly average

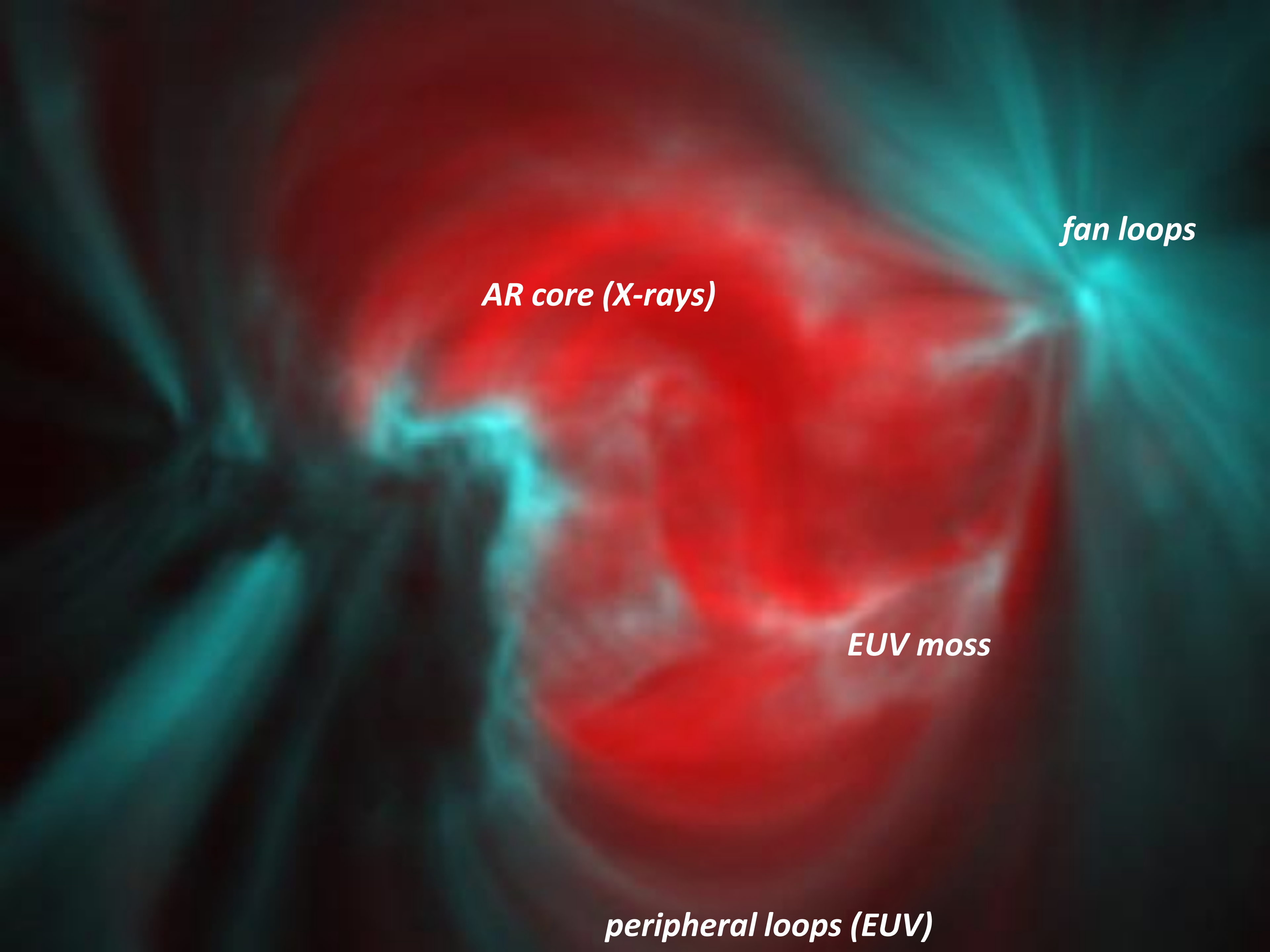
fan loops
AR core (X-rays)
EUV moss
peripheral loops (EUV)

TRACE 171 warm loops

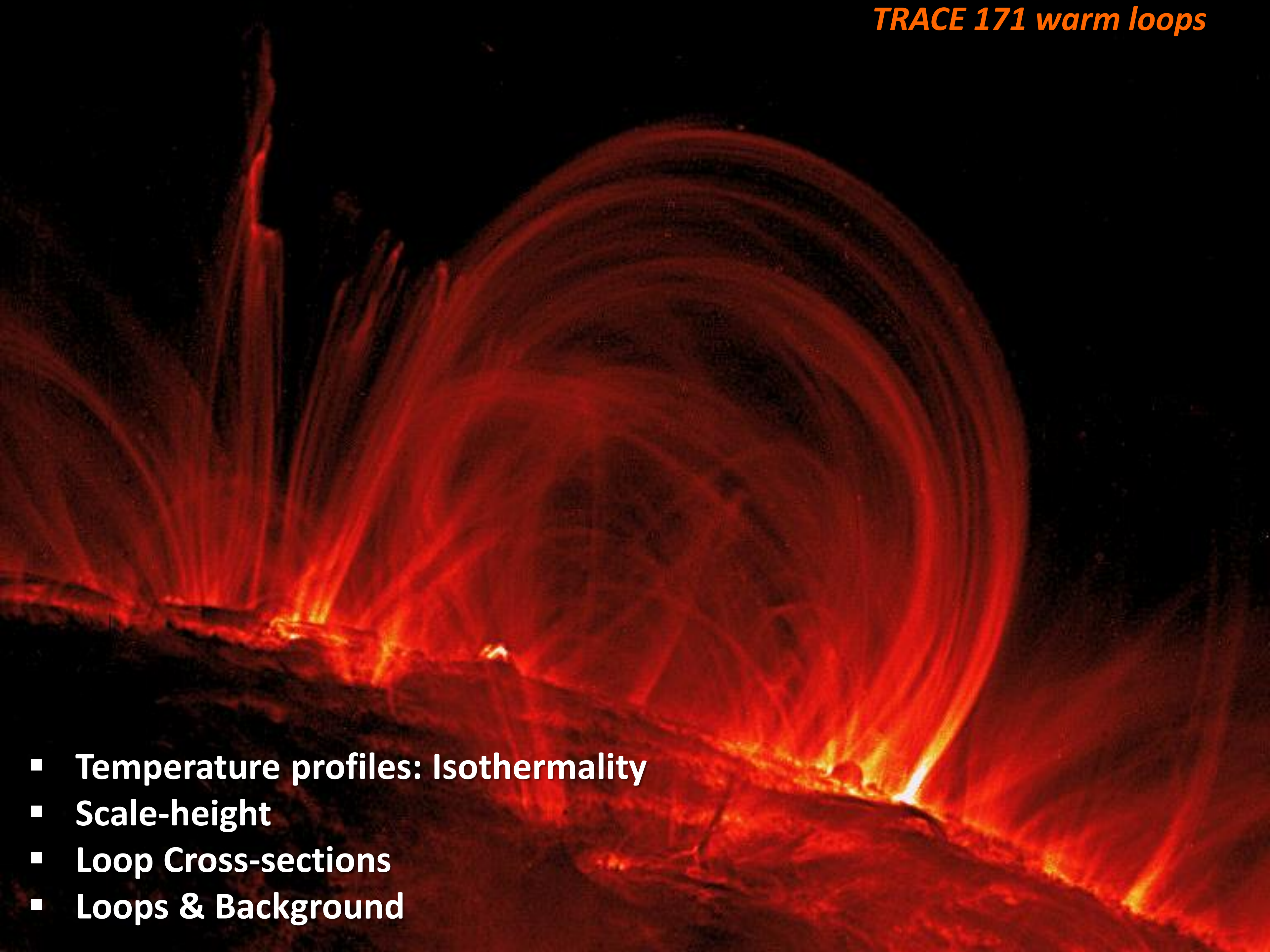

- **Temperature profiles: Isothermality**
- **Scale-height**
- **Loop Cross-sections**
- **Loops & Background**

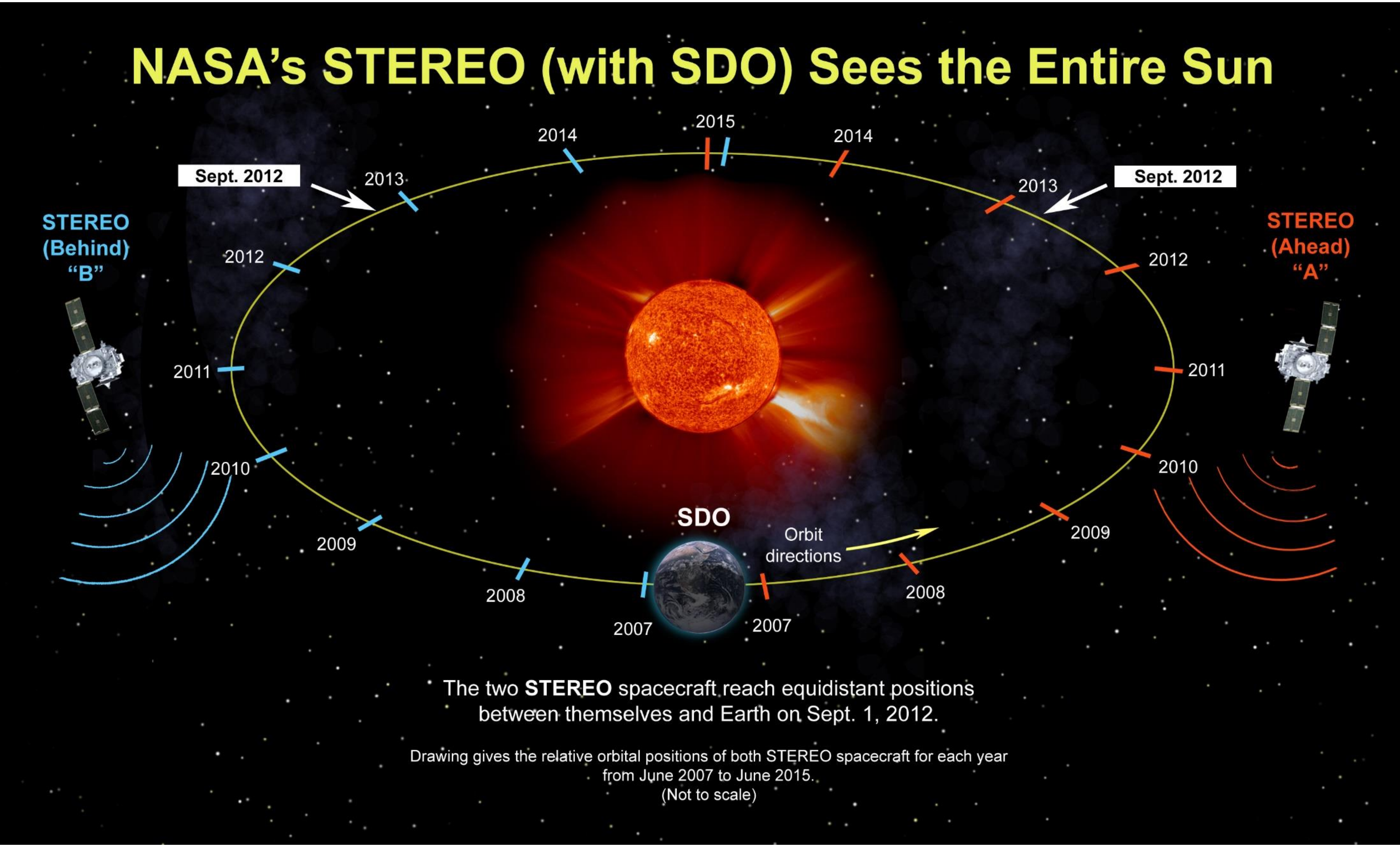
NASA's STEREO (with SDO) Sees the Entire Sun
STEREO (Behind) "B"
STEREO (Ahead) "A"
Sept. 2012
Sept. 2012
2007
2008
2009
2010
2011
2012
2013
2014
2015
2014
2013
2012
2011
2010
2009
2008
2007
SDO
Orbit directions
The two STEREO spacecraft reach equidistant positions between themselves and Earth on Sept. 1, 2012.
Drawing gives the relative orbital positions of both STEREO spacecraft for each year from June 2007 to June 2015.
(Not to scale)

Geometry of Coronal Loops

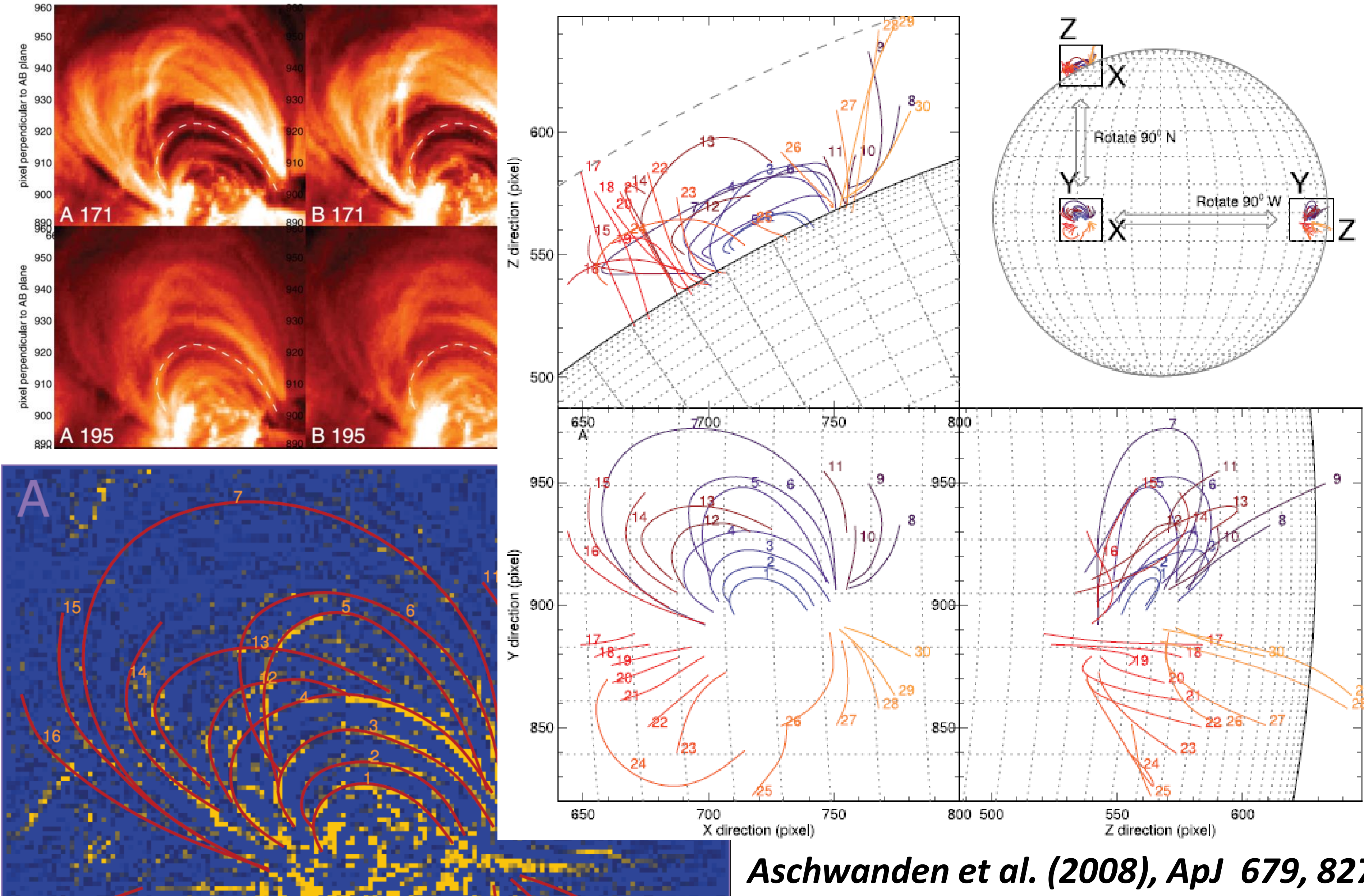

Aschwanden et al. (2008), ApJ 679, 827

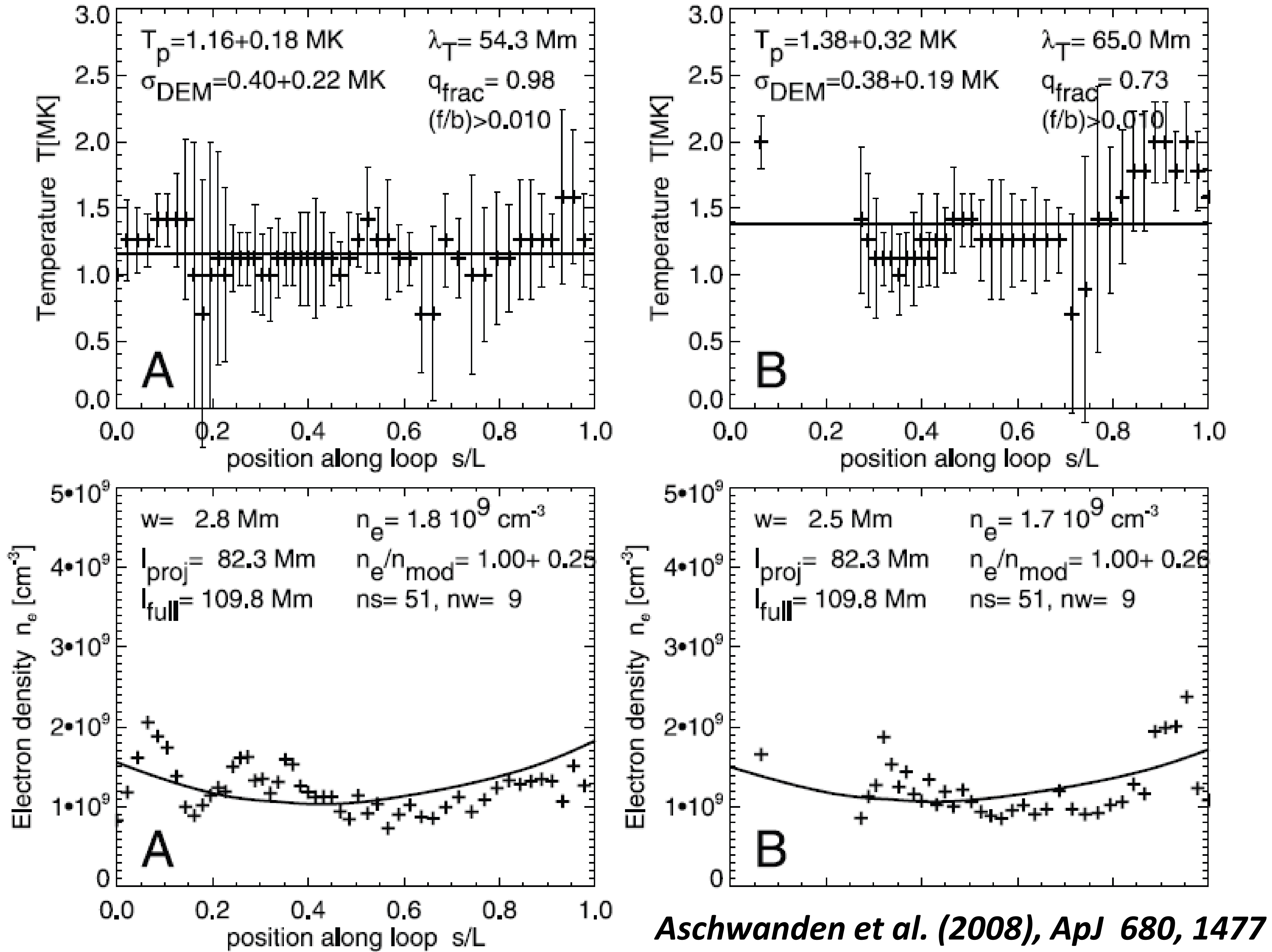

Aschwanden et al. (2008), ApJ 680, 1477

Loops can be Hydrostatic

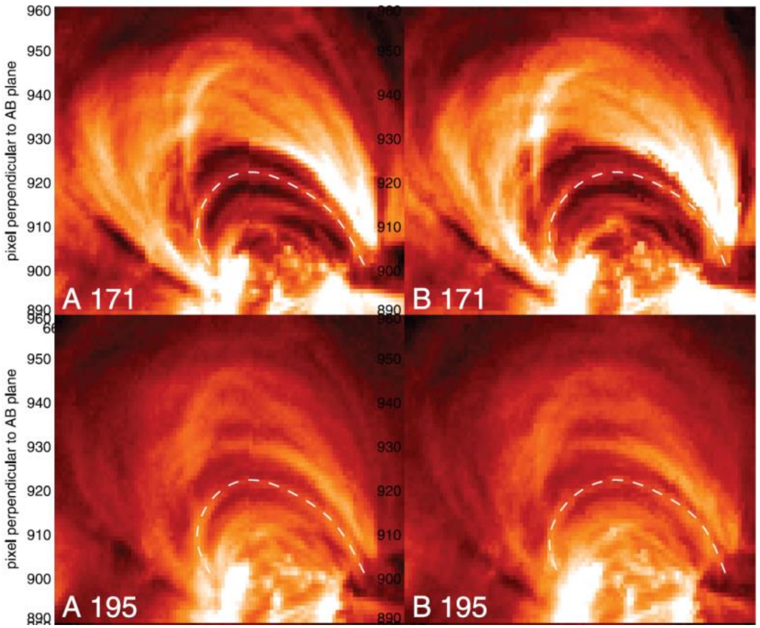

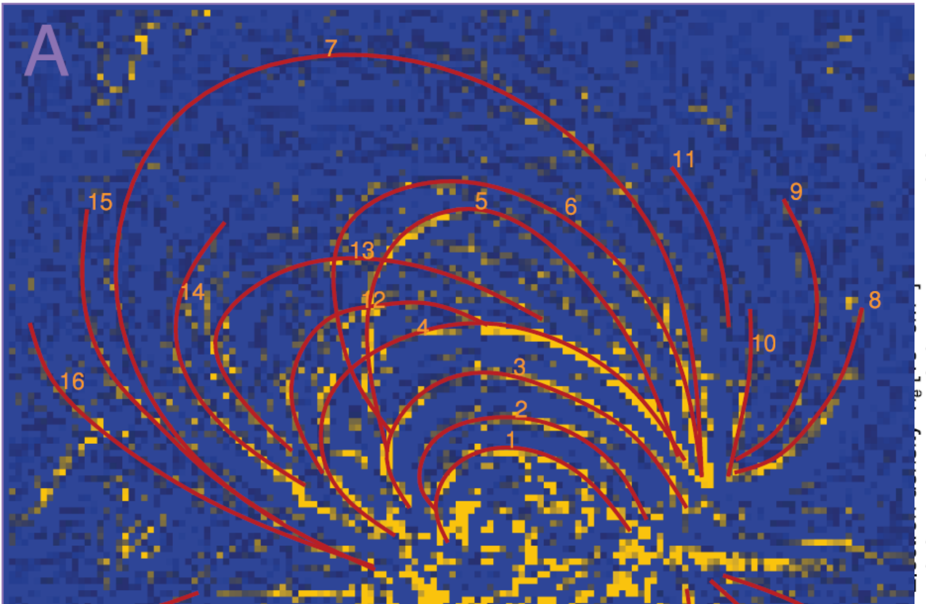

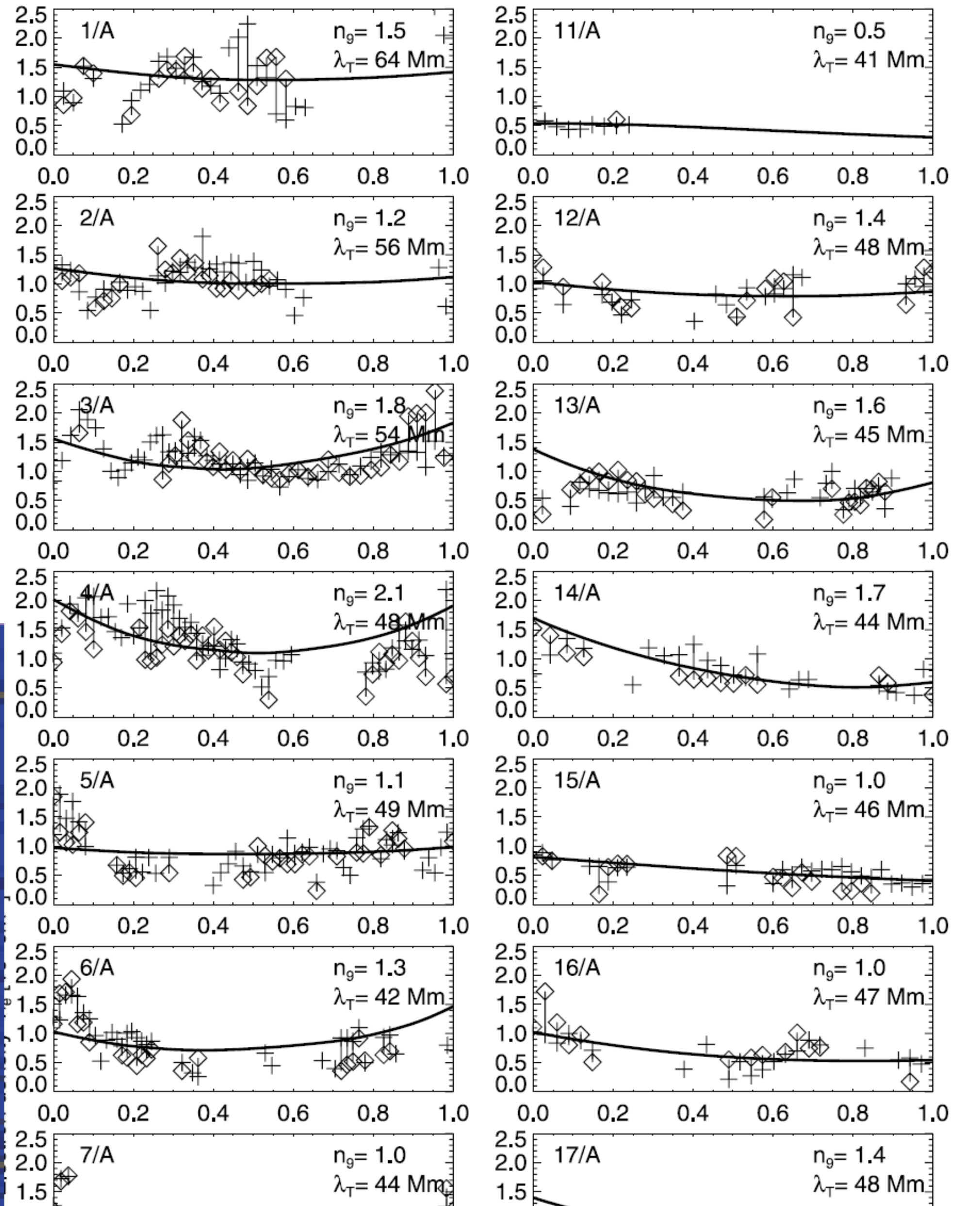

Coronal Background

- **Background** can be ~ **80%** of the actual observed signal:

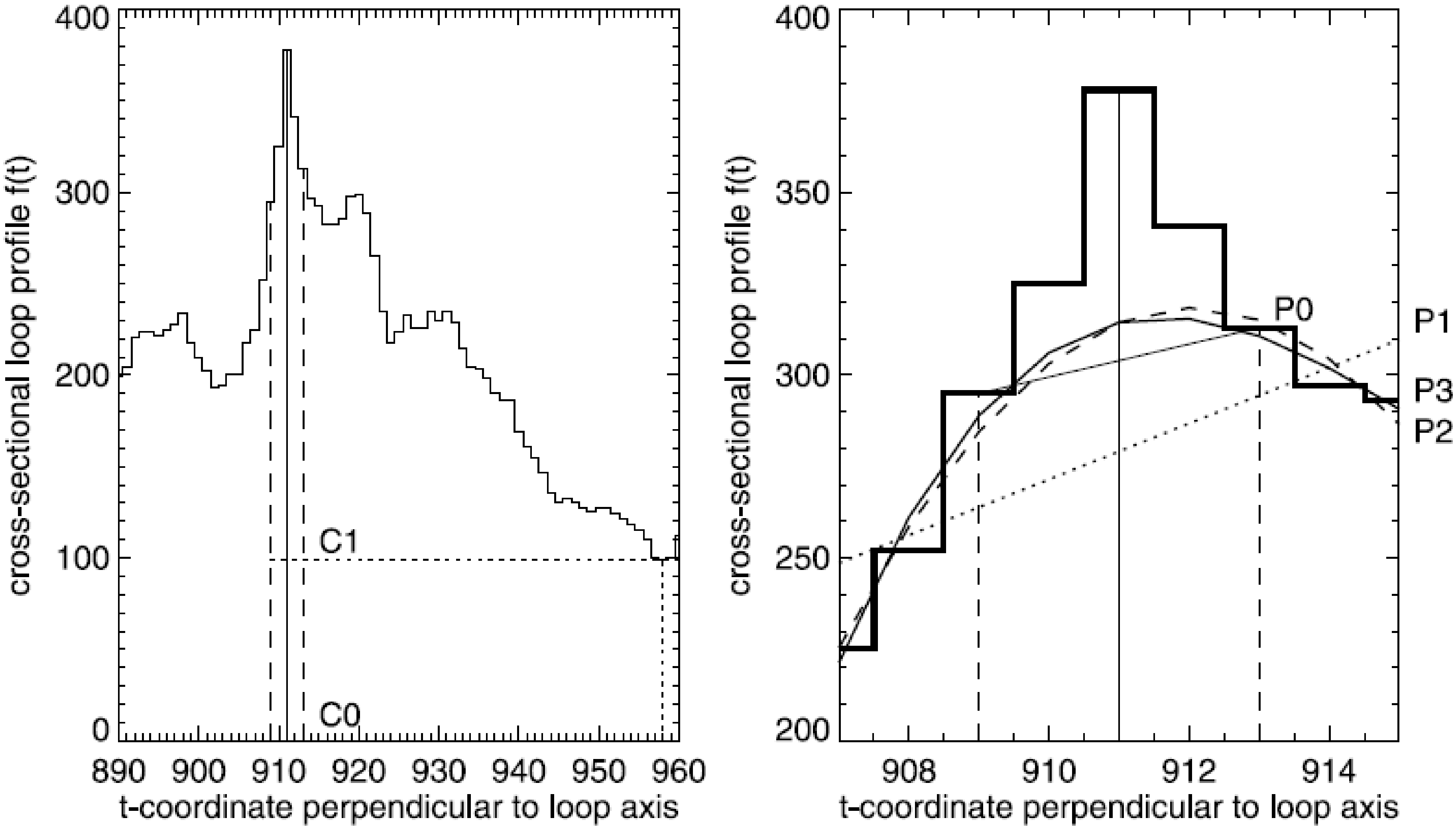

Aschwanden et al. (2008), ApJ 680, 1477

Loops or Strands…

Aschwanden et al. (2000), ApJ 541, 1059

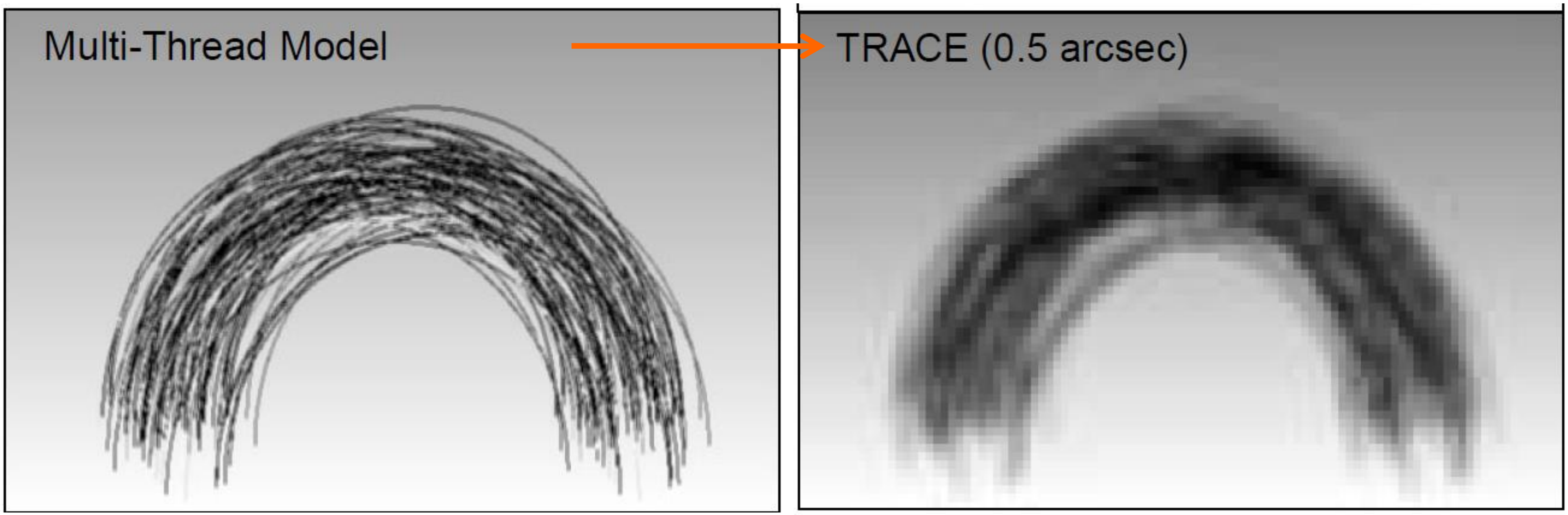

- **Loop**: coherent structure in an observed image of the corona
- **Strand**: Fundamental, independent, elementary structure with an **isothermal cross-field profile**, thickness down to gyro-radius < 1 m

- ***Reale & Peres (2000), ApJ 521, L45: Multithermal, multi-strand loop, with different temperature structure for each strand, can produce false "isothermal" loop if unresolved***

Isothermal or Multithermal?

Schmelz et al. (2009): ApJ 691, 503: "Are Coronal Loops Isothermal or Multithermal?"

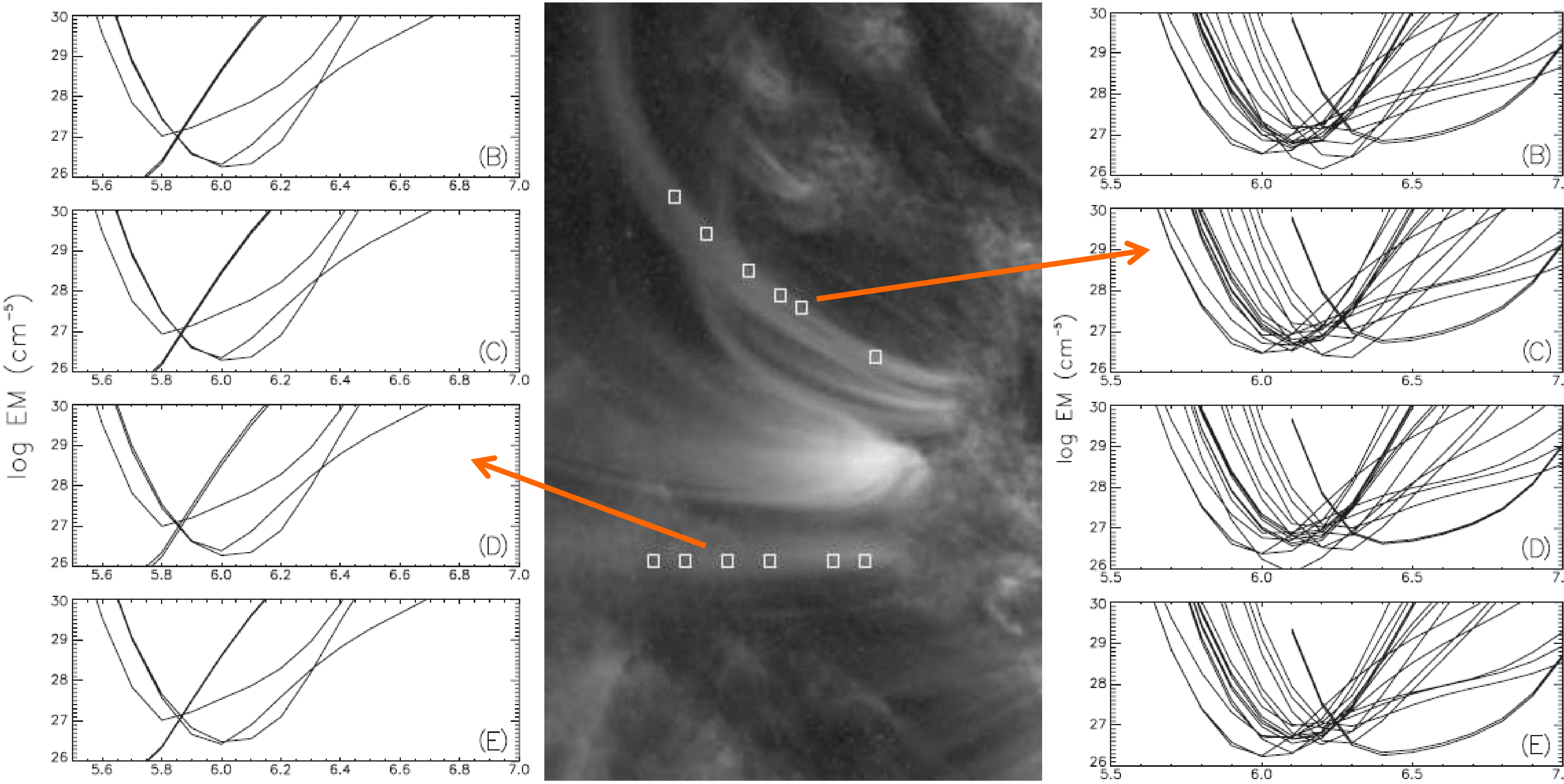

Conclusion: ***Yes***

Loop Dynamics

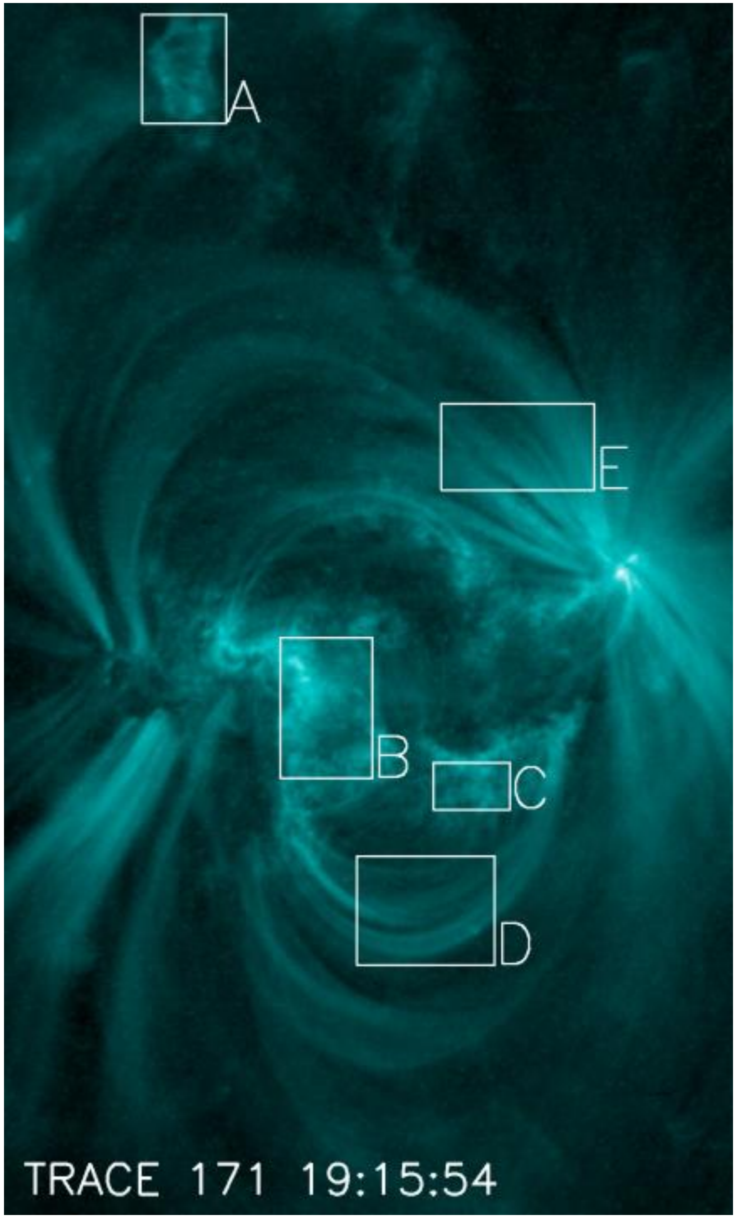

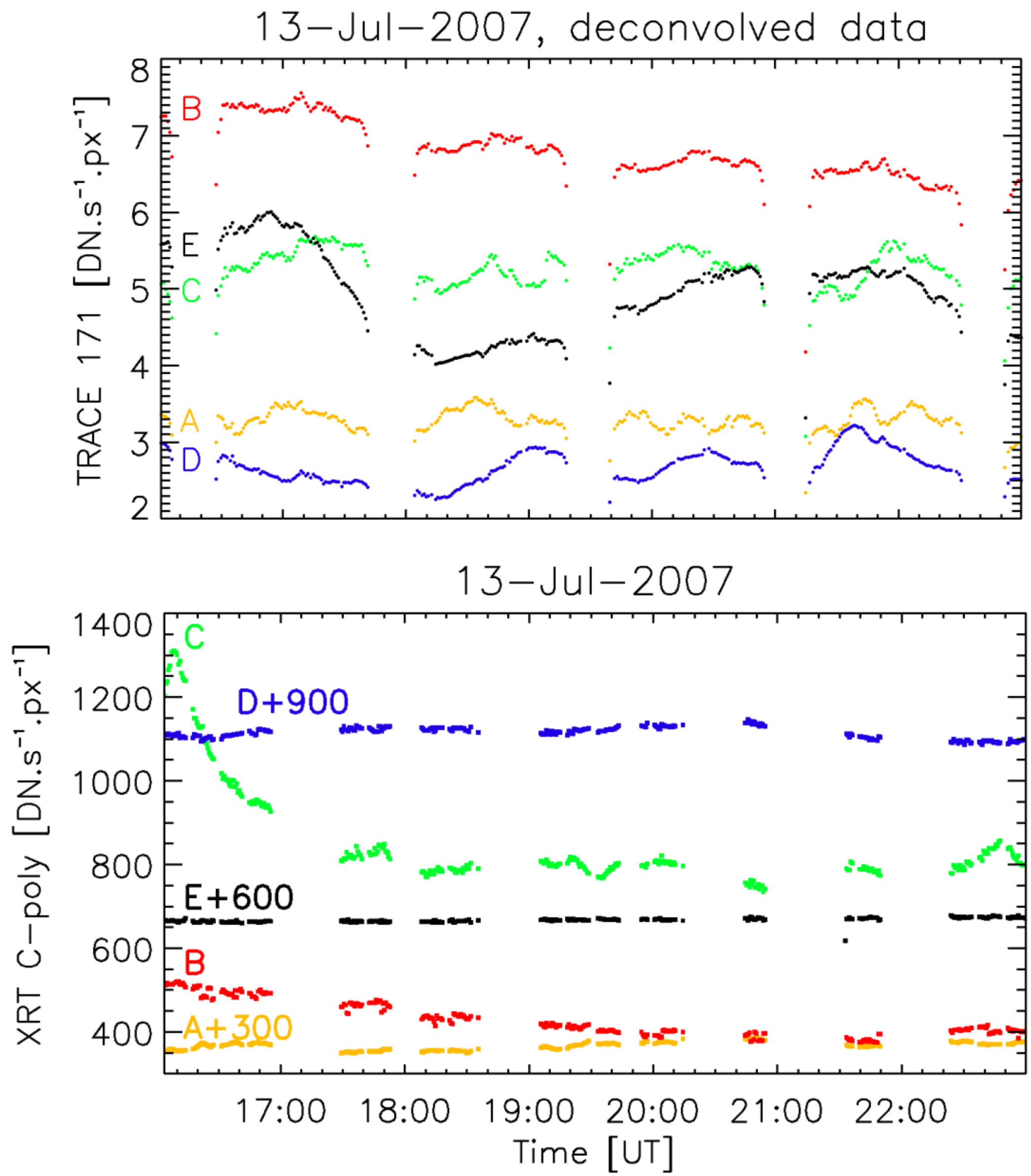

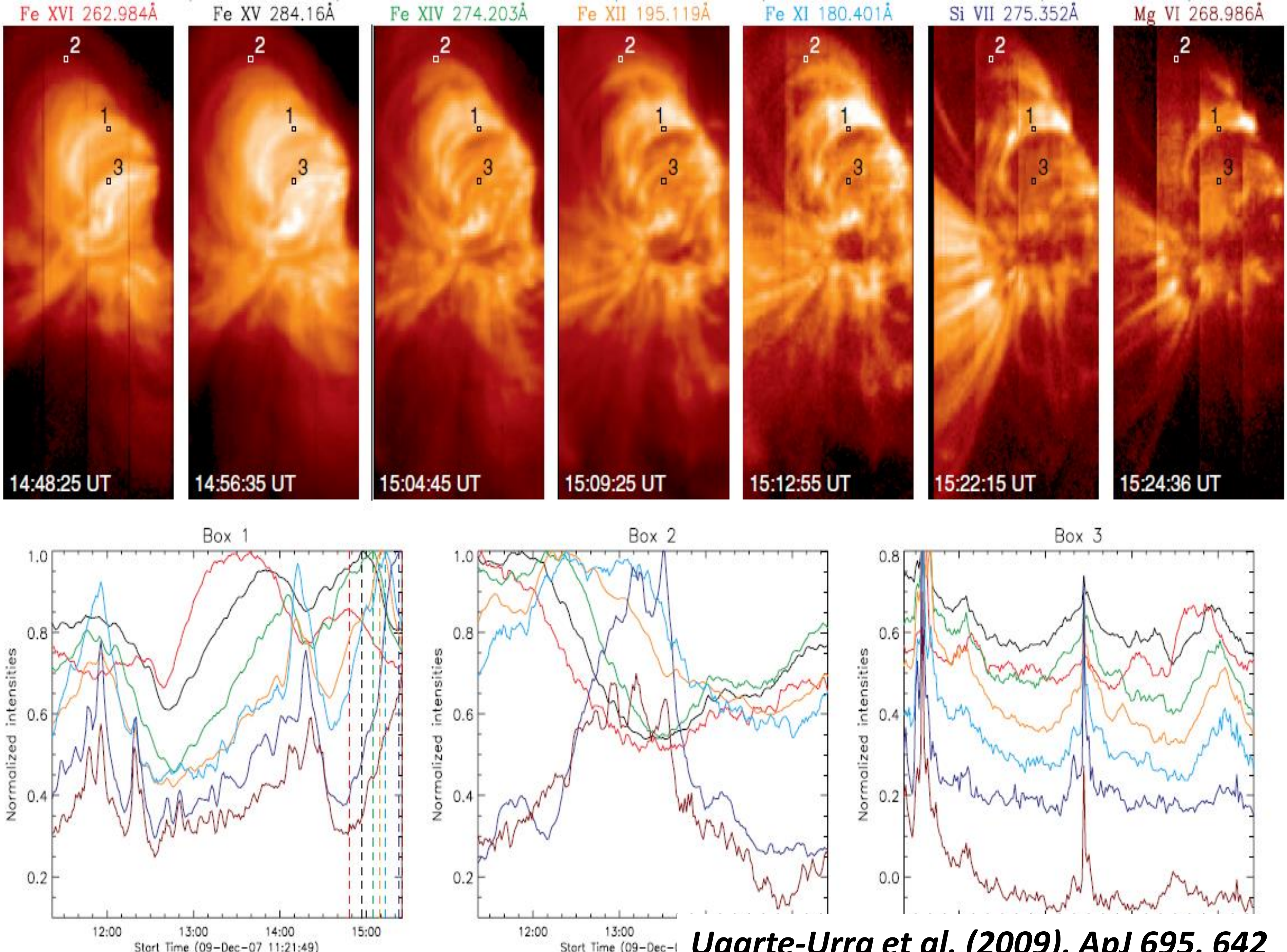

Ugarte-Urra et al. (2009), ApJ 695, 642

Nanoflare Storms

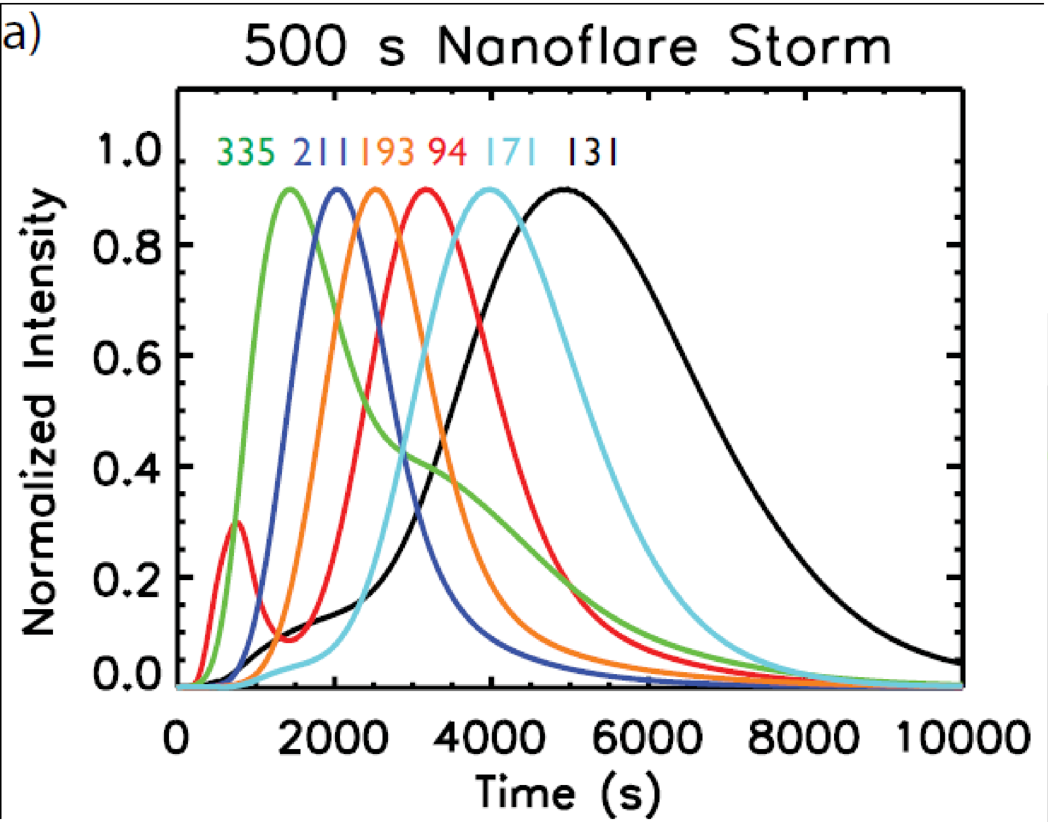

Theoretical light curves ^

- Multi-strand loop
- One strand heated at a time, then next one is heated
- Short heating followed by cooling

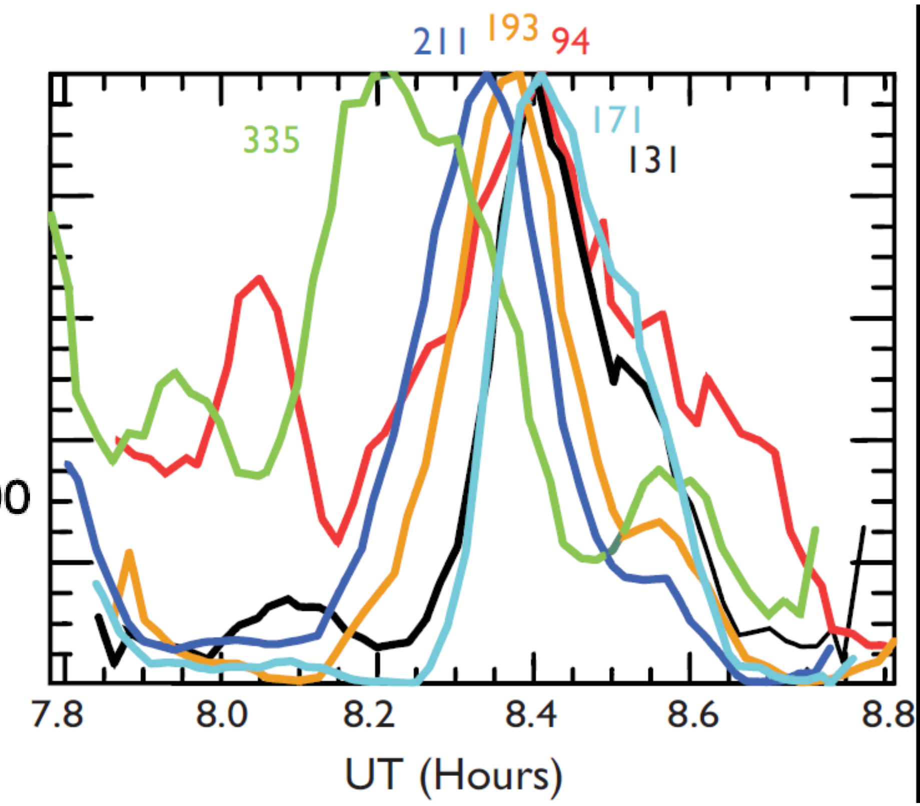

Observed light curves >
for an AR core loop

Viall & Klimchuk (2011), ApJ 738, 24

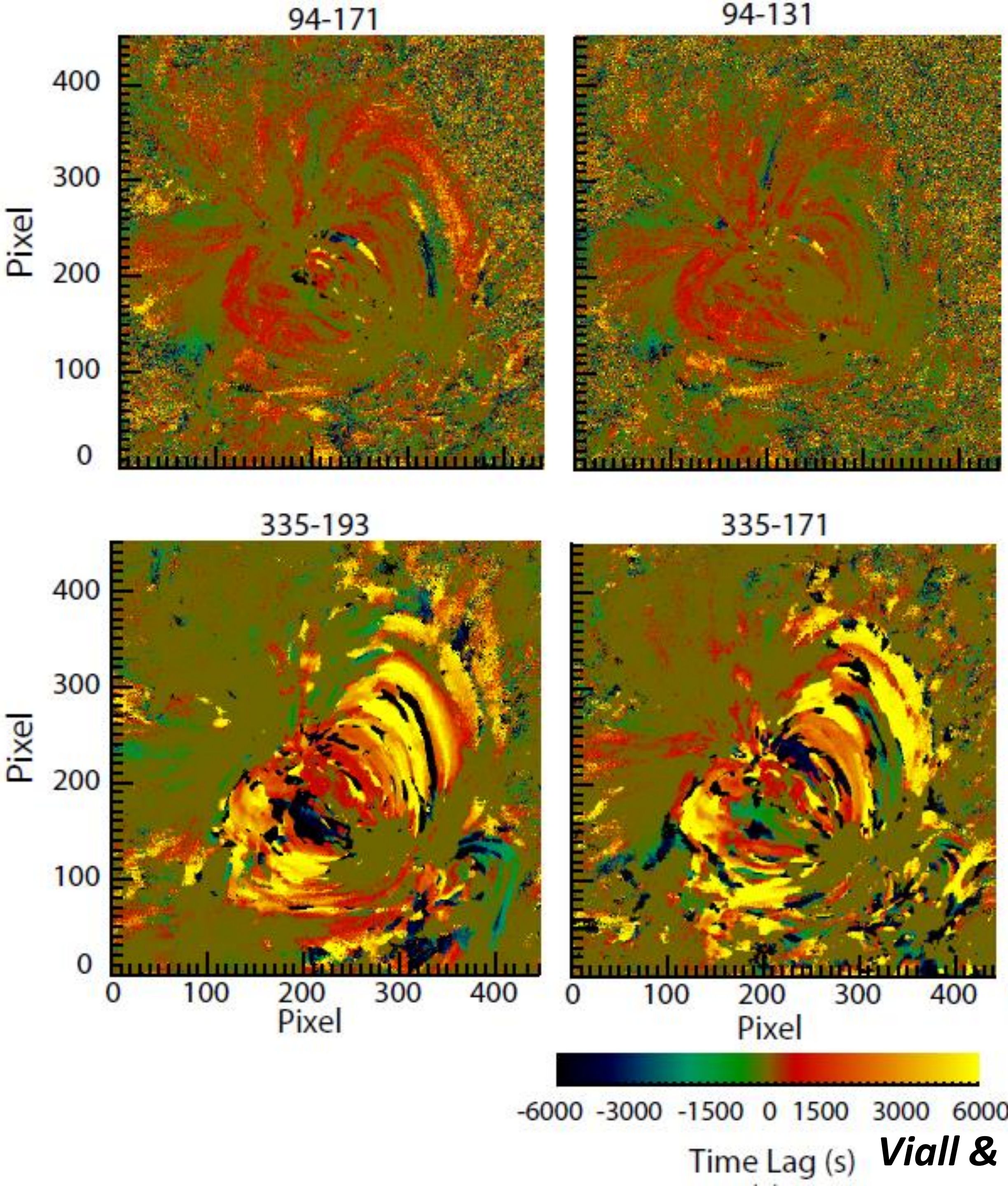

Viall & Klimchuk (2012), ApJ 753, 35

Coronal Heating Problem

- The Corona is heated to temperatures of several MK. But how?

- Small-scale reconnection – Parker's nanoflares
- Wave heating – transfer of energy
  from waves
  to particles

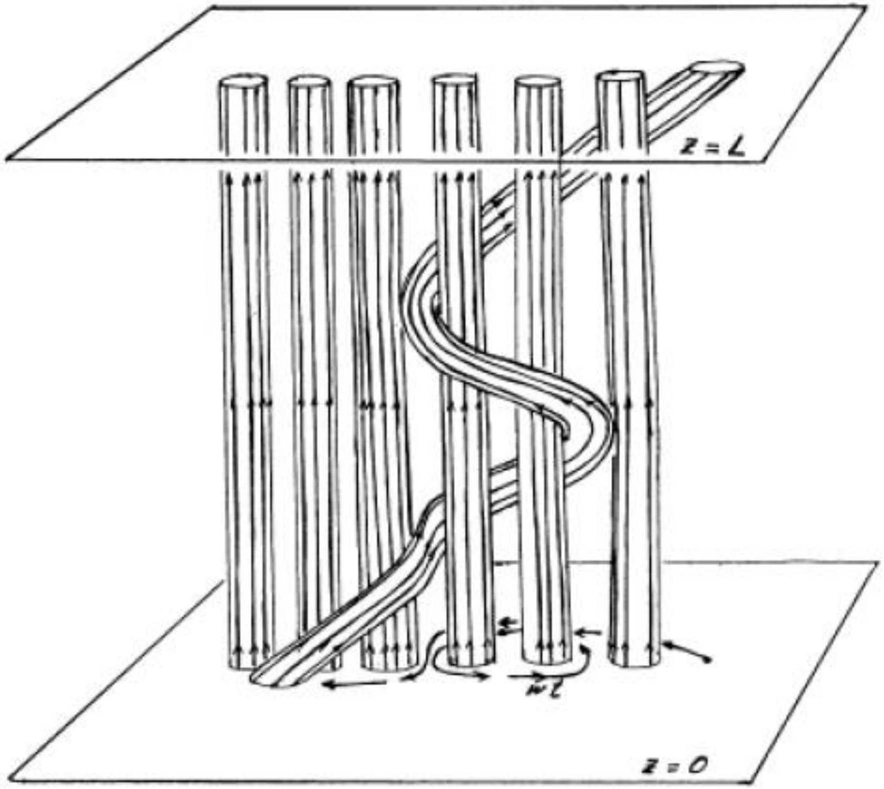

- Note on terminology:
  The current "nanoflare" models simply refer to any impulsive energy release
  (papers by the Klimchuk group),

  i.e., not only reconnection,
  but also (any) bursty wave heating

Heat Flux Required

- Exponentially decreasing heating has heating flux of

$$F_{\mathrm{H}} = E_{\mathrm{H0}} s_{\mathrm{H}}$$

$$\approx 5 \times 10^3 \left(\frac{n_e}{10^8\ \mathrm{cm}^{-3}} \right)^2 \left(\frac{T}{1\ \mathrm{MK}} \right) \quad [\mathrm{ergs\ cm^{-2} s^{-1}}]$$

$$\uparrow$$

$$E_{\mathrm{H0}} \approx E_{rad} = n_e^2 Q(T)$$

- Simplest assumption: radiation losses balanced by heating flux
- Coronal hole: $T \approx$ 1 MK, $n_e \approx 10^8$ cm^{-3} : $F_{\mathrm{H}} \approx 5 \times 10^3$ ergs cm^{-2} s^{-1}
- Active region: $T \approx 2.5$ MK, $n_e \approx 2 \times 10^9$ cm^{-3} : $F_{\mathrm{H}} \approx 5 \times 10^6$ ergs cm^{-2} s^{-1}

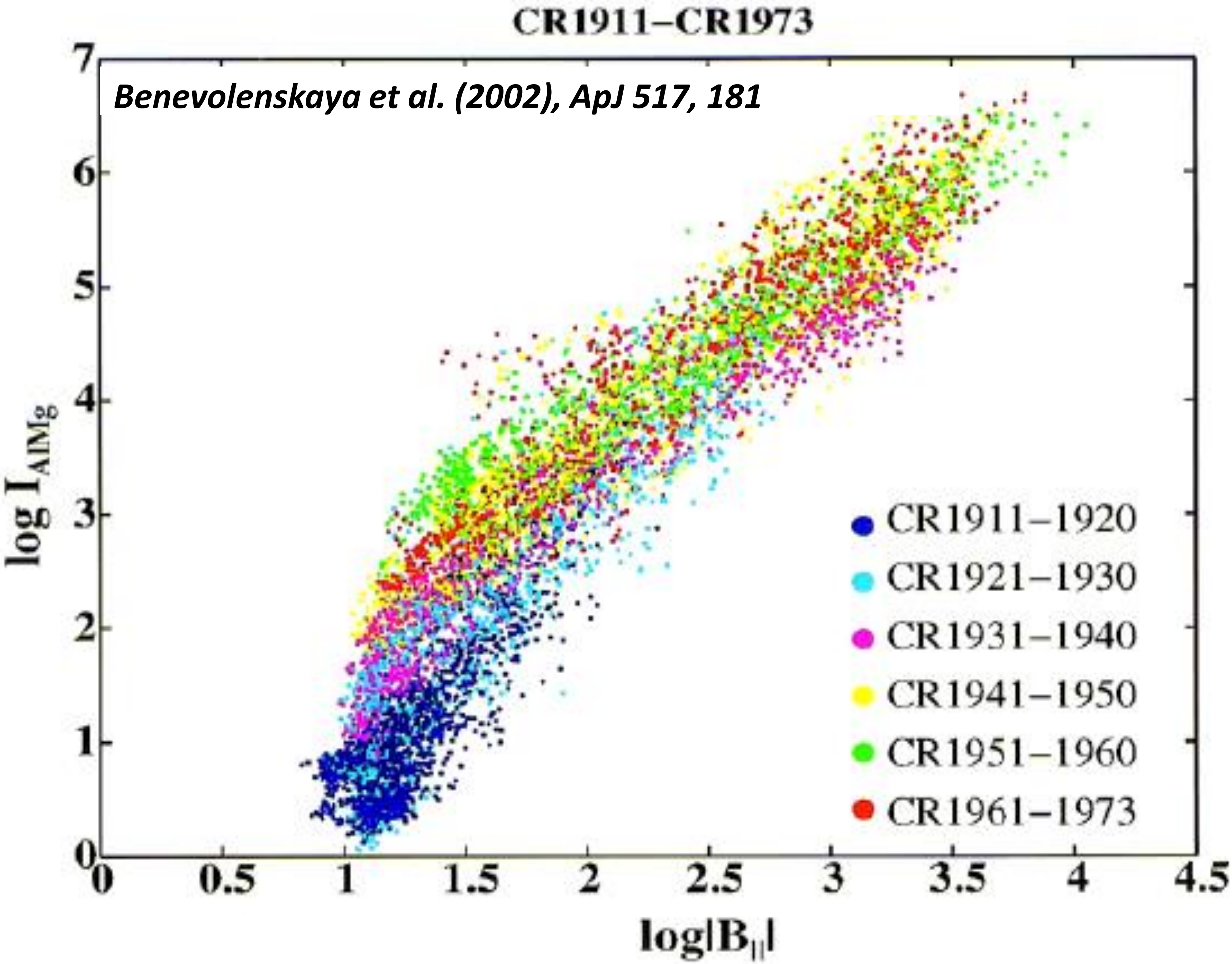
CR1911–CR1973
Benevolenskaya et al. (2002), ApJ 517, 181
log I_AIMg
log|B_||
0
0.5
1
1.5
2
2.5
3
3.5
4
4.5
0
1
2
3
4
5
6
7
CR1911–1920
CR1921–1930
CR1931–1940
CR1941–1950
CR1951–1960
CR1961–1973

Statement of the Problem: MHD

$$\rho\left(\frac{\partial\vec{v}}{\partial t}+\left(\vec{v}.\vec{\nabla}\right)\vec{v}\right)=-\vec{\nabla}p_{\mathrm{G}}+\vec{j}\times\vec{B}+\rho\vec{g},$$

$$\frac{1}{\gamma-1}\left(\frac{\partial T}{\partial t}+\vec{v}.\vec{\nabla}T\right)=-T\vec{\nabla}.\vec{v}+\frac{1}{qk_{\mathrm{B}}n_{\mathrm{e}}}\left(E_{\mathrm{H}}-n_{\mathrm{e}}^{2}Q(T)+\vec{\nabla}.\vec{F}_{\mathrm{C}}\right),$$

$$\frac{\partial\vec{B}}{\partial t}=\vec{\nabla}\times\left(\vec{v}\times\vec{B}\right),$$

$$\frac{\partial\rho}{\partial t}+\vec{\nabla}.\left(\rho\vec{v}\right)=0, \qquad \vec{j}=\frac{1}{\mu}\vec{\nabla}\times\vec{B},$$

$$\vec{\nabla}.\vec{B}=0, \qquad p=qn_{\mathrm{e}}k_{\mathrm{B}}T=\frac{\rho k_{\mathrm{B}}T}{\bar{\mu}m_{\mathrm{H}}},$$

$$F_{\mathrm{C},\parallel}=\kappa_{0}T^{5/2}\frac{dT}{ds}, \qquad F_{\mathrm{C},\perp}=0.$$

Scaling Laws: Simple Solutions

Assumptions:

- No time derivatives
- No flows
- Geometrically symmetric loop with symmetric heating
- Vanishing thermal conductivity at loop apex and footpoints

Rosner, Tucker, Vaiana (1978)
Serio et al. (1981)
Aschwanden & Schrijver (2002)
Dudík et al. (2009)
Martens (2010)

$$p_0\left(L_0, s_{\mathrm{H}}, T_1\right) = L_0^{-1} T_1^3 S_1^{-3},$$

$$E_{\mathrm{H0}}\left(L_0, s_{\mathrm{H}}, T_1\right) = L_0^{-2} T_1^{7/2} S_2,$$

$$S_1^{\mathrm{RTV}} = 1{,}4 \times 10^2 \quad [\mathrm{K\ s^{2/3} kg^{-1/3}}],$$

$$S_2^{\mathrm{RTV}} = 9{,}5 \times 10^{-6} \quad [\mathrm{kg\ m\ s^{-3} K^{-7/2}}].$$

$$S_1^{\mathrm{Serio}} = 1.4 \times 10^2\ \mathrm{e}^{-\left(0{,}08 L_0/s_{\mathrm{H}} + 0{,}04 L_0/s_p\right)},$$

$$S_2^{\mathrm{Serio}} = 9{,}5 \times 10^{-6}\ \mathrm{e}^{\left(0{,}78 L_0/s_{\mathrm{H}} - 0{,}36 L_0/s_p\right)}.$$

Comparison to Observations

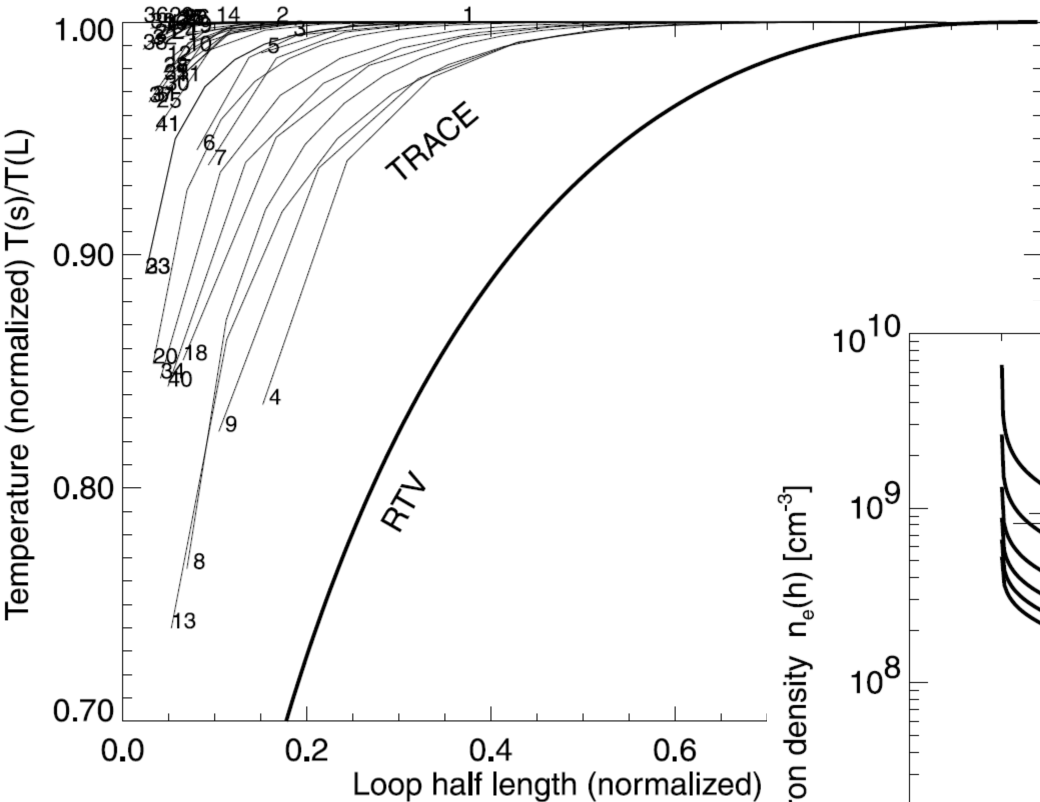

Aschwanden et al. (2000), ApJ 541, 1059

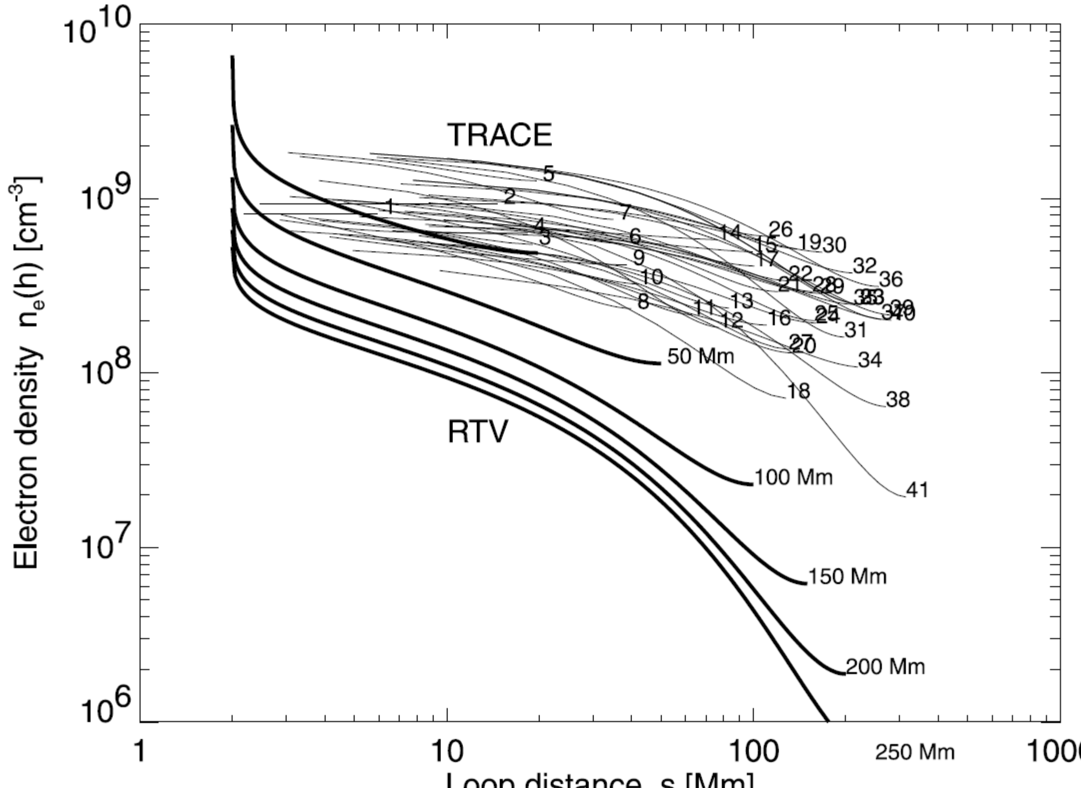

Proposed Heating Models

Lundquist et al. 2008, ApJ 689, 1388

TABLE 1
HEATING SCALE RELATIONSHIPS

Description	Number	Reference	MDK Scaling	B Case a	B Case b	B Case c	L
Stochastic buildup	1	1	$B^2L^{-2}V^2\tau$	B^2	B^1	B^2	L^{-2}
Critical angle	2	2	$B^2L^{-1}V^1\tan\theta$	B^2	$B^{1.5}$	B^2	L^{-1}
Critical twist	3	3	$B^2L^{-2}V^1R^1\phi$	B^2	B^1	...	L^{-2}
Reconnection $\propto v_A$	4	4	$B^1L^{-2}\rho^{0.5}V^2R^1$	B^1	...	$B^{0.5}$	$L^{-2.45}$
Reconnection $\propto v_{A\perp}$	5	5	$B^{1.5}L^{-1.5}\rho^{0.25}V^{1.5}R^{1.5}$	$B^{1.5}$	...	$B^{0.75}$	$L^{-1.725}$
Current layers (DC)	6	6	$B^2L^{-2}V^2\tau\log R_m$	B^2	...	...	L^{-2}
	7	7	$B^2L^{-2}V^2S^{0.1}\tau$	B^2	...	...	L^{-2}
	8	8	$B^2L^{-2}V^2\tau$	B^2	...	...	L^{-2}
Current sheets	9	9	$B^2L^{-1}R^{-1}V_{ph}^2\tau$	B^2	...	$B^{2.5}$	L^{-1}
Taylor relaxation	10	10	$B^2L^{-2}V_{ph}^2\tau$	B^2	...	...	L^{-2}
Turbulence (DC) with:							
Constant dissipation coefficients	11	11	$B^{1.5}L^{-1.5}\rho^{0.25}V^{1.5}R^{1.5}$	$B^{1.5}$	...	$B^{0.75}$	$L^{-1.725}$
Closure	12	12	$B^{1.67}L^{-1.33}\rho^{0.17}V^{1.33}R^{0.33}$	$B^{1.67}$	...	$B^{1.505}$	$L^{-1.483}$
Closure + spectrum ($s = 0.7$)	13	13	$B^{1.7}L^{-1.7}\rho^{0.15}V^{1.3}R^{0.7}$	$B^{1.7}$	...	$B^{1.35}$	$L^{-1.835}$
Closure + spectrum ($s = 1.1$)	14	13	$B^{2.1}L^{-2.1}\rho^{-0.05}V^{0.9}R^{1.1}$	$B^{2.1}$	...	$B^{1.55}$	$L^{-2.055}$
Resonance ($m = -1$)	15	14	B^0L^{-2}	B^0	...	...	L^{-2}
Resonance ($m = -2$)	16	14	$B^{-1}L^{-1}\rho^{0.5}$	B^{-1}	...	...	$L^{-1.45}$
Resonant absorption I ($m = -1$)	17	15	B^0L^0	B^0	...	...	L^0
Resonant absorption I ($m = -2$)	18	15	$B^{-1}L^1\rho^{0.5}$	B^{-1}	...	...	$L^{0.55}$
Resonant absorption II ($m = -1$)	19	16	$B^0L^1\rho^1$	B^0	...	...	$L^{0.1}$
Resonant absorption II ($m = -2$)	20	16	$B^{-1}L^2\rho^{1.5}$	B^{-1}	...	...	$L^{0.65}$
Current layers (AC)	21	17	$B^1L^{-1}\rho^{0.5}V^2$	B^1	...	...	$L^{-1.45}$
Turbulence (AC)	22	18	$B^{1.67}L^{-1.33}R^{0.33}$	$B^{1.67}$	...	$B^{1.505}$	$L^{-1.33}$

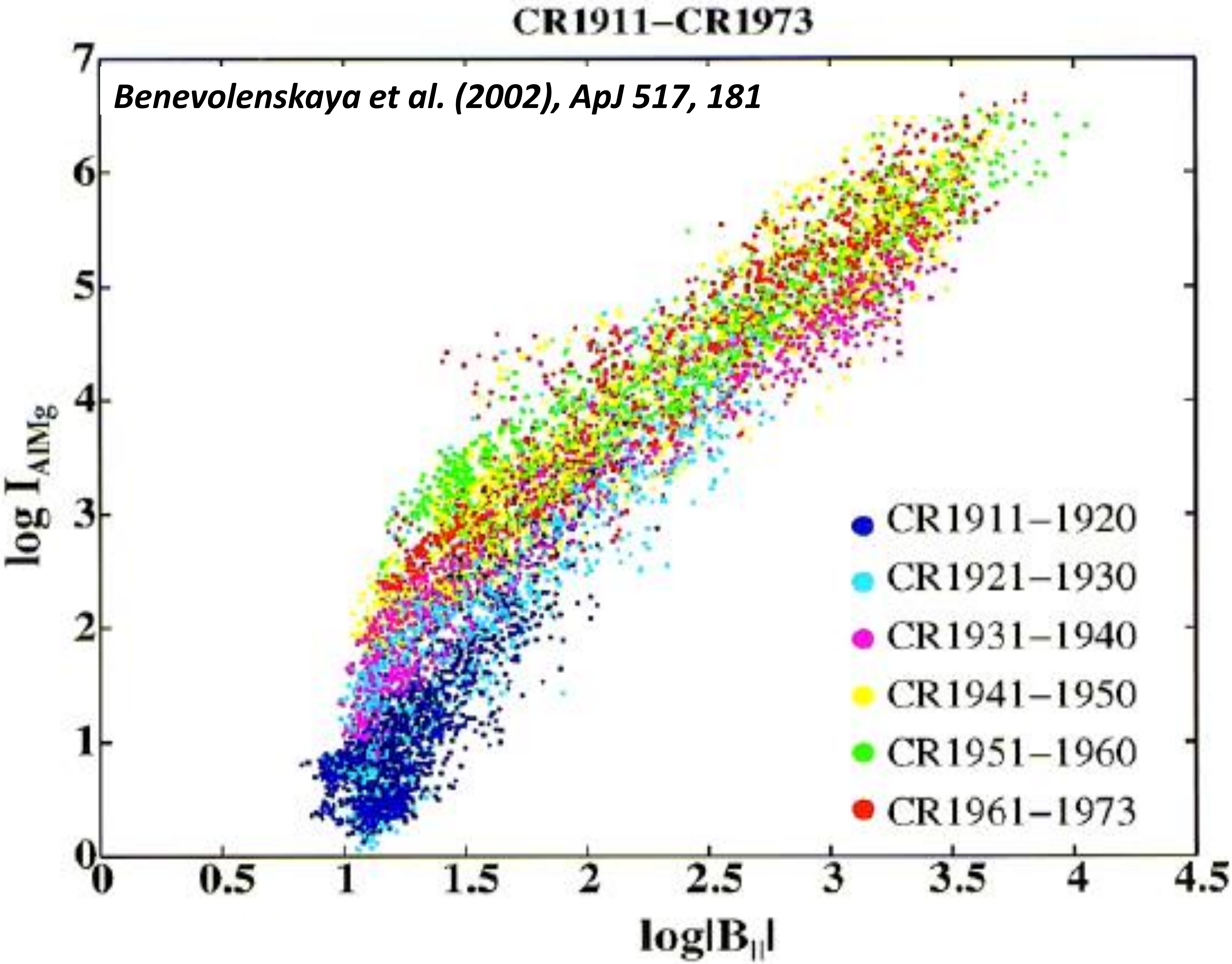
CR1911–CR1973
Benevolenskaya et al. (2002), ApJ 517, 181
log I_AIMg
log|B_||
CR1911–1920
CR1921–1930
CR1931–1940
CR1941–1950
CR1951–1960
CR1961–1973

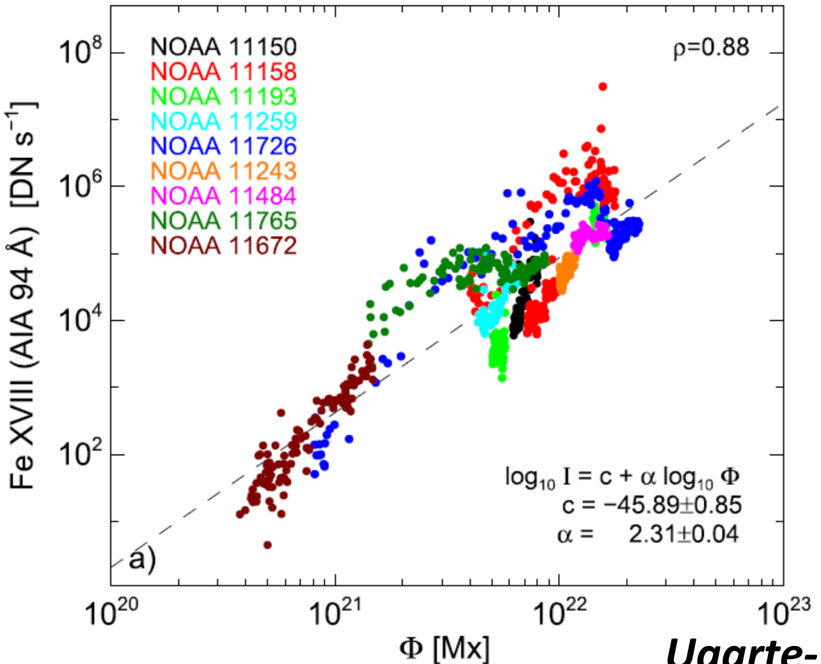

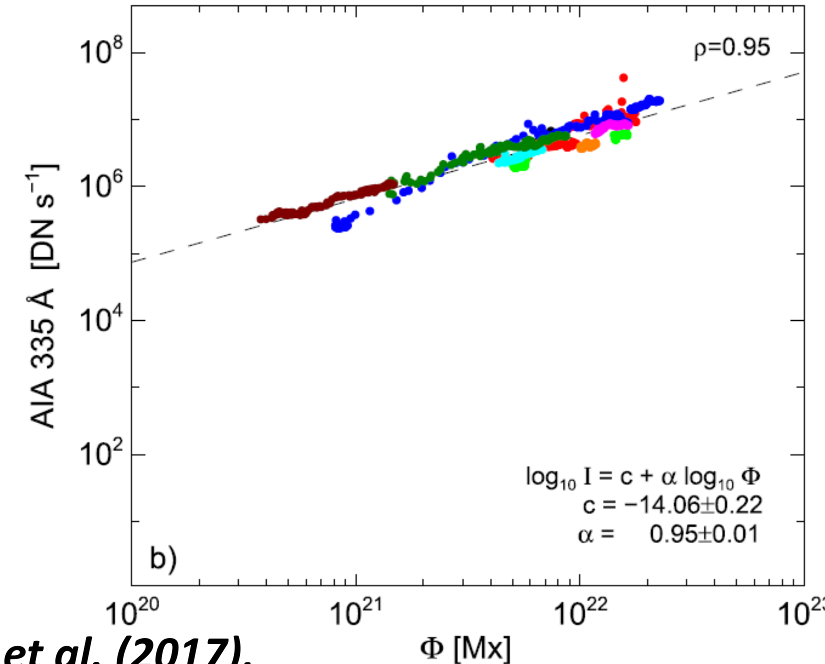

Ugarte-Urra et al. (2017), ApJ 846, 165

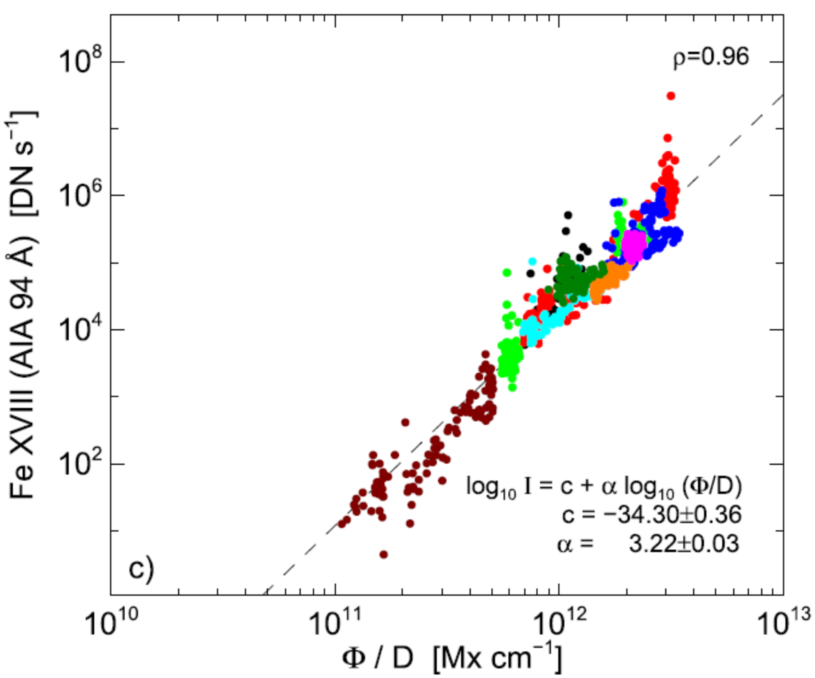

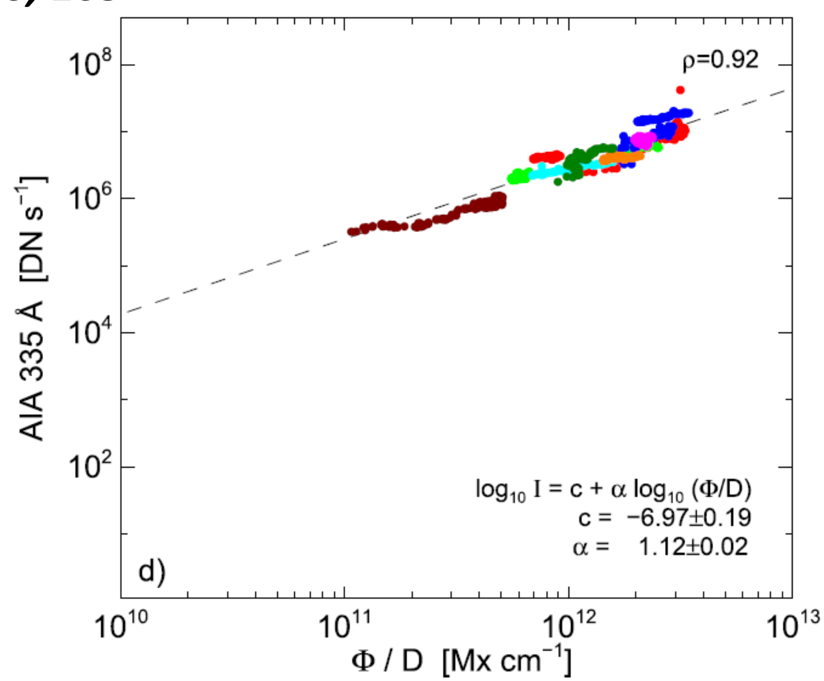

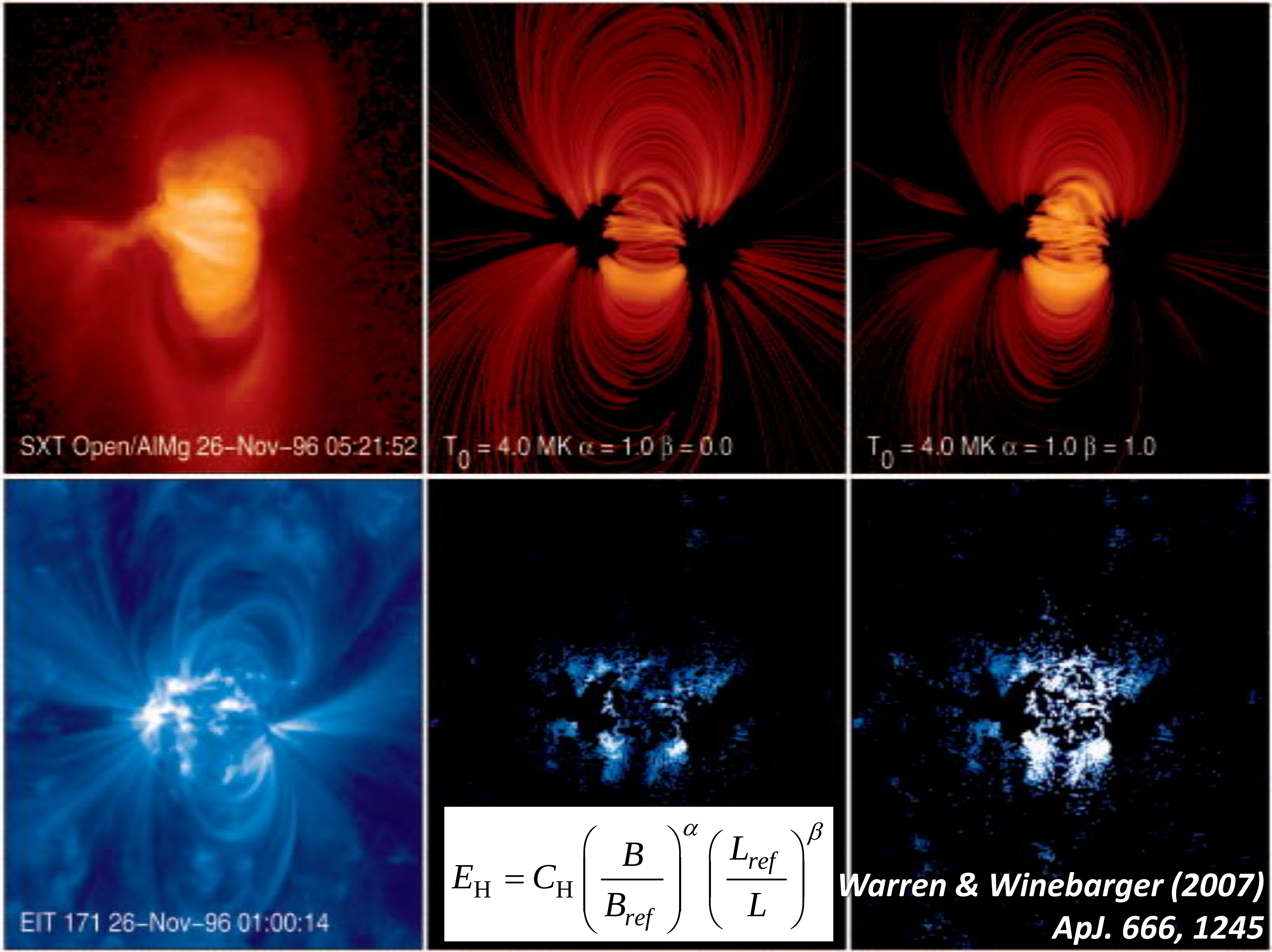

$$E_{\mathrm{H}} = C_{\mathrm{H}} \left(\frac{B}{B_{ref}} \right)^{\alpha} \left(\frac{L_{ref}}{L} \right)^{\beta}$$

Warren & Winebarger (2007)

ApJ. 666, 1245

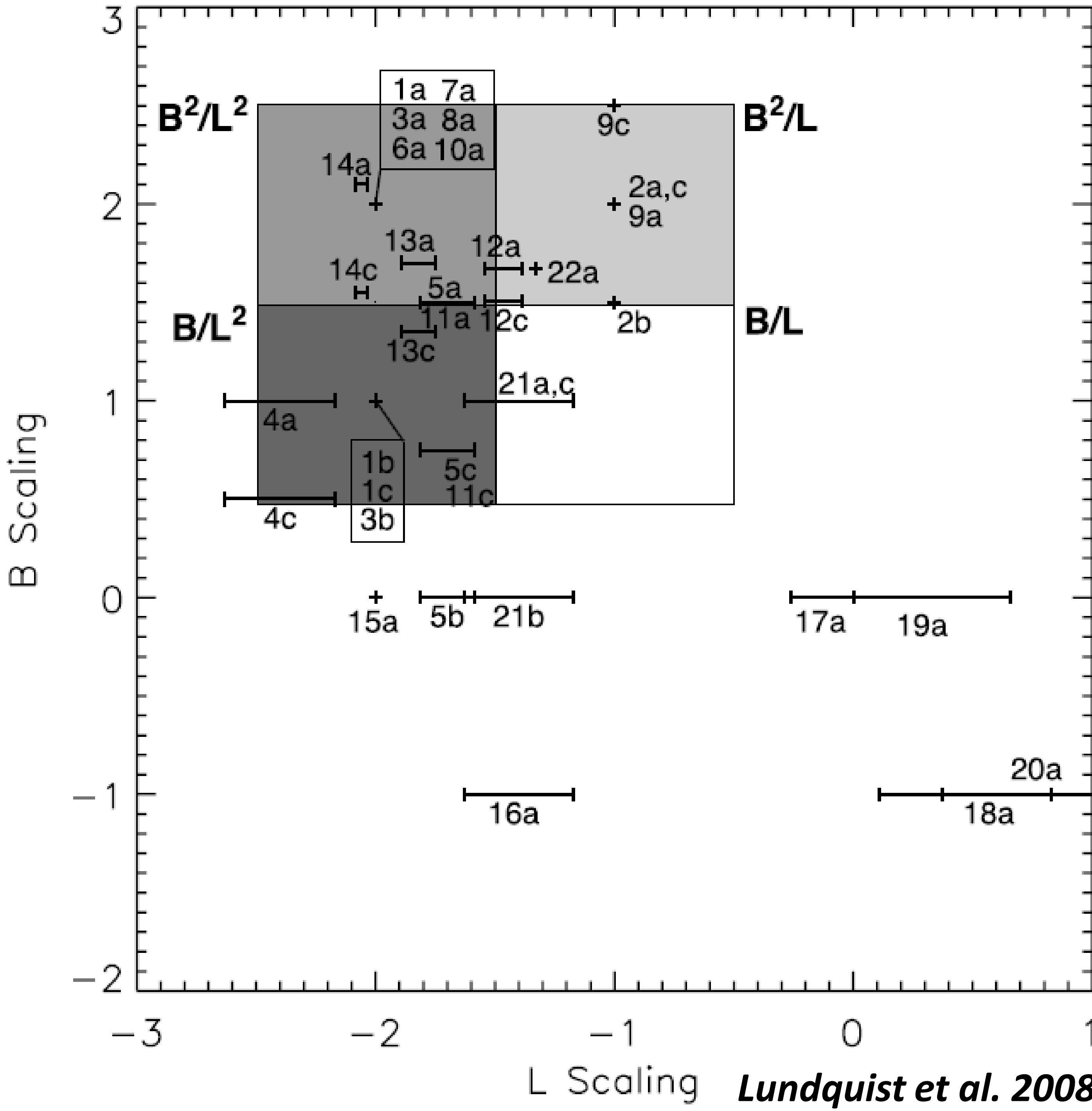

Lundquist et al. 2008, ApJ 689, 1388

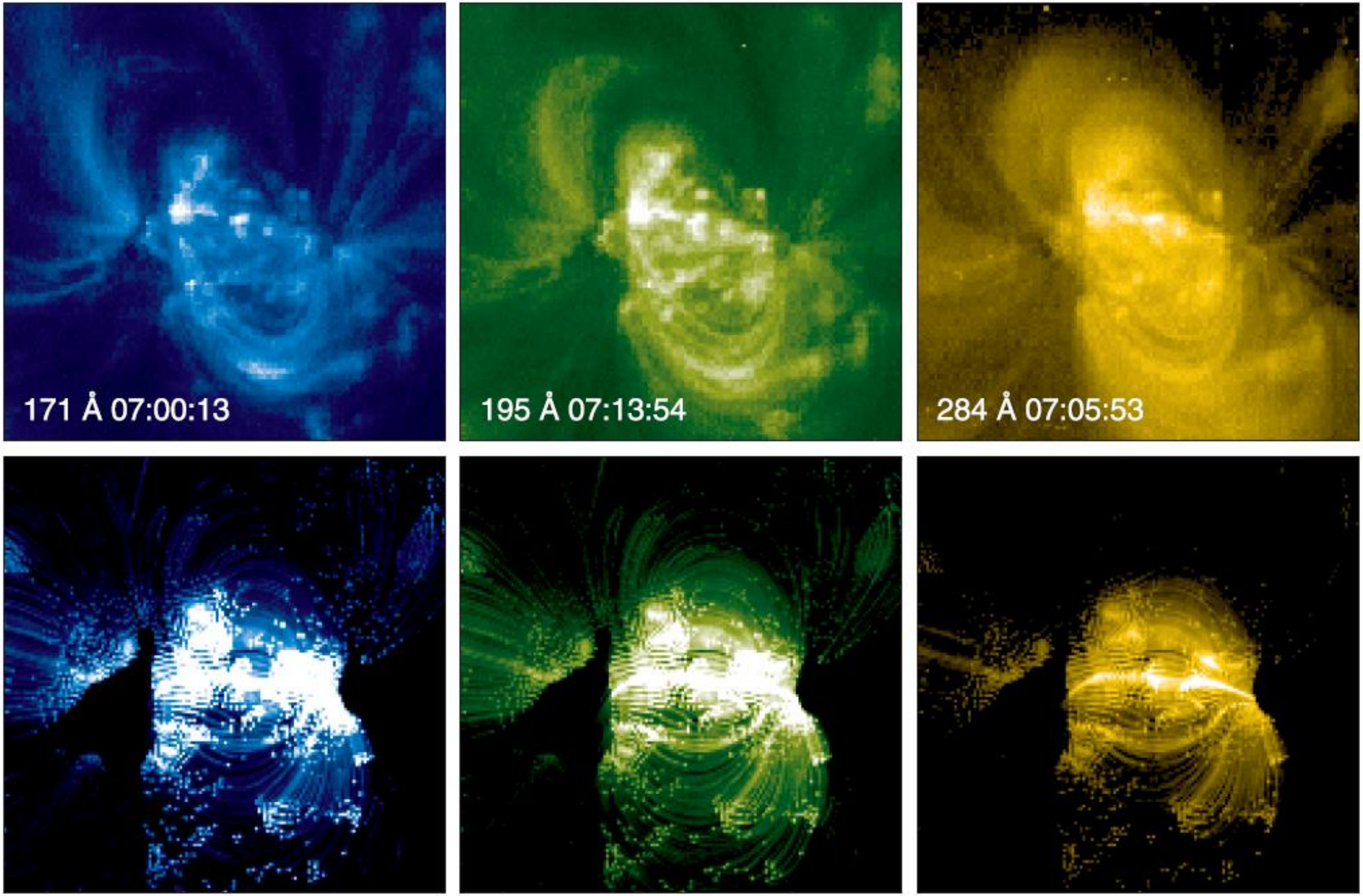

Warren & Winebarger (2007), ApJ. 666, 1245

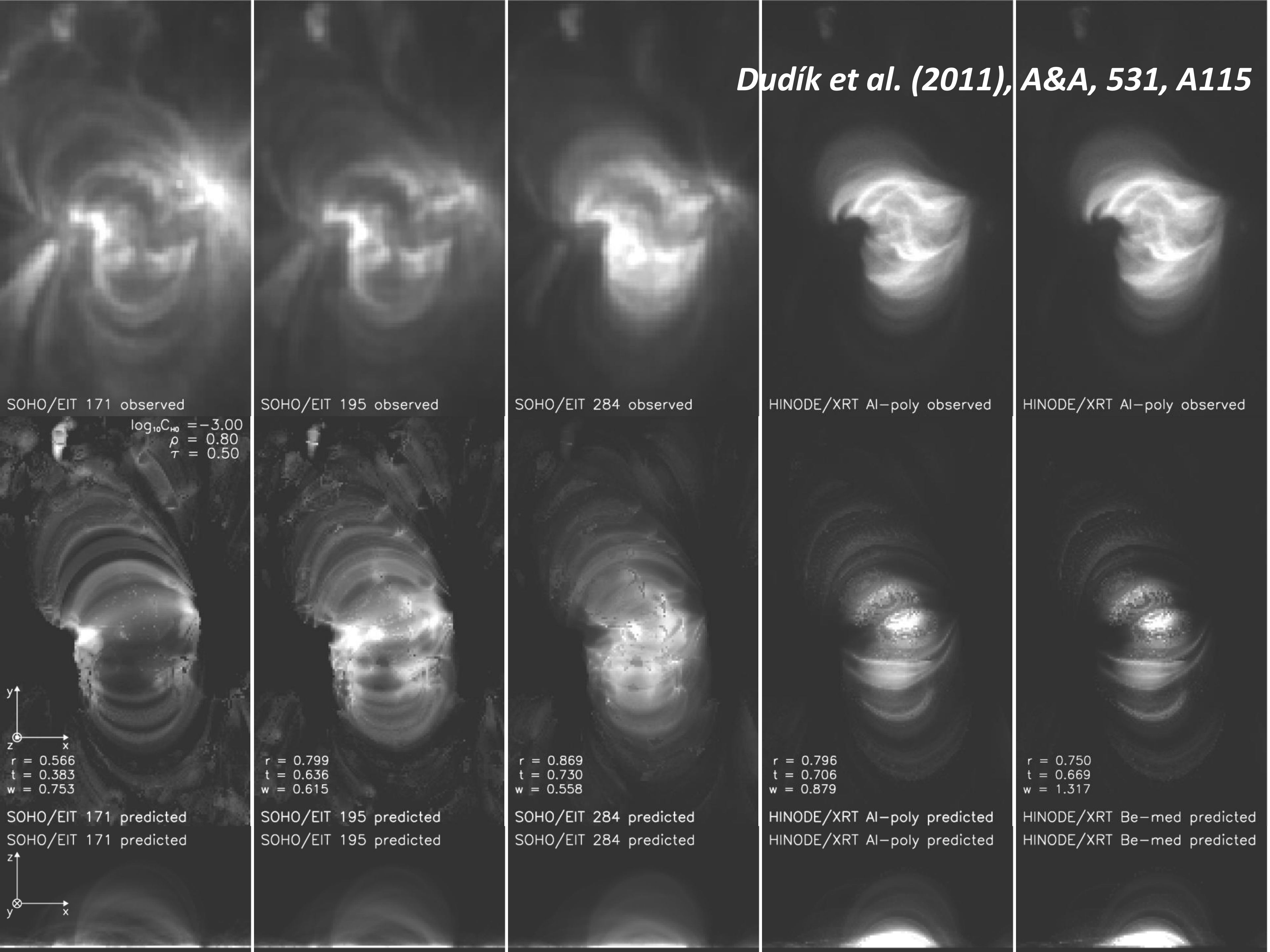
Dudík et al. (2011), A&A, 531, A115
SOHO/EIT 171 observed
SOHO/EIT 195 observed
SOHO/EIT 284 observed
HINODE/XRT Al−poly observed
HINODE/XRT Al−poly observed
$\log_{10}C_{H0}$ = −3.00
ρ = 0.80
τ = 0.50
y
z
x
r = 0.566
t = 0.383
w = 0.753
r = 0.799
t = 0.636
w = 0.615
r = 0.869
t = 0.730
w = 0.558
r = 0.796
t = 0.706
w = 0.879
r = 0.750
t = 0.669
w = 1.317
SOHO/EIT 171 predicted
SOHO/EIT 195 predicted
SOHO/EIT 284 predicted
HINODE/XRT Al−poly predicted
HINODE/XRT Be−med predicted
SOHO/EIT 171 predicted
SOHO/EIT 195 predicted
SOHO/EIT 284 predicted
HINODE/XRT Al−poly predicted
HINODE/XRT Be−med predicted
z
y
x

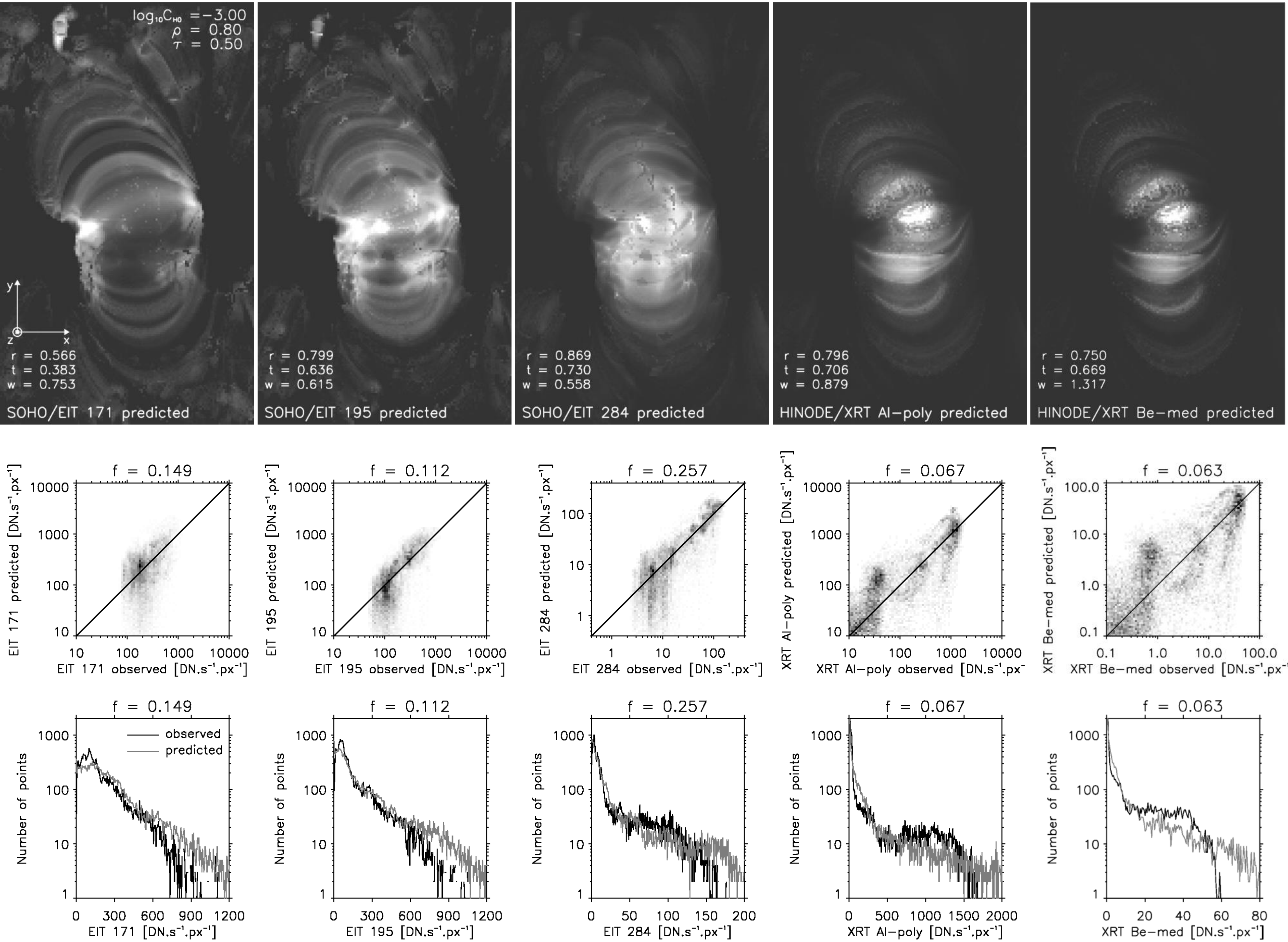

log10CH0 = −3.00
ρ = 0.80
τ = 0.50
r = 0.566
t = 0.383
w = 0.753
SOHO/EIT 171 predicted
r = 0.799
t = 0.636
w = 0.615
SOHO/EIT 195 predicted
r = 0.869
t = 0.730
w = 0.558
SOHO/EIT 284 predicted
r = 0.796
t = 0.706
w = 0.879
HINODE/XRT Al-poly predicted
r = 0.750
t = 0.669
w = 1.317
HINODE/XRT Be-med predicted
f = 0.149
f = 0.112
f = 0.257
f = 0.067
f = 0.063
EIT 171 predicted [DN.s⁻¹.px⁻¹]
EIT 171 observed [DN.s⁻¹.px⁻¹]
EIT 195 predicted [DN.s⁻¹.px⁻¹]
EIT 195 observed [DN.s⁻¹.px⁻¹]
EIT 284 predicted [DN.s⁻¹.px⁻¹]
EIT 284 observed [DN.s⁻¹.px⁻¹]
XRT Al-poly predicted [DN.s⁻¹.px⁻¹]
XRT Al-poly observed [DN.s⁻¹.px⁻
XRT Be-med predicted [DN.s⁻¹.px⁻¹]
XRT Be-med observed [DN.s⁻¹.px⁻
observed
predicted
Number of points
EIT 171 [DN.s⁻¹.px⁻¹]
EIT 195 [DN.s⁻¹.px⁻¹]
EIT 284 [DN.s⁻¹.px⁻¹]
XRT Al-poly [DN.s⁻¹.px⁻¹]
XRT Be-med [DN.s⁻¹.px⁻¹]

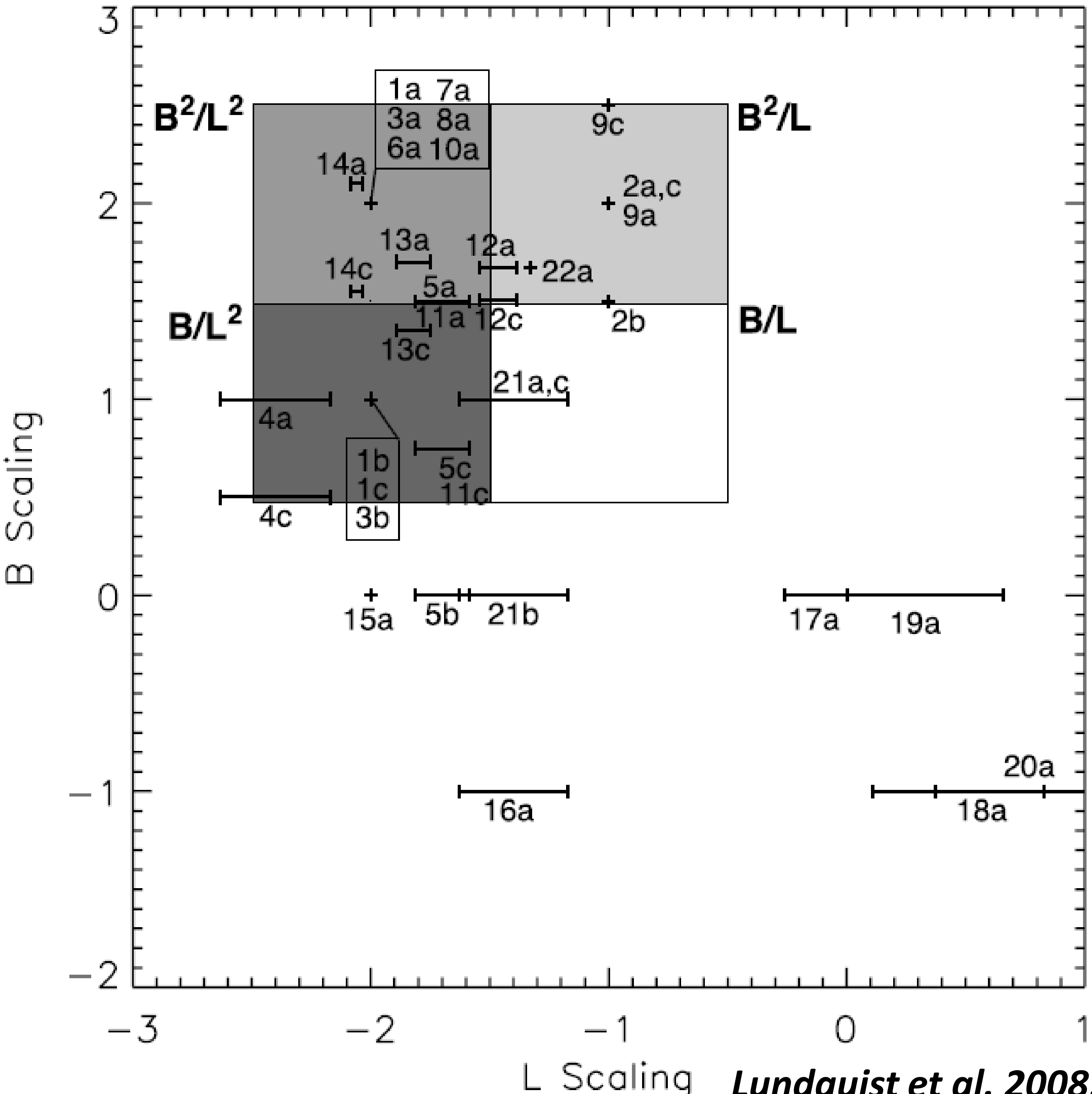

Lundquist et al. 2008, ApJ 689, 1388

Do We Understand the Geometry?

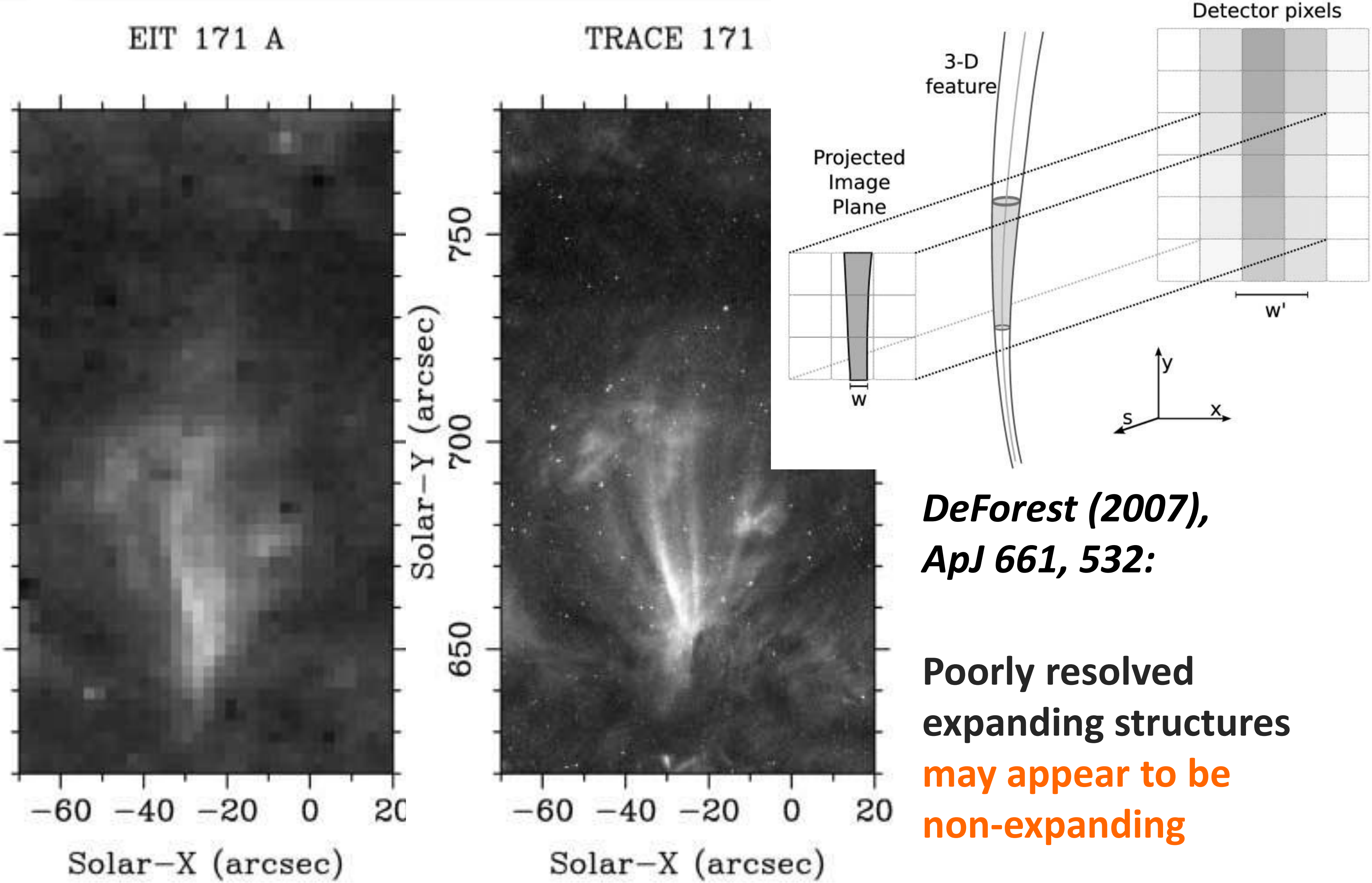

DeForest (2007), ApJ 661, 532:

Poorly resolved expanding structures may appear to be non-expanding

But some loops are resolved…

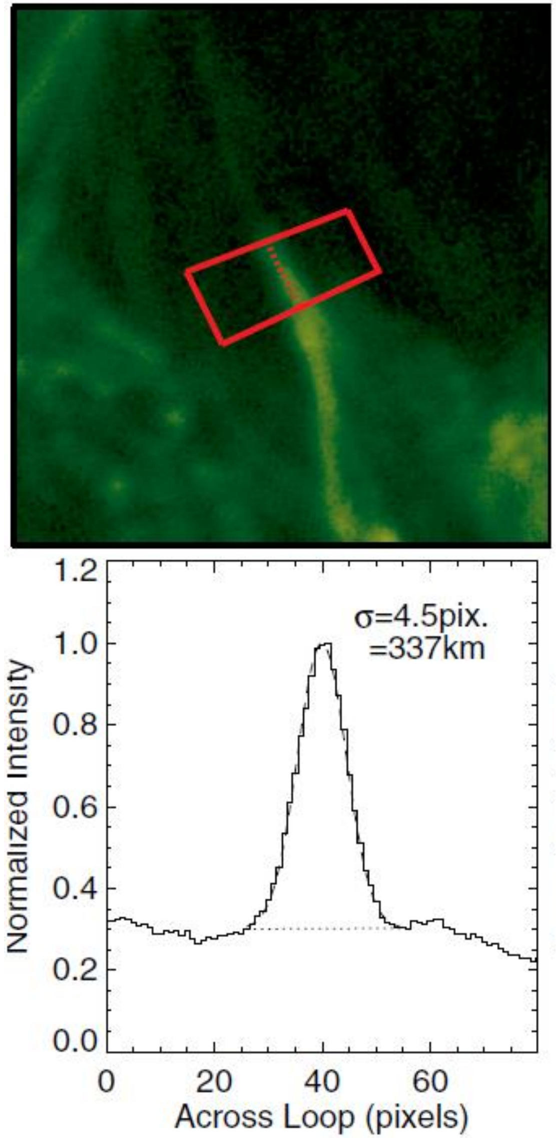

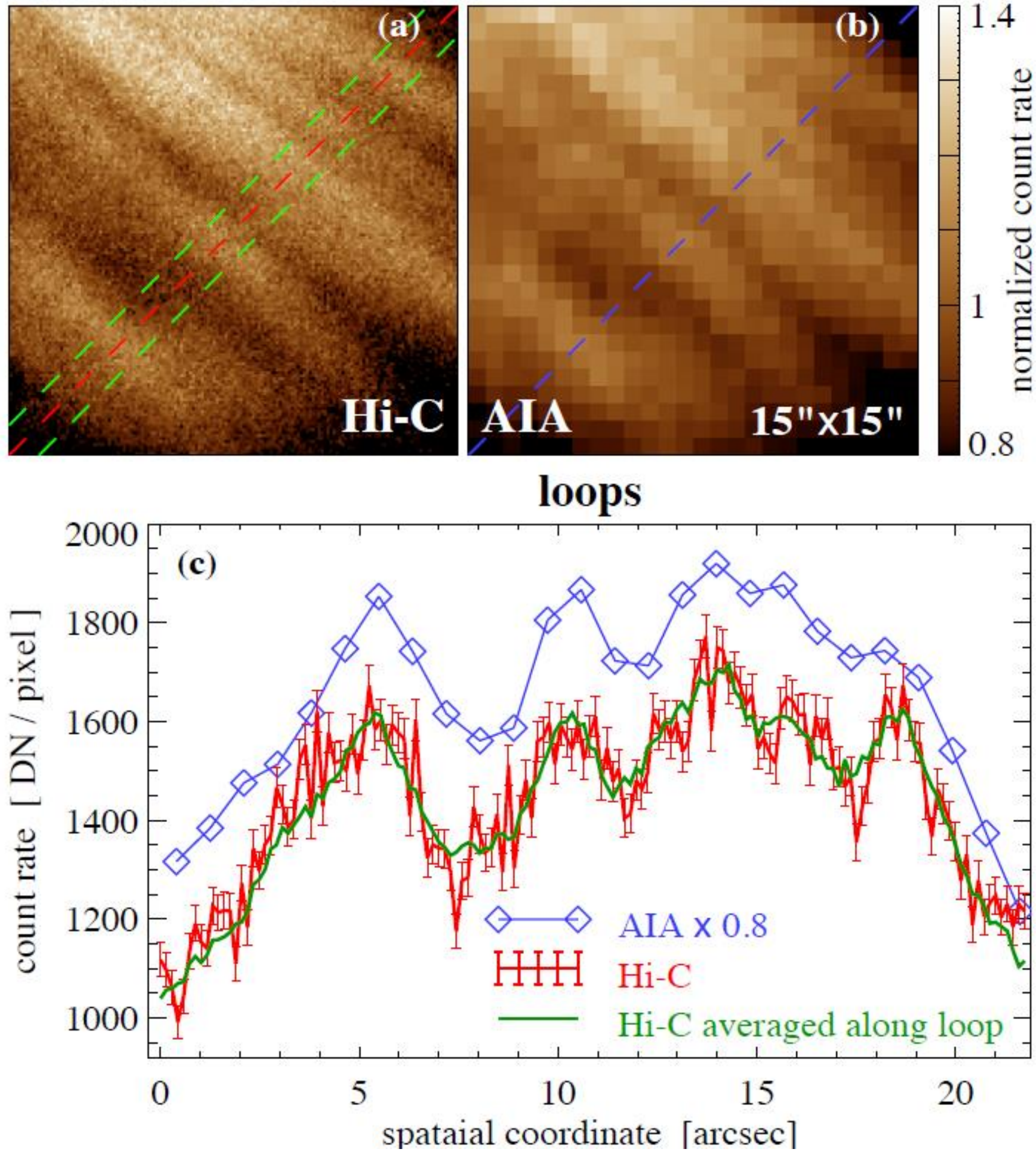

Brooks et al. (2013), ApJ 772, L19

Peter et al. (2013) A&A 556, A104

Geometry… Part 2

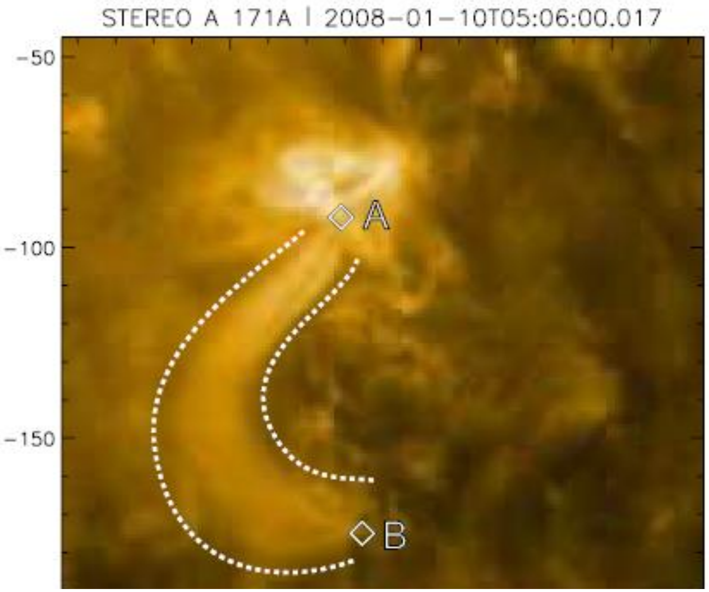

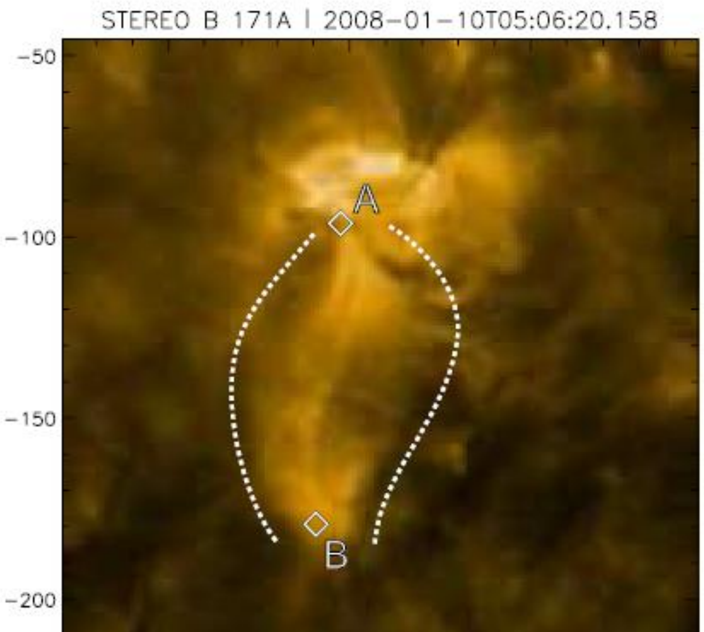

Malanushenko & Schrijver (2013), ApJ 775, 120

- No circular cross-sections
- Introduces bias in loop selection

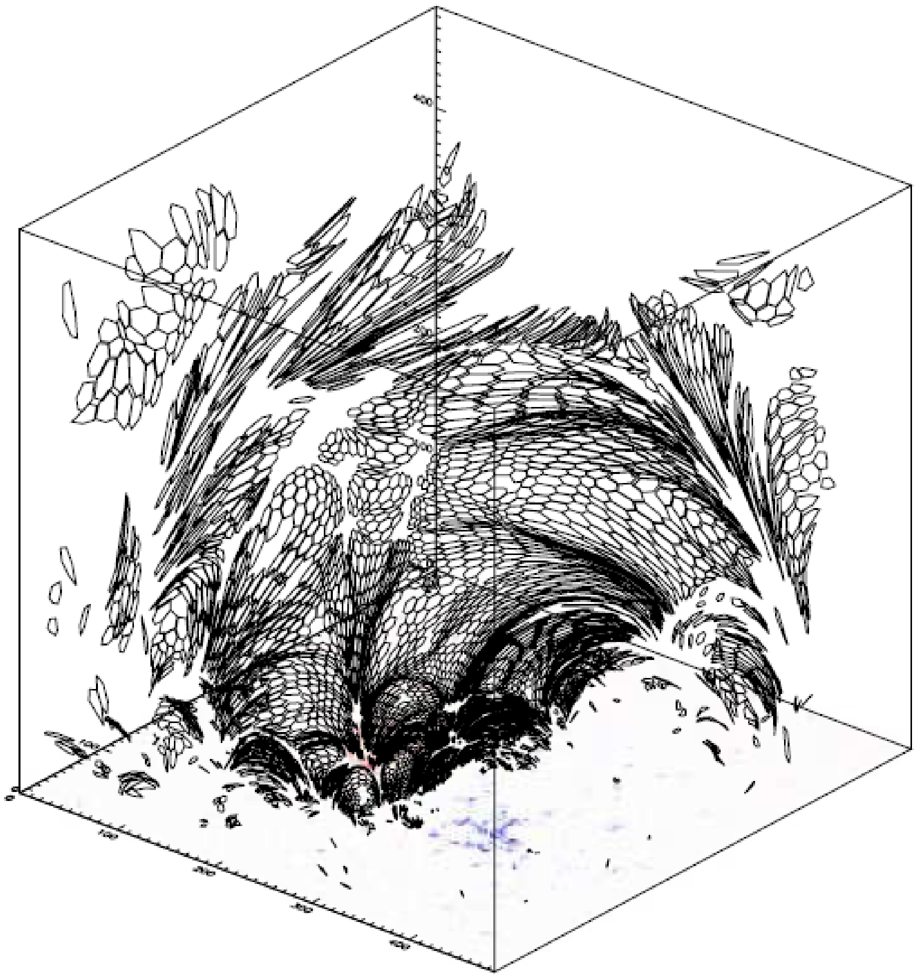

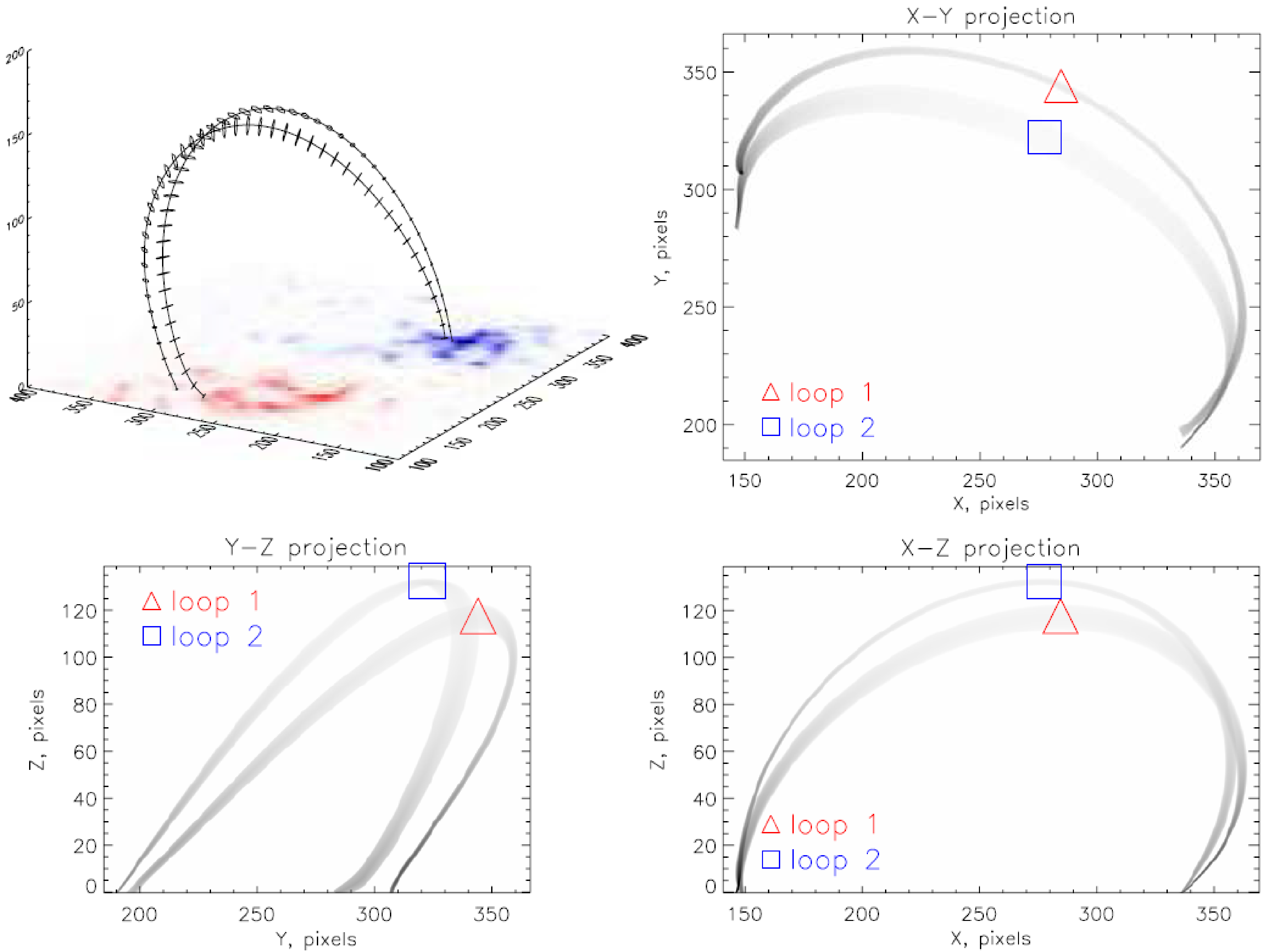
X–Y projection
Y, pixels
X, pixels
loop 1
loop 2
Y–Z projection
Z, pixels
Y, pixels
X–Z projection
Z, pixels
X, pixels

Expanding Loop: Thermal Struct.

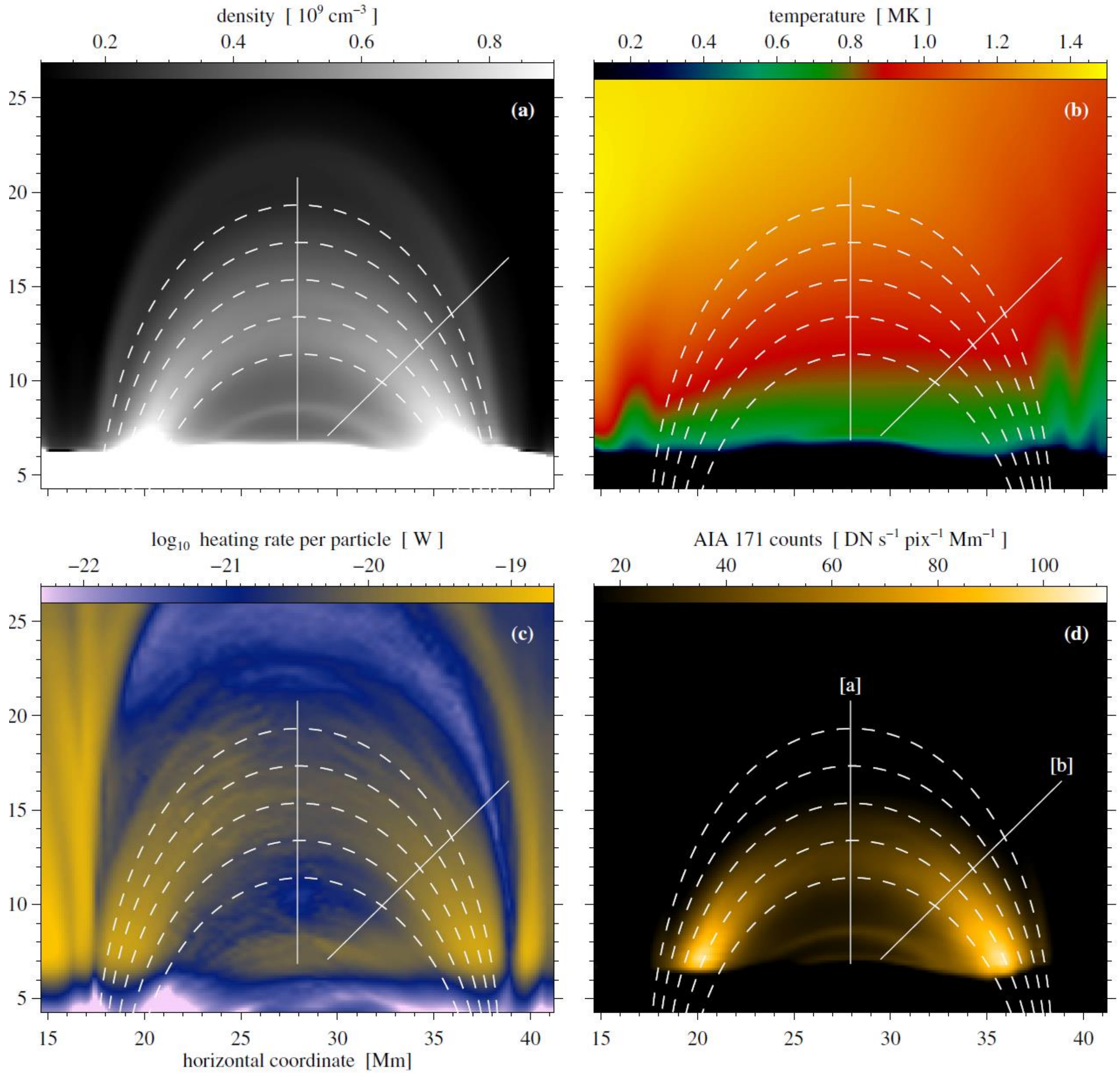

Peter & Bingert (2012), A&A 457, A1

- **MHD model of the solar corona**
- **Magnetic flux-tube with expanding area (cross-section)**
- **Interplay between temperature and density structure**
- **Leads to *apparently non-expanding* AIA loop**
- **Even if well-resolved**

Hinode/SOT and SDO/AIA

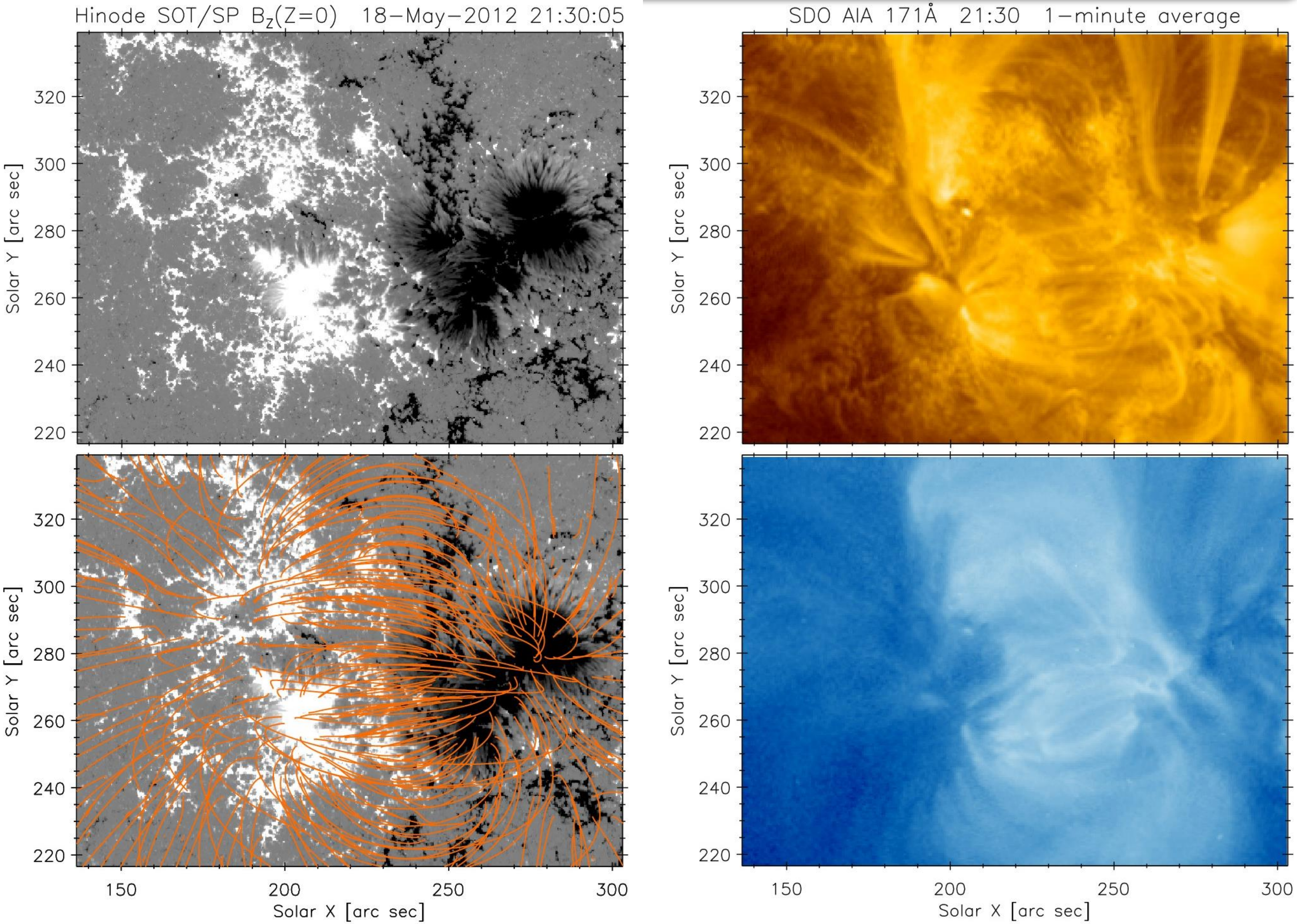

“Fundamental Flux-tubes”

Dudík et al. (2014), ApJ, 796, 20

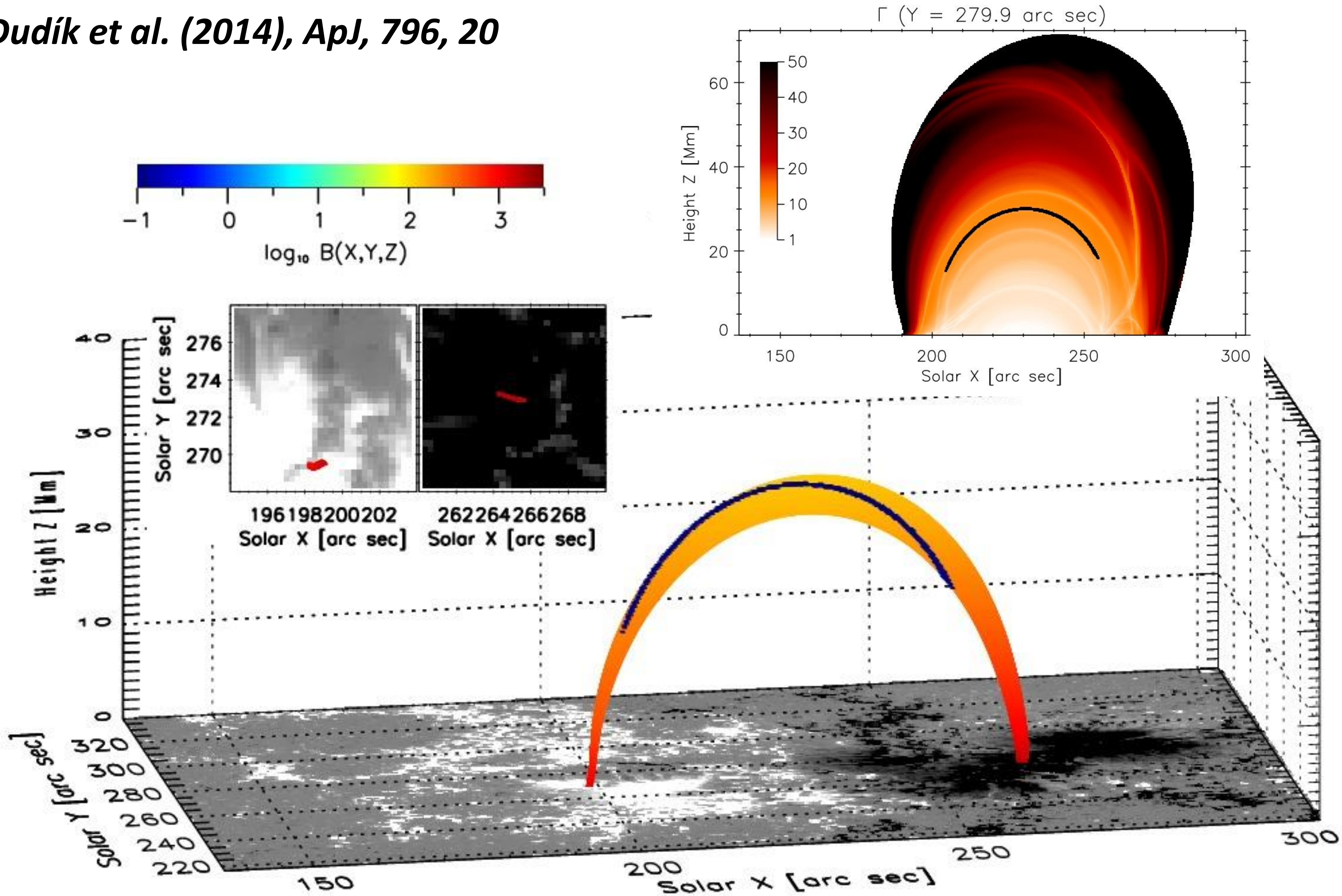

"Fundamental Flux-tubes"

Dudík et al. (2014), ApJ, 796, 20

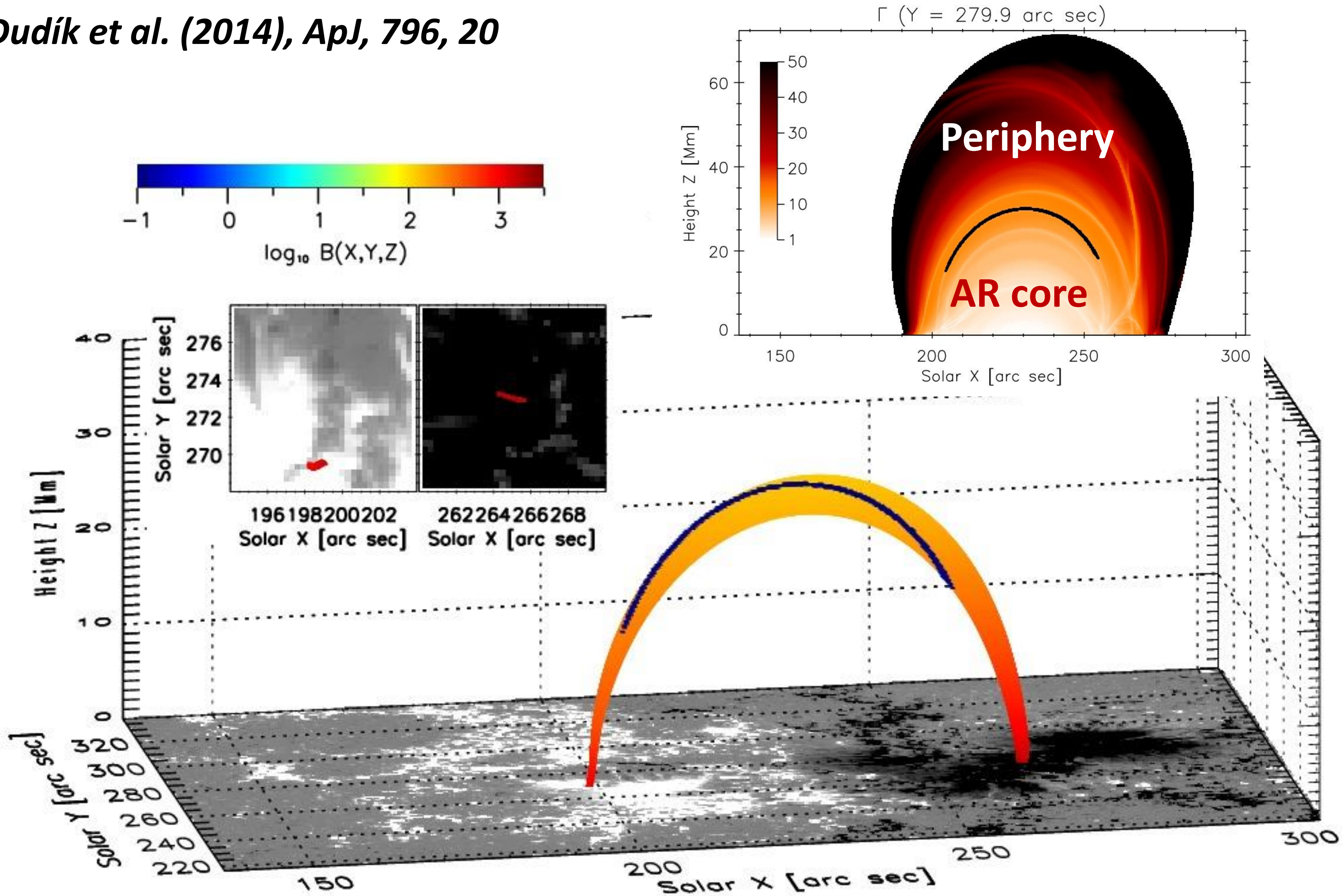

Highly Squashed Cross-sections

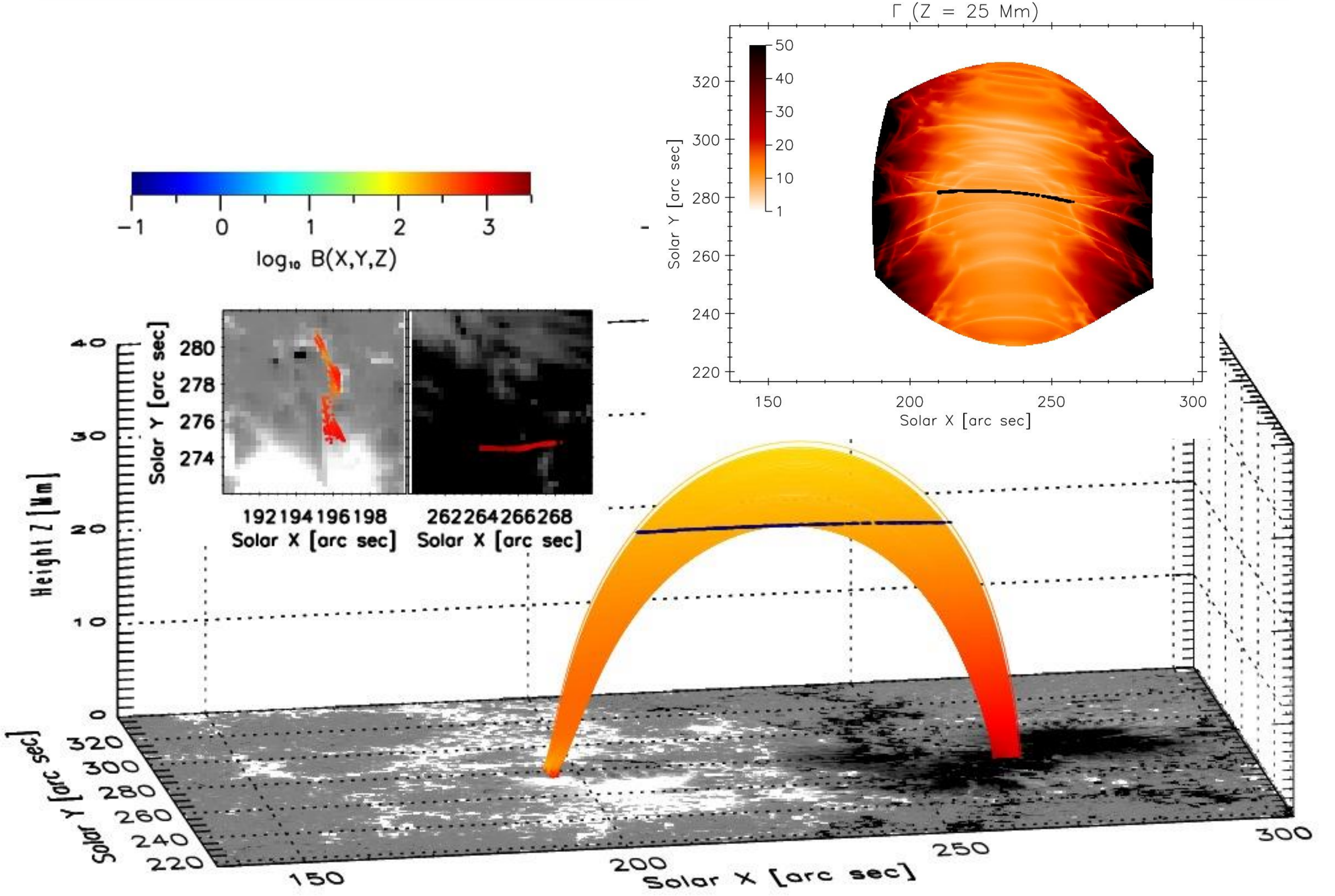

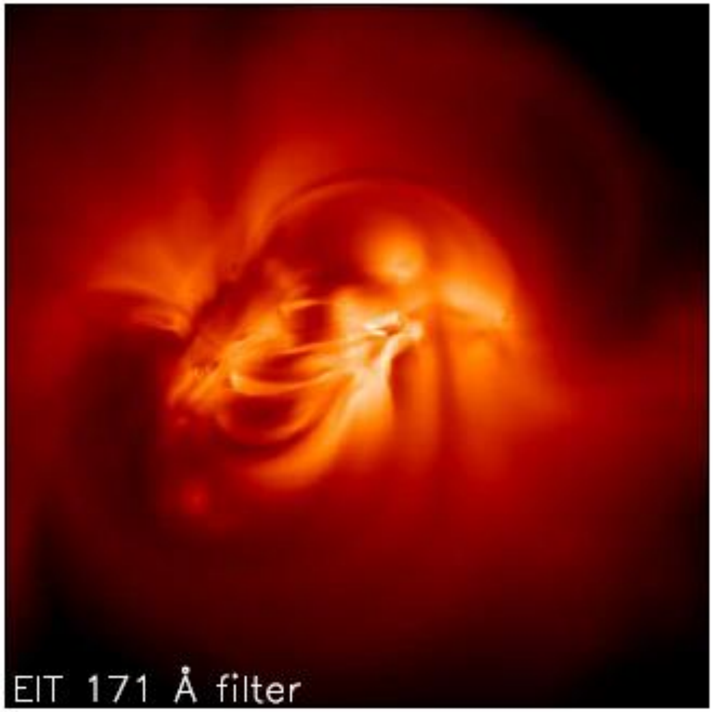
EIT 171 Å filter

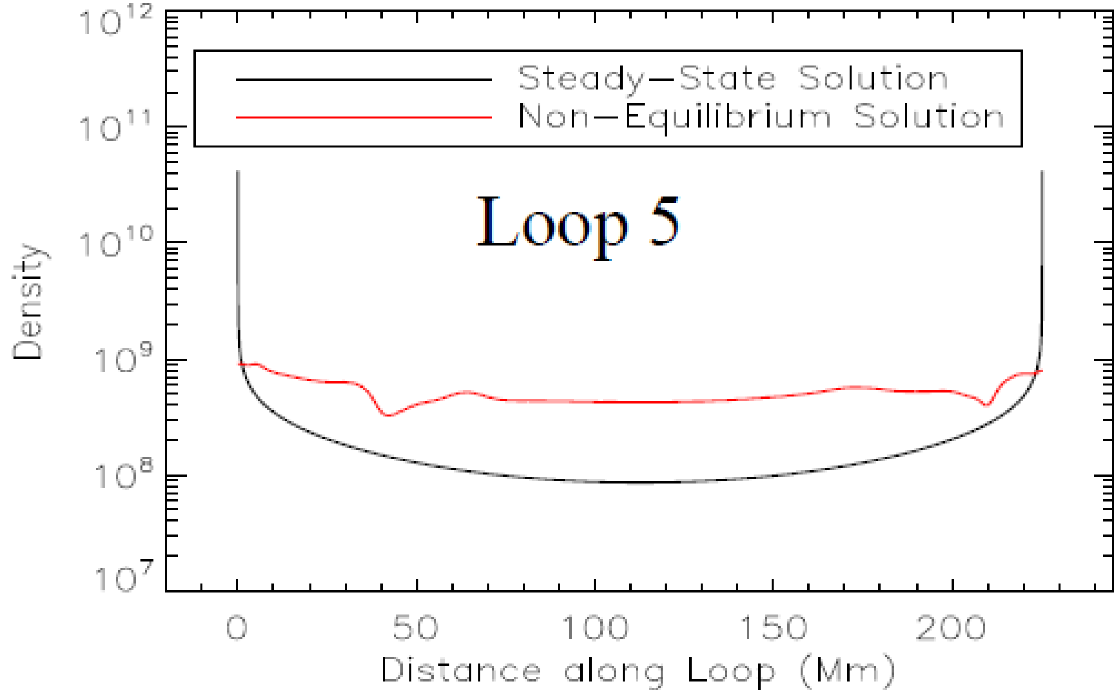
Steady−State Solution
Non−Equilibrium Solution
Loop 5
Density
10^{12}
10^{11}
10^{10}
10^{9}
10^{8}
10^{7}
0
50
100
150
200
Distance along Loop (Mm)

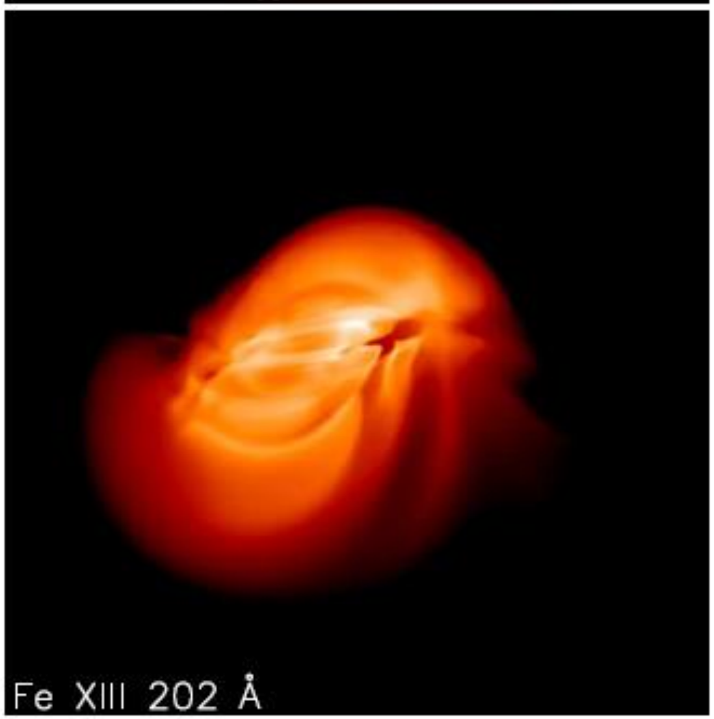
Fe XIII 202 Å


Lionello et al. (2011)
Loops Workshop V presentation
5
6
Fe XIII 202 Å

Thermal Non-Equilibrium

$$E_H - n_e^2 Q(T) = -\nabla . F_C$$

1. If the heating is too localized near the footpoints,
   thermal conduction cannot balance the radiative losses near the apex.
2. As a result, loop apex cools
3. Cooling increases radiative losses!
4. Condensation develops, grows and falls down. Loop empties
5. Empty loop is heated, resulting in chromospheric evaporation. Cycle renews.

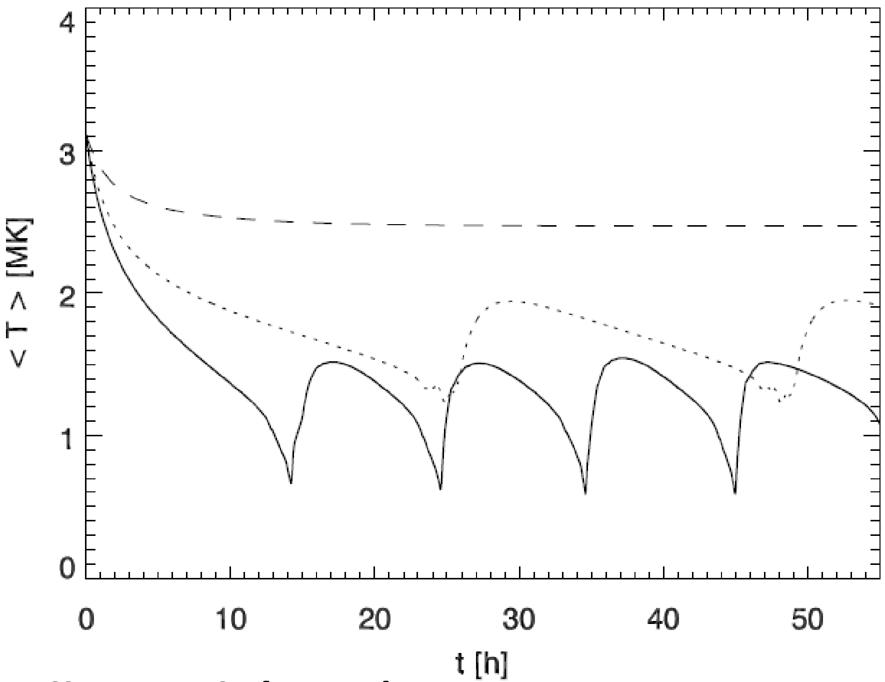

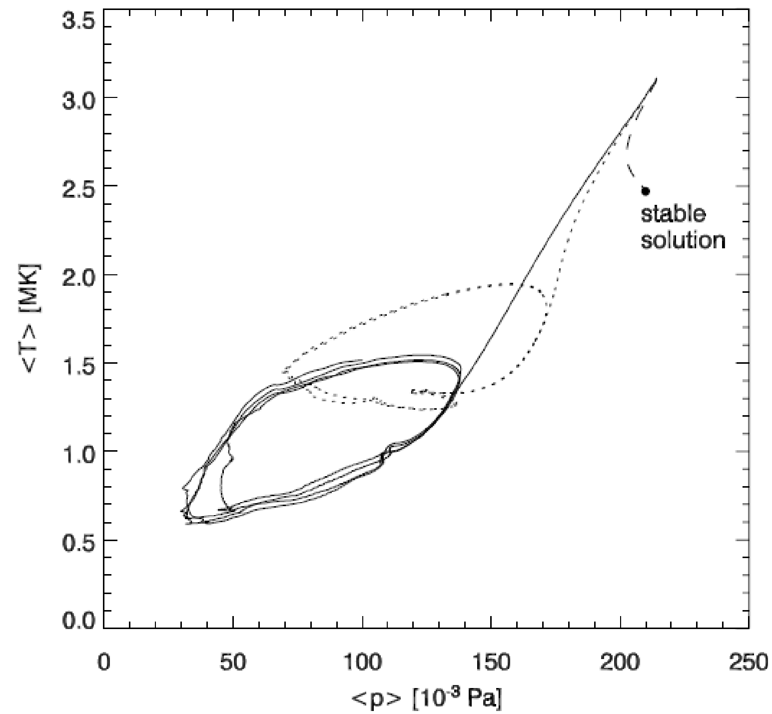

Muller et al. (2005), AA 463, 1067

Complete Condensations

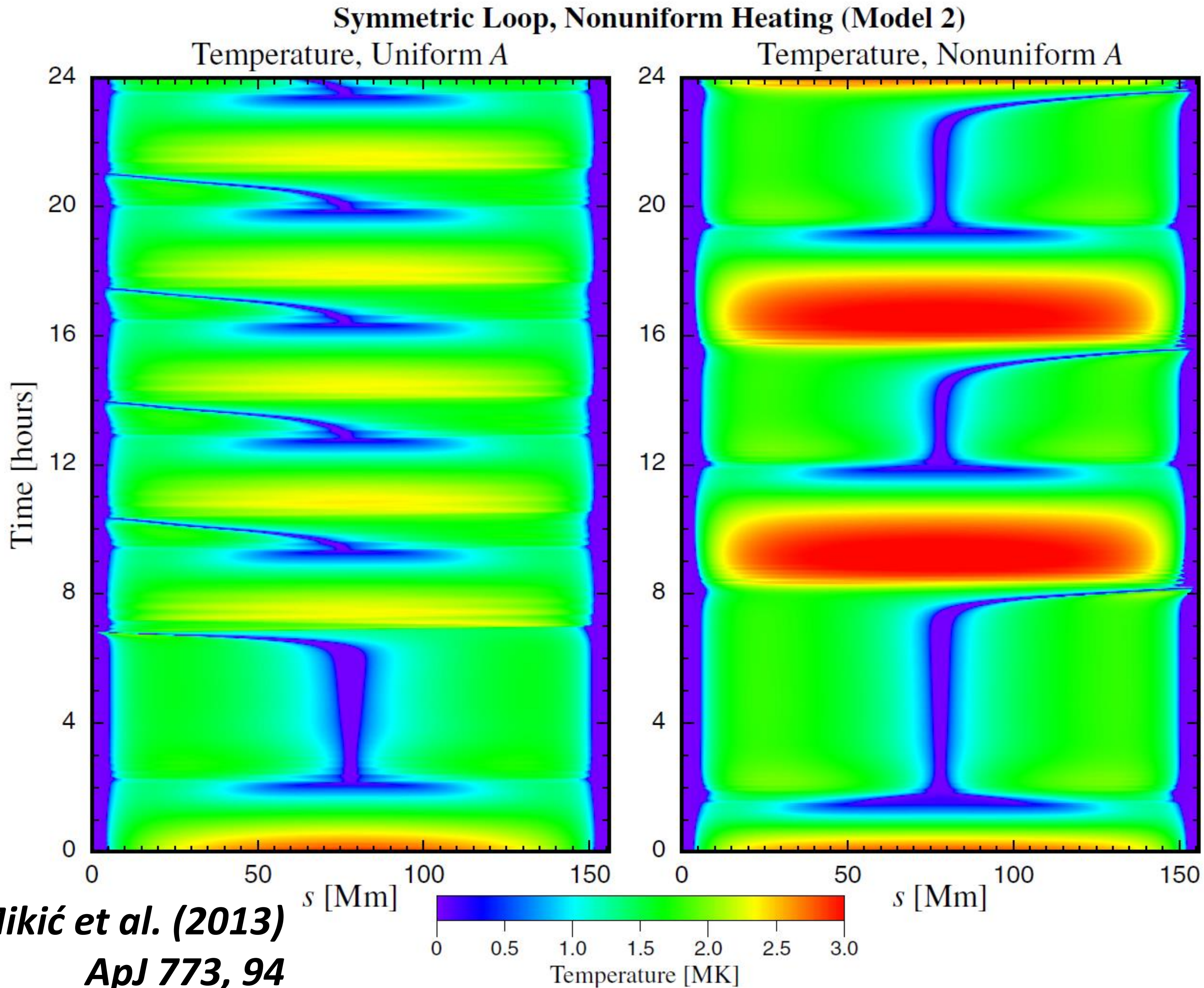

Mikić et al. (2013) ApJ 773, 94

(In)Complete Condensations

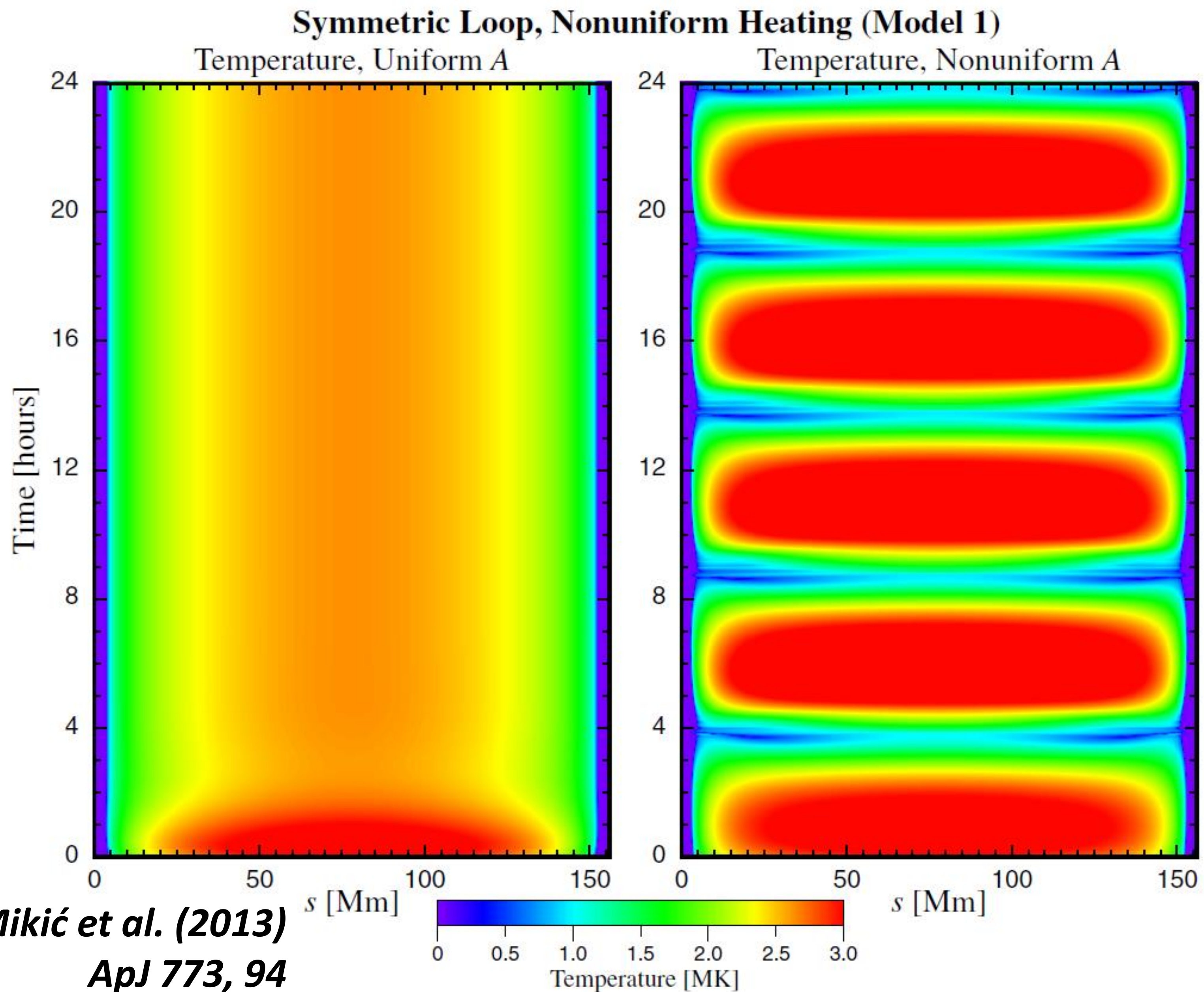

Mikić et al. (2013)
ApJ 773, 94

(In)Complete Condensations

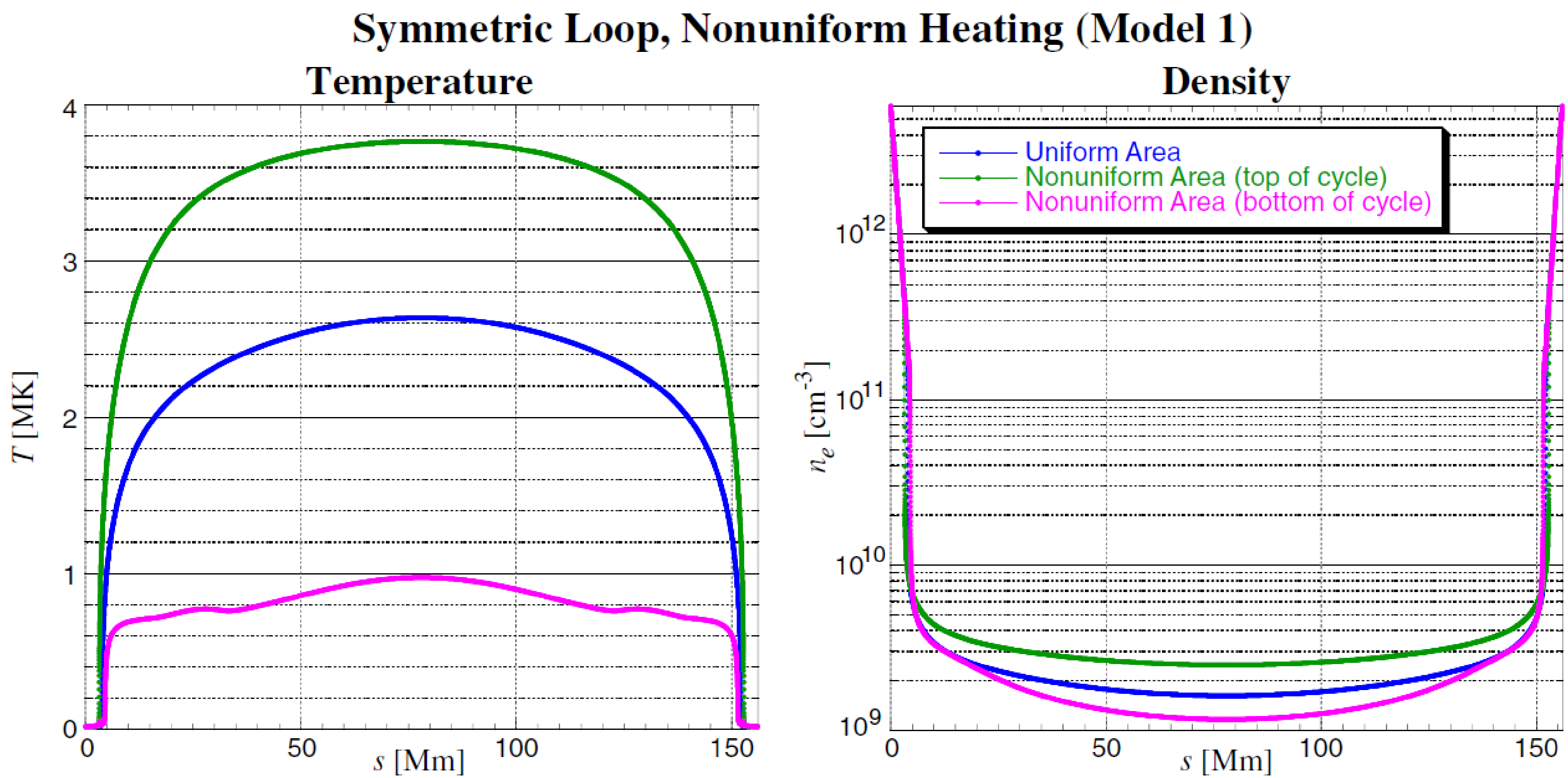

Mikić et al. (2013)
ApJ 773, 94

Coronal Rain

Antolin & Roupe van der Voort (2012), ApJ, 745, 152

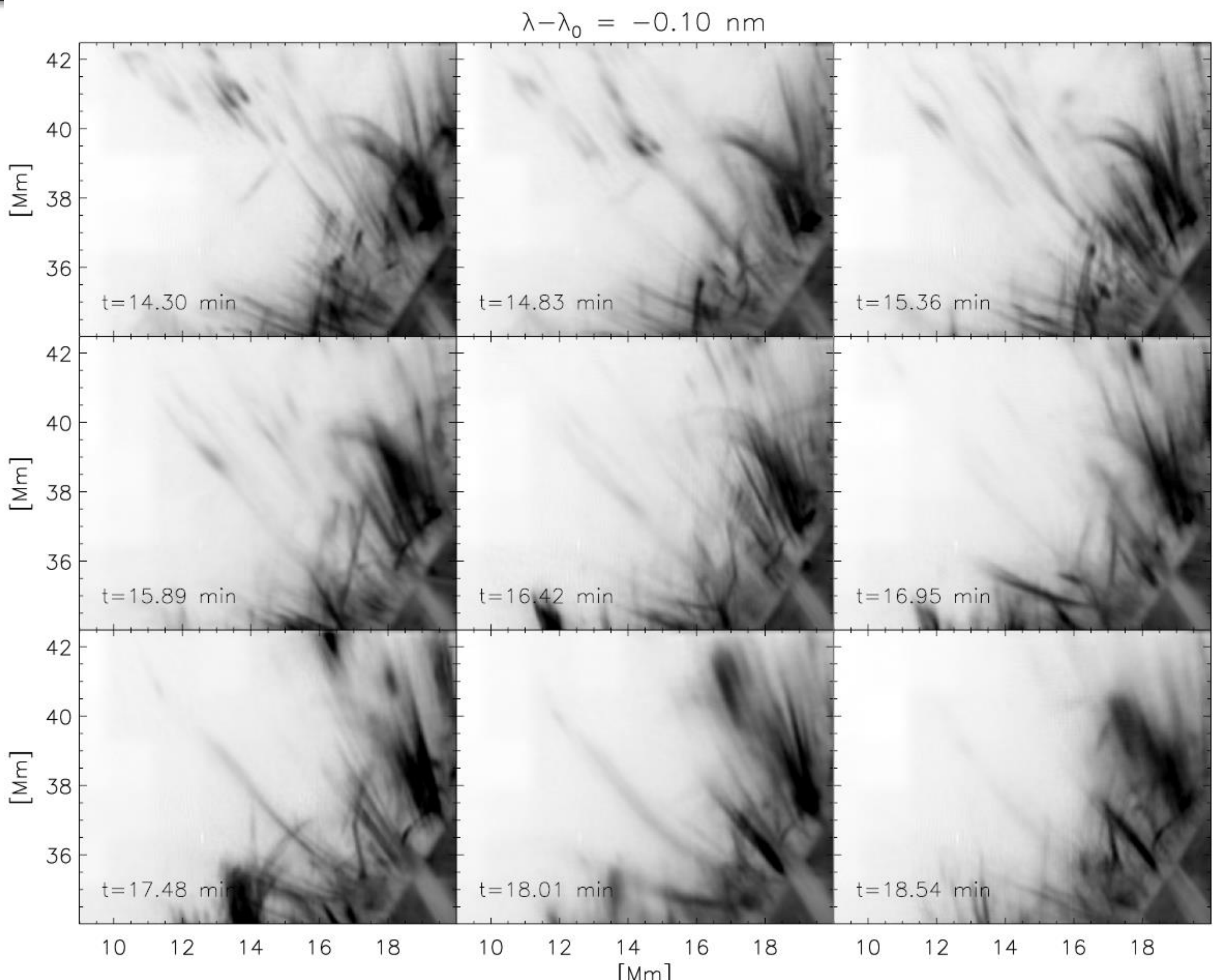

Thermal Non-Eq.: Recent Obs.

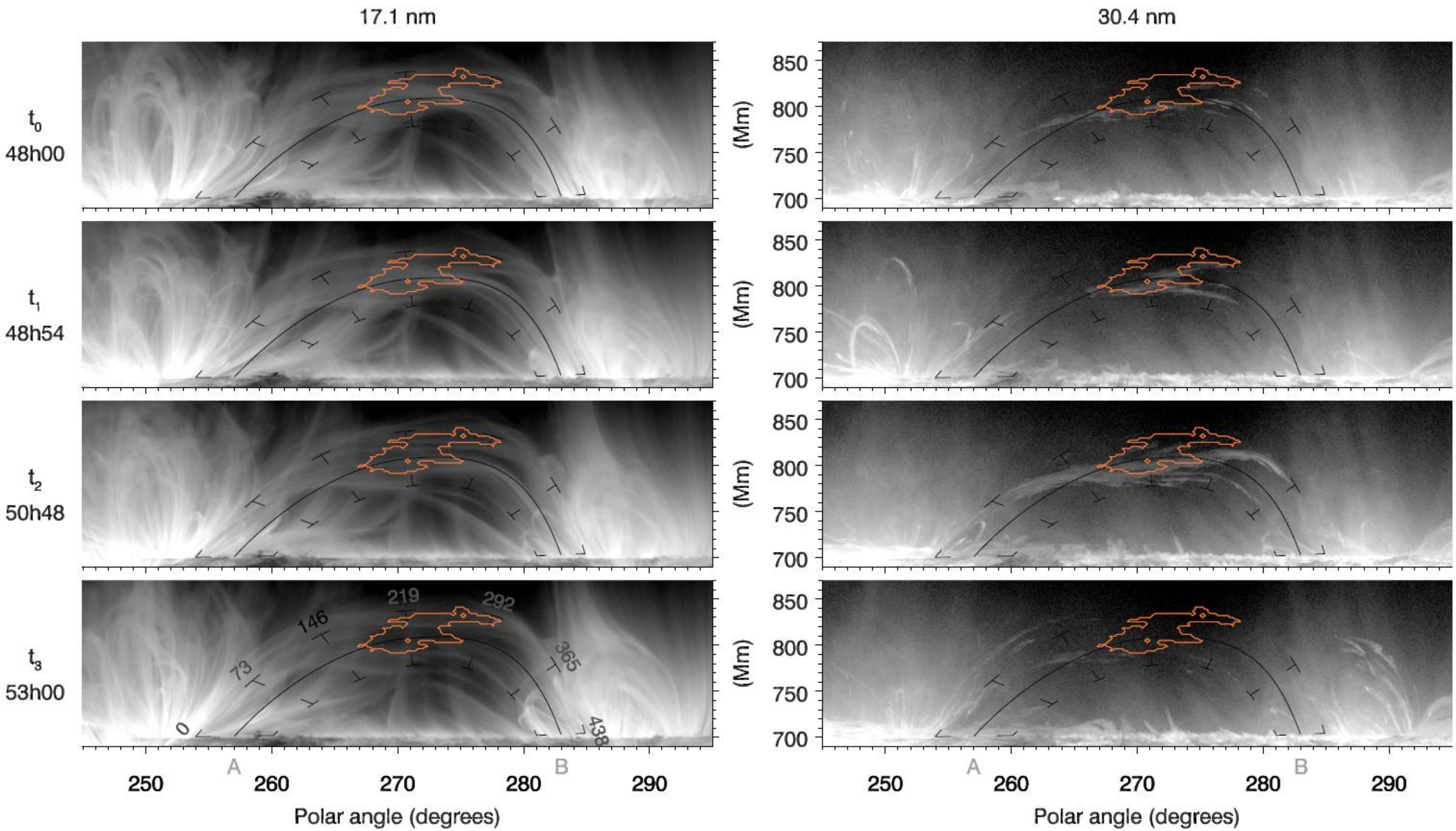

Auchère et al. (2018), ApJ, 853, 176

Thermal Non-Eq.: Recent Obs.

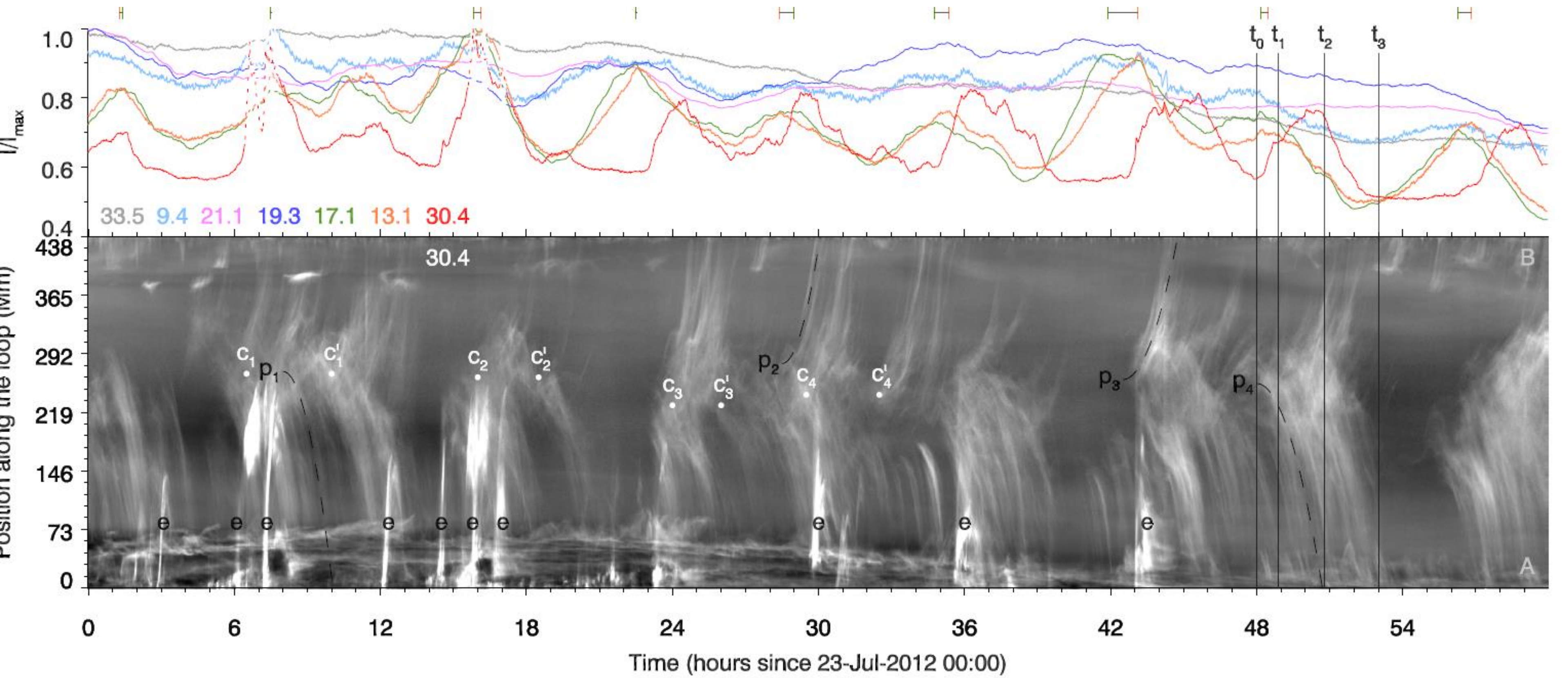

Auchère et al. (2018), ApJ, 853, 176

- Co-spatial and periodic (6.6 hr) showers
- Complete condensations seen at transition-region temperatures (0.1 MK)
- "It is raining as usual": Most of the trails follow parabolas (constant acceleration)
- Evidence for steady footpoint heating